

Diss. ETH No 21690

Investigation of Ion Transmission in  
Inductively Coupled Plasma  
Mass Spectrometry for  
Different Configurations of a  
Vacuum Interface

A dissertation submitted to attain the degree of  
DOCTOR OF SCIENCES of ETH ZURICH  
(Dr. sc. ETH Zurich)

Presented by  
TATIANA EGOROVA  
born 13<sup>th</sup> February 1983  
citizen of Russian Federation

accepted on the recommendation of  
prof. Detlef Günther  
prof. Wendelin Stark  
dr. Bodo Hattendorf

2013



# Contents

---

Abstract.....	5
Zusammenfassung.....	7
Acknowledgements.....	11
1. Introduction.....	13
1.1.    The Inductively Coupled Plasma Mass Spectrometer.....	13
1.2.    Sample introduction systems for ICPMS .....	14
1.3.    Inductively Coupled Plasma as Ion Source.....	15
1.4.    The ICPMS Vacuum Interface.....	17
1.5.    Improving Ion Transmission of the conventional Vacuum Interface.....	24
1.6.    The Ion Funnel.....	25
2. Characteristics of an ion funnel coupled to the vacuum interface of an ICP MS.....	29
2.1.    Experimental .....	29
2.2.    Results and Discussion.....	32
2.3.    Conclusions .....	41
3. Directly Coupled Ion Funnel .....	42
3.1.    Experimental .....	42
3.2.    Plasma Expansion .....	46
3.3.    DC Influence.....	47
3.4.    RF Influence .....	49
3.5.    Summary .....	49
4. Additional Extraction Interface .....	51
4.1.    Introduction .....	51
4.2.    Experimental .....	51
4.3.    Results and Discussions.....	61
4.4.    Angular Resolved Current Measurements.....	68
4.5.    Conclusions .....	74
5. Plasma Extraction through a Nozzle Interface.....	77
5.1.    Introduction.....	77
5.2.    Experimental.....	78
5.3.    Results and discussion.....	81
5.4.    Summary.....	99
6. Conclusion and Outlook .....	103
7. Reference List .....	107
8. Appendix.....	113
8.1. Simlon simulations parameters: .....	113
8.2. Reflections of the plasma from the cylindrical detector.....	115
9. Acronyms and Abbreviations .....	117
10. Curriculum Vitae .....	119



# I. Abstract

---

This work has investigated several approaches to improve ion transmission efficiency and thus sensitivity in inductively coupled plasma mass spectrometry. In a first step, properties of an electrodynamic ion funnel as an ion guide were investigated. Such ion funnel setups were found very efficient for electro spray ionization mass spectrometry instruments, where up to 100 % ions ion transmission was obtained in previous studies. It consists of a stack of ring electrodes with successively decreasing inner diameter and superimposed DC gradient along its axis and an RF field. The RF field creates a so called effective potential near the electrodes and potential-well region in the center of the funnel. Ions are thermalized by collisions and fall towards the centerline of the funnel while the DC gradient accelerates them towards the funnel exit. This configuration achieves a large acceptance area and effective focusing to a narrower conductance-limiting aperture. Higher operating pressures in comparison to common multipole ion guides additionally leads to efficient collisional thermalization of ions.

The adaption of an ion funnel as ion guide for ions extracted from an atmospheric inductively coupled plasma ion source was investigated in different approaches. Initial tests had shown for the first time that an ion funnel of specific geometry can be utilized to transfer also elemental ions through the 2<sup>nd</sup> vacuum stage of a modified commercial ICPMS instrument. However, at optimized conditions, ion transmission was found to be lower in average by one order of magnitude compared with the conventional setup utilizing electrostatic ion optics. Nevertheless the ion transmission was sensitive to the RF and DC fields applied, indicating that the funnel can be used as transfer element instead of the classical ion optics. Parameters for optimum ion transmission were found to depend on  $m/Q$ . With the ion funnel made of 0.5 mm thick electrode rings and 0.5 mm spacing, transmission was optimized for an RF field with amplitudes in the range of 25V to 50V at 600 MHz frequency and a DC gradient of -20V to -40V along the funnel axis.

Partly enclosing the ion funnel enabled its operation as a gas collision cell for the use of reactive or non-reactive gases. An effective reduction  $Ar^+$  and Ar-containing molecular ions was achieved using  $N_2$  and  $H_2$ . The latter is rather favorable in this context as it does not affect the transmission of low  $m/Q$  analyte ions to a great extent.

The coupling of the ion funnel directly downstream the sampler cone in an ICPMS vacuum interface however was not possible because the high electron number density within the plasma expansion just after the sampler orifice led to electric shorting between the funnel electrodes and a breakdown of the RF-field inside the funnel. An additional pumping stage before the ion funnel was again necessary to reduce the plasma load. This ensured stable operation of the RF field and allowed operation of the funnel in a wider pressure range. The transmission could be improved by the applied DC field, though the potential drop between the terminal funnel electrodes was most critical. Nevertheless no improvement of sensitivity was achieved by the applied RF field, which indicated that space charge effects most likely still limit the total current that can be transferred through the smallest apertures at the funnel exit to several nA. Angular resolved measurements of the ion

current exiting the funnel yet indicated an interesting aspect of the RF and DC potential. Both fields caused the angular spread to become narrower without significantly affecting the current measured at the axis. This is interpreted as an effect similar to that of a solid slit by cutting off the fraction of ions from the entire beam that has too low kinetic energies to overcome the effective potential at the exit of the ion funnel.

Another attempt to increase ion transmission through the first vacuum stage was made by investigating the effect of nozzles instead of the conventional sampler. Due to the narrower opening angle of nozzles the expansion degree of the plasma can be decreased, leading to visible changes of the supersonic expansion and corresponding shock structures. A narrower and denser expanding plasma jet occurs, which provides a higher electron and ion density along the expansion axis. Thus higher potential gradients were necessary to achieve charge separation of ions and electrons. Nonetheless a significantly higher ion transmission was attained through a skimmer cone into the 2<sup>nd</sup> vacuum stage. Nozzles with opening angles between 7° and 56° for the conventional sampler cone were investigated together with different skimmer cone orifices in a conventional ICPMS instrument. Smaller opening angles lead to a higher gas load to the 2<sup>nd</sup> vacuum stage and thus require smaller skimmer cone openings in order to maintain the pressure conditions in the mass spectrometer region. The skimmer cone aperture however was found the critical parameter for total ion transmission. The sensitivities for smaller orifice sizes were lower in all cases and yet the confined expansion from the smaller nozzle opening angles could not compensate for the loss when maintaining the pressure limit. Nonetheless the nozzles caused the mass discrimination to decrease and reduced the kinetic energy spread of the ions extracted from the ICP. This would indicate that the ion higher collision frequency near the skimmer orifice can effectively thermalize the ion motion.

The current configuration of the ion funnel yields and the use of the nozzles ultimately did not improve analyte sensitivity in comparison to ICPMS instruments with conventional electrostatic ion optics or the conventional sampler cone, which is most likely caused by the high ion current introduced from the ICP source. Thus the space-charge limit is the crucial issue to be overcome for improving ion transmission. It will thus remain to be investigated further whether there is an opportunity to minimize space charge effects for example by selective reduction of the dominating Ar<sup>+</sup> ions and transfer of the main current to ions of low  $m/Q$  which may be removed from the entire beam in a more convenient way. The results obtained during this study however may also be used to the advantage of other mass spectrometric techniques. In particular, the narrowing of ion energy spread inside the ion funnel or even in the expansion of a supersonic jet can be an advantage for techniques, where, similar to ICPMS, a wide energy distribution can occur for the ions generated for example by laser ablation or glow discharge ionization methods.

## II. Zusammenfassung

---

In dieser Arbeit wurden unterschiedliche Ansätze untersucht, um die Effizienz der Ionen­transmission und damit Empfindlichkeit der Massenspektrometrie mit induktiv gekoppelter Plasma­ionen­quelle (inductively coupled plasma mass spectrometry - ICPMS) zu verbessern. Zunächst wurden die Eigenschaften eines elektrodynamischen Ionen­trichters als System zur Ionen­führung untersucht. Solche Ionen­trichter Ansätze konnten bereits erfolgreich für Massenspektrometrie mit Elektrospray-Ionisation eingesetzt, wobei bis zu 100% Ionen­transmission erreicht wurde. Der Ionen­trichter besteht aus einem Stapel von Ringe­elektroden mit kontinuierlich abnehmendem Innendurchmesser an denen ein Hochfrequenzfeld (HF-Feld) mit gegenseitiger Polarität mit einem Gleichspannungsgradienten entlang der Achse angelegt wird. Das HF-Feld erzeugt ein sogenanntes effektives Potential in der Nähe der Elektrodeninnenseiten während an der Achse der Anordnung nur geringe Feldstärken erreicht werden. Ionen, deren kinetische Energie durch Kollisionen abnimmt, können so nahe der Achse angereichert werden. Das Gleichspannungspotential dient dann noch zur Beschleunigung zur Austrittsöffnung des Trichters. Diese Konfiguration ermöglicht eine große Akzeptanz für den Eintritt der Ionen bei gleichzeitiger Fokussierung. Höhere Betriebsdrücke im Vergleich zu herkömmlichen Multipolionen­führungen führt zusätzlich zu einer effizienten Thermalisierung der Ionen durch Stöße mit dem Kollisionsgas.

Die Adaption eines Ionen­trichters zur Führung von Ionen aus einer atmosphärischen Plasma­ionen­quelle, wurde in verschiedenen Ansätzen untersucht. In ersten Tests konnte zum ersten Mal gezeigt werden, dass ein Ionen­trichter mit der hier verwendeten Geometrie eingesetzt werden kann, um auch atomare Ionen durch die zweite Vakuumstufe eines modifizierten, kommerziellen ICPMS Instruments zu leiten. Unter optimierten Bedingungen war die Ionen­transmission allerdings noch um durchschnittlich eine Größenordnung geringer als mit dem herkömmlichen Aufbau mit elektrostatischer Ionenoptik. Nichtsdestotrotz konnten die Transmissionseigenschaften der unterschiedlichen Isotope durch der Wahl der Betriebsbedingungen angepasst werden. Dies zeigt, dass der Trichter prinzipiell als Komponente anstelle einer klassischen Ionenoptik verwendet werden kann. Die Betriebsbedingungen für optimale Ionen­transmission hängen ausserdem vom Masse/Ladung-Verhältnis der einzelnen Isotope ab. Der hier verwendete Ionen­trichter mit Elektroden von je 0,5 mm Dicke und Abstand zeigte höchste Transmission für atomare Ionen bei einem HF-Feld mit einer Amplitude im Bereich von 25V bis 50V, einer Frequenz von 600 MHz und einem Gleichspannungsgradienten von -20 V bis -40V.

Durch eine teilweise Überdeckung des Ionen­trichters ergibt sich ausserdem die Möglichkeit ihn als Reaktions-Kollisionszelle mit reaktiven oder nicht-reaktiven Gasen zu betreiben. Eine effiziente Reduktion der dominierenden  $\text{Ar}^+$ -Ionen sowie Moleküli­onen konnte durch Zugabe von  $\text{N}_2$  und  $\text{H}_2$  erreicht werden. Da der Einsatz von  $\text{H}_2$  in diesem Zusammenhang eine bessere Transmission von Analyt­ionen mit niedrigerem  $m/Q$  erreicht, ist der Einsatz dieses Gases hier vorteilhaft.

Die Verwendung des Ionen­trichters unmittelbar in der ersten Vakuumstufe eines ICPMS war allerdings nicht möglich, da die hohe Elektronenzahldichte im Plasma zu einem elektrischen

Kurzschluss zwischen den Elektroden des Trichters und damit zu einem Zusammenbruch des HF-Feldes führte. Dies machte den Einsatz einer weiteren Vakuumstufe zwischen Ionentrichter und Samplerkonus erforderlich, um die Plasmadichte innerhalb des Trichters zu reduzieren. Dadurch konnte ein stabiler Betrieb des HF-Feldes auch über einen weiten Druckbereich erreicht werden. In dieser Konfiguration konnte durch den axialen Potentialgradienten eine deutliche Erhöhung der Transmission erreicht werden, wobei sich die Spannungsdifferenz zwischen den letzten beiden Trichterelektroden als kritisch herausstellte. Eine Verbesserung konnte durch das HF-Feld jedoch nicht erreicht werden. Insofern scheint der maximal erreichbare Ionenstrom von einigen nA durch Raumladungseffekte, insbesondere an den Ringelektroden mit kleinstem Innendurchmesser, limitiert.

Messungen der Winkelabhängigkeit des Ionenstroms am Ausgang des Trichters offenbarten eine interessante Wirkung von Potentialgradient und HF-Feld. Durch anlegen beider Felder wurde die Winkeldispersion des Ionenstrahls erheblich reduziert, ohne den axial gemessenen Ionenstrom zu beeinflussen. Dieser Effekt ist ähnlich zu dem eines massiven Spaltes wobei zusätzlich der Ionenanteil mit geringer kinetischer Energie aus dem Ionenstrahl herausgefiltert werden konnte.

In einem weiteren Versuch, die Ionenstrahltransmission durch die erste Vakuumstufe zu erhöhen, wurde untersucht, welchen Einfluss ein Einsatz von Düsen anstelle des konventionellen Samplerkonus hat. Durch die kleineren Öffnungswinkel der Düsen kann der Expansionsgrad des Plasmas in der Überschallexpansion reduziert werden, was zu sichtbaren Veränderungen der entsprechenden Schockstrukturen führt. Generell konnte eine deutlich höhere Ionenstrahltransmission durch einen Skimmer Konus in die 2. Vakuumstufe erreicht werden. Düsen mit Öffnungswinkel zwischen  $7^\circ$  und  $30^\circ$  sowie für den herkömmlichen Samplerkonus wurden zusammen mit verschiedenen Durchmessern der Öffnung im Skimmerkonus in einem kommerziellen ICPMS Gerät untersucht. Kleinere Öffnungswinkel führten dabei zu einer deutlich höheren Gaslast in der zweiten Vakuumstufe und die Betriebsbedingungen des MS konnten nur durch kleinere Öffnungen im Skimmerkonus aufrechterhalten werden. Dieser Parameter hat sich allerdings als kritische Größe für die maximale Ionenstrahltransmission herausgestellt. Die Empfindlichkeit für alle Isotope nahm jeweils mit kleineren Öffnungen ab. Es wurde allerdings beobachtet, dass durch die Düsen mit kleinerem Öffnungswinkel eine geringere Massendiskriminierung im resultierenden Ionenstrahl erreicht wird und dass die kinetischen Energien der Ionen zunehmend ähnlicher werden. Dies deutet darauf hin, dass eine grössere Kollisionswahrscheinlichkeit der Ionen nahe der Skimmeröffnung besteht, die die Ionenenergien effektiv reduzieren können.

Die aktuelle Konfiguration des Ionentrichters oder die Verwendung von Düsen anstelle des konventionellen Samplerkonus ermöglichen im Vergleich zum kommerziellen ICPMS Instrument leider keine Verbesserung der Empfindlichkeit für die atomaren Ionen aus einer ICP Ionenquelle. Die ist höchstwahrscheinlich bedingt durch den hohen Ionenstrom der Quelle und daraus resultierende Raumladungseffekte.

Um den Ionentrichter zur Führung des Ionenstrahls eines ICPMS einsetzen zu können müssten zunächst Möglichkeiten gefunden werden, den Gesamtionenstrom zu reduzieren.



Raumladungseffekte scheinen momentan das grösste Hindernis darzustellen, um die Analytione von der Plasmaquelle effizient durch die Trichteranordnung zu überführen. Ein möglicher Weg wäre  $\text{Ar}^+$ , welches den grössten Anteil des Stroms ausmacht selektiv zu neutralisieren, die Ladung auf eine Spezies mit tiefem  $m/Q$  zu übertragen und sie durch Anpassung der Betriebsbedingungen des Ionentrichters aus dem Strahl zu entfernen.

Einige Resultate, die während dieser Studie erhalten wurden, können allerdings auch vorteilhaft in anderen massenspektrometrischen Methoden zum Einsatz kommen. Im Besonderen ist dies die effiziente Verringerung des Energiespektrums der atomaren Ionen, die insbesondere in der Glimmladungs- und Lasermassenspektrometrie, in denen ähnlich breite Energieverteilungen auftreten wie in der ICPMS, eine bessere Fokussierung des Ionenstrahls ermöglichen sollten.



### III. Acknowledgements

---

This work could be not possible to accomplish it without many people, who assisted, supported and inspired me and whom I would like to thank.

First of all, I would like to thank **Detlef Günther** for giving me an opportunity to work in his group at ETH and his inspiration, which he always brings with himself. I am thankful for believing in me and supporting me with patience and understanding.

I would like also to express my sincere gratitude to **Bodo Hattendorf**, his tremendous support and his patience. He is an example for a true scientist, with ideas and openness for discussions, which were not limited to science only, but also showed me a deep interest in combination with judiciousness to the world.

I also appreciate deeply the assistance of **Rolf Dietiker**, who was always ready to help. Without his practical support this project would never been realized.

I wish to thank **Henry Longerich**, who made a great favor and assisted with the writing. He made great advices which were very useful to improve the thesis.

I would like to thank **Karin Birbaum** for the friendless and support, **Gisela Fontaine** for her optimism, inspiration and interesting discussions, **Beat Aeschlimann** for his funny stories and friendliness. I very appreciate the help of **Olga Borovinskaya** and **Daniel Tabesrky** with the preparation to the defense and **Natalie Fedotova** for the support. And I am thankful the entire **Günther group** I was so happy to work with. It was a great time for me, which granted me memorable moments and I learnt a lot.

I also want to thank my family for the support and especially my husband for his belief in me and his support in difficult moments of fears and doubts.



# 1. Introduction

---

## 1.1. The Inductively Coupled Plasma Mass Spectrometer

Inductively coupled plasma mass spectrometry (ICPMS) is a widely used technique for trace and ultra-trace multi-element analysis in many fields of analytical chemistry. It provides high precision and accuracy, and achieves low limits of detection and can be used with a wide range of sample introduction systems. With a limit of detection between the sub-pg/L to ng/L range for most elements, the ICPMS is a very powerful method used in many applications, including geochemistry (*e.g.* fluid inclusions analysis), geochronology, environmental monitoring, material science, life science, food, chemical, semiconductor and nuclear industries, forensic science, archeology, cosmochemistry, speciation analysis, provenance studies, etc. [1–20]. After it was first introduced in the early 1980s [21], the basic configuration of an ICPMS has not changed in a dramatic way. The two stage differential pumping interface introduced by Douglas and French [22] remains the essential part of all currently commercially available ICPMS instruments, as this allows the generation of elemental ions within an atmospheric source and continuously transfer them into a low pressure vacuum chamber holding a mass spectrometer. ICPMS hardware generally may be separated into four major components: the sample introduction system, the plasma ion source, the two stage vacuum interface with sampler and skimmer cones and ion optics system and a mass spectrometer with detector. Despite the generally similar concepts of the instrumentation, the sensitivity of the instruments has been significantly improved during the past 30 years, but even with the high sensitivity reached by today's instruments, the majority of the ions generated inside the ICP do not reach the detector, with most of this loss of ion transmission in the interface region [23].

Currently available ICPMS instruments with standard solution sample introduction systems typically achieve sensitivities from  $\approx 50$  to  $\approx 500$  cps/ng/L for ions of intermediate  $m/Q$  using quadrupole mass filters. Sector field magnetic sector instruments mass analyzers usually yield about 10 times higher sensitivities (Table 1). With specific modifications even higher sensitivity can be achieved. The so-called "S-option" [24] utilized additional pumping capacity and smaller sampler cone orifices to enhance sensitivity, an approach currently revisited in the jet interface offered for the Element XR instrument. Considering that the liquid intake into the ICP is typically in the range of 20  $\mu\text{L}/\text{min}$  for conventional nebulizer/spray chamber systems, this results in a detection efficiency of  $10^{-5}$  –  $10^{-4}$  ions per atom presented to the ICP.

Table 1. Sensitivities for different ICPMS instruments from manufacturers' specifications.

Instrument	Sensitivity, cps/mg/L
Sector field MS	
Thermo Scientific ELEMENT 2/XR	$^{115}\text{In} > 1 \cdot 10^9$
NU Instruments Attom	$^{115}\text{In} > 1 \cdot 10^9$
Quadrupole MS	
Perkin Elmer NexION series	$^{115}\text{In} > 5 \cdot 10^7$
Agilent 7700/8800 series	$^{89}\text{Y} > 1.6 - > 2.2 \cdot 10^8^*$
Thermo ICApQ series	$^{115}\text{In} > 1.5 - > 4 \cdot 10^8^*$
Bruker Aurora/Aurora Elite	$^{115}\text{In} > 0.05 - > 1 \cdot 10^9^*$

\* Range of specifications for different available models

An overall gain in sensitivity of ICPMS instruments would be beneficial to all fields of applications, because it would allow to either extend the measurement range to even smaller concentrations of the elements in any sample or to utilize less sample material for analysis. It would however be especially useful for the direct analysis of solids using laser ablation sampling. This is because of the ongoing demand towards sampling at ever smaller laser spot sizes or sample volumes. Higher sampling resolution requires increasing sensitivity, especially when considering that a lot of effort has been put in reducing the ablation pit diameters, in order to attain higher spatial resolution. Considering however that a sample volume of 1  $\mu\text{m}$  diameter and depth for a silicate glass with a density of 2.2  $\text{g}/\text{cm}^3$  contains only  $42 \cdot 10^5$  atoms of In per mg/kg illustrates the need for a higher sensitivity or order to achieve trace element sensitivity at one micrometer spatial resolution. A similarly relevant example is the determination of major and trace elements in single fluid inclusions [1], which can reveal information about ore formation process and hydrothermal transport of elements, is limited by the availability of higher instrument sensitivity. Another emerging application field for ICPMS is nanoparticle analysis where single particles with diameters of less than several tens of nm need to be analyzed [3].

## 1.2. Sample introduction systems for ICPMS

The majority of samples regularly analyzed with ICPMS are liquid samples, which are introduced to the ICP in the form of droplets generated typically by pneumatic nebulization. Since the evaporation of big droplets delays the sample atomization and ionization within the plasma, spray chambers are used to make a droplet selection which allows only smaller droplets pass to the ICP, while larger droplets are removed via collision on the walls of the spray chamber and pumped off. The aerosol is generated with the nebulizer by a high velocity gas jet rupturing the liquid at an exit opening into fine droplets. These droplets then pass through the spray chamber where big droplets are removed by collisions with the spray chamber wall. The most widely used spray chambers are the Scott-type [25] spray chamber which is a double-pass design. Another more recently popular type of

spray chamber is based on cyclonic motion to aid in droplet selection. It has a smaller volume (~ 50 mL) and surface area and thus equilibration and washout times are significantly shorter. It further often achieves higher sensitivity by a factor of 1.2 – 1.5 relative to the double-pass type of a spray chamber. This has made the cyclonic type the most common spray chamber in use now for routine conventional solution analysis. Most conventional combinations of concentric nebulizer and spray chamber achieve an efficiency of 2 – 5% analyte transfer to the ICP [26]. These systems typically operate around 1 mL/min solution uptake and are compatible with a variety of nebulizers and most of them are based on a high velocity gas jet tearing the sample solution into droplets.

So called “microflow” (low flow) nebulizers on the other hand can operate with uptake rates in the range of around 0.1 to 0.01 mL/min and achieve higher transport efficiency but suffer from sample clogging in the fine capillary, when operated with solutions of high salt content. A way to improve the sampling efficiency to up to 30 % and sensitivity by a factor of 10 is to use an ultrasonic nebulizer, where fine droplets (typically < 5 µm) are generated on a surface, which oscillates at a frequency of between 200 kHz and 10 MHz [27]. The main disadvantage of this type of nebulizer is a significantly higher cost and high solvent load to the ICP, which requires a further desolvation step. It is further prone to high memory effects, and slow wash-out, increasing the total analysis times.

A laser ablation is widely used to introduce solid samples into the ICP MS. The material absorbed the laser energy, heats rapidly and evaporates or sublimates the sample in the ablation chamber, which is flushed with a suitable carrier gas [28, 29]. The main advantage of laser ablation sampling is the ability to carry out spatially resolved analysis at high resolution, reduce the solvent load in the ICP and more rapid sample analysis capabilities without needing to digest solids before analysis.

### **1.3. Inductively Coupled Plasma as Ion Source**

The ICP as emission or ion source used in spectrometry consists of a plasma torch usually made from three concentric quartz tubes of and a load coil, based on the initial design of Wendt and Fassel *et al.* for ICPOES [30], and is known as the Fassel torch (Figure 1.1).

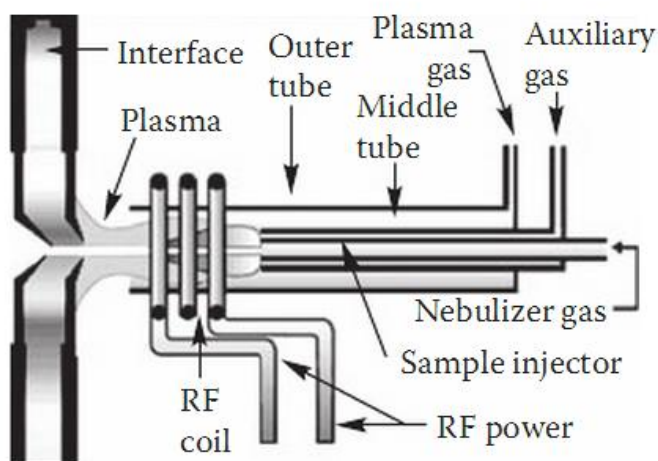


Figure 1.1. Schematic view of a plasma torch and radio-frequency (RF) coil, positioned near the inductively coupled plasma mass spectrometer vacuum interface. [26]

The plasma is sustained within the load coil region by applying a radiofrequency electromagnetic field. As power is supplied to the load coil from the RF-generator, oscillating electric and magnetic fields are established in the torch. When a spark is applied to the gas flowing through the torch, a fraction of the argon atoms can get ionized. The ions and electrons are accelerated in the magnetic field and collide with other argon atoms and successively can ionize more argon atoms and form a permanent discharge or plasma by the continuous chain-reaction. The electrical spark is discontinued and the plasma is sustained by the RF energy transfer through the inductively coupling process. The plasma is characterized by different temperature zones as a function of the axial and longitudinal location. The hottest part of the plasma at its core can reach temperatures of up to 10 000° K [23, 26].

The sample is introduced into the system as an aerosol through the central tube with carrier gas argon flow born with the nebulizer. As the sample aerosol travels through the plasma, droplets are dried and evaporate into a gas, which is further atomized and ionized. Based on the optical emission characteristics, the plasma is divided into three zones: the initial radiation zone (IRZ), normal analytical zone (NAZ), and the plasma tail [23]. The IRZ contains mostly neutral argon atoms and analytical species, while inside the NAZ atomic analyte ions are formed, which can ultimately recombine and/or react forming neutral atoms and molecules in the plasma tail.

The axial position of the zones depends on the carrier gas flow rate, the other two gas flows (plasma or cool gas and intermediate or auxiliary gas), RF-power, solvent loading and the nature of the analyte [23]. At a higher gas flow rate the plasma temperature decreases and the IRZ shifts downstream toward the sampler. The same effect occurs with the decreasing the RF power. On the other hand, the addition of molecular gases like water vapor or N<sub>2</sub> can shift the IRZ upstream due to enhanced energy transfer between the plasma core and the central channel carrying the analyte [31]. The sampling depth (the distance from the end of the load coil to the sampler tip) affects the



sampling of the analyte ions from the plasma. Thus increasing the sampling depth within some range, effectively samples ions from the plasma at an apparently higher temperature, due to their longer residence time.

#### **1.4. The ICPMS Vacuum Interface**

The purpose of the vacuum interface is to transfer ions as efficiently as possible from the atmospheric plasma to a low pressure chamber holding the mass spectrometer. Within first three years after the implementation of the ICPMS the original stagnant layer type sampling interface with a one-cone structure [21] has been replaced by the supersonic sample-skimmer interface with corresponding improvement of performance in ion sampling [32]. A typical current ICP MS interface is comparable to a Campargue type supersonic beam source [33] and consists of the sampler and skimmer cones with a system of ion lenses installed downstream of the skimmer. This configuration allows the plasma expansion through the sampler cone into a region of moderate pressure (about 500 Pa), evacuated by a mechanical rotary vane pump.

Downstream the sampler cone a skimmer cone is mounted, with the tip located in the zone of silence of the expanding supersonic jet, to extract the central part of the plasma. The region downstream the skimmer is evacuated by additional pumps, with turbomolecular pumps being most commonly used today. The pressure in this region is lowered to a range of around  $10^{-2}$  Pa. Ions from the center of the plasma jet exiting the sampler orifice pass the skimmer (approximately 1% [34] to > 3% [35]) and reach the ion optics that further focus the ions towards the MS analyzer, usually comprised of quadrupole mass filter, sector field double focusing mass spectrometers or time of flight instruments.

##### **1.4.1. The Sampling Process**

The sampling process was described in detail by Douglas and French in 1988 [34] based on gas dynamics. The atmospheric plasma expands adiabatically through the sampler cone with an aperture diameter  $D_0$  (Figure 1.2) into a region of finite pressure ( $P_1$ ) and forms a free jet. During the expansion the gas density and gas kinetic temperature initially decrease monotonically. The decrease of temperature corresponds to a narrowing of the width of the velocity distribution as the random thermal motion is converted into directed flow with a relatively uniform velocity. The estimated temperature in the zone of silence was calculated to be about 150 K.

At some point the expansion reaches sub-sonic velocities and collisions with the background gas form a surrounding barrel shock and a terminal Mach disc, enclosing the zone of silence (Figure 1.2). At the shock border the gas reheats to a temperature close the plasma source ( $T_0$ ). Several processes can take place within the shock structure. The expanding jet interacts with the background

gas that can cause a scattering and ion recombination or reactions with the gas. At the Mach disc or downstream from it an extensive scattering of sampled particles is observed.

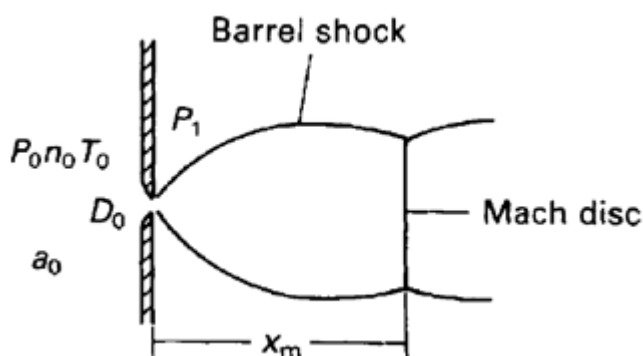


Figure 1.2. Sketch of the supersonic expansion of the plasma into the region of finite pressure. [34].

Douglas and French [34] have shown that in the flow through the sampler, the density and gas kinetic temperature of the plasma drop so rapidly that the degree of ionization can be considered as “frozen” at the degree of ionization of the source and little ion-molecule chemistry should occur. They calculated the Debye length in the plasma to be at the order of  $2 \cdot 10^{-4}$  mm, which would indicate that plasma flows through a sampler cone aperture with  $> 1$  mm diameter with only little charge separation. Measurements of the actual plasma potential within the vacuum interface however indicated that charge separation might still occur as a result of penetration of the plasma potential through the orifice into the jet [36, 37]. This idea was disproved later by Houk, *et al.*, who investigated the ion spread behind the skimmer and found it to be not ideal but at least narrower than it would be in case of significant space-charge effects between the sampler and the skimmer [38]. The current common theory assumes a quasi-neutral plasma beam behind the sampler, where the charge densities from electrons and ions are balanced [23]. The positive offset of the plasma was explained as a consequence of the plasma RF converted into an apparent positive DC offset due to rectification of the RF-induced currents at the sampler orifice. Later, Houk *et al.* [39] found, that the relative abundance of  $M^+$  ions in the mass spectrum closely reflects the corresponding abundance in the ICP just outside the sampler. This confirms the suggestion by Douglas and French that the plasma is sampled as a bulk and no significant changes in its composition occurs immediately behind the sampler orifice.

At the cold sampler walls a thin boundary layer is formed near the edge of the orifice [23, 34, 40], which is characterized by higher gas density and lower temperature and velocities. Downstream on the central axis of the flow, it may be considered as an ideal fluid, whose behavior can be described by fluid dynamics [34, 40]. The bulk gas flows through the sampler without passing through this cool boundary layer and sheath. Therefore the plasma immediately behind the sampler has nearly the same composition as inside the ICP, though the boundary layer results in a reduction of the total flow

through the orifice [40]. Two populations of ions were found in the expanding plasma in the 1<sup>st</sup> interface stage: cold and fast atoms, whose population decreases downstream, while the second type of slow and hot ions appears at approximately 10 mm downstream the sampler orifice [41]. In that study the Mach disc was observed 17 mm downstream from the sampler orifice and most ions were reheated and decelerated before that. The calculated Mach disc position corresponds to the point where intrusion of background gas into the expansion is complete and less than 10% of the gas has the temperature and velocity characteristics of a supersonic expansion. The authors conclude that this shock structure is not a good definition of an edge of the zone of silence because the zone of silence is assumed to be the region where there is no influence from the background gas. Because of the diffuse nature of the shock structure, care must be taken to avoid placing the skimmer in a position where there is already a significant population of hot, slow atoms.

The theory of the sampling process was developed mostly based on the data of neutral argon atoms. The difference of the acceleration between neutral argon species and calcium ions has been measured by Farnsworth, *et al.* [42]. That study has shown that initially similar velocities of argon atoms and calcium ions begin to differ with distance but remain practically constant between 1 mm and 10 mm downstream of the sampler orifice. Since the mass of argon atoms and calcium ions are nearly the same, the difference of velocity is explained by the ambipolar electric field due to the electron density and temperature gradients which result in an additional acceleration of ions relative to the neutral species. The ambipolar diffusion has longitudinal and radial components. The radial ambipolar diffusion rate will induce a mass bias, which causes a proportionally higher transmission of heavier ions.

#### **1.4.2. The Skimming Process**

A skimmer is used to limit penetration of the background gas into the ion optics downstream. This additional differential pumping aperture also allows the use of a larger sampler orifice, resulting in a significantly improved performance in terms of sensitivity relative to the initial configuration and reduces the susceptibility to clogging of the sampler cone by salt deposition. Typically the skimmer tip is located inside the assumed zone of silence of the supersonic jet. In this configuration the Mach disk would appear downstream the skimmer orifice, and only ions from the core of the expanded beam are extracted. The optimum skimming position as estimated by Douglas and French in 1988 [34] to be located at approx. 2/3 of distance between the sampler aperture and the onset of the Mach disc. This corresponds approximately to the position where highest transmission of the neutral beam can be achieved. This position of the skimmer also improves skimmer stability because the skimmer tip is located inside the “cold” region of the expanding jet. The shock structure where species in the beam are reheated by collisions with background gas will touch the skimmer near to its base, closer to the cooling circuit. In case when the Mach disc would be located near the skimmer tip, the hot gas would quickly degrade the skimmer surface due to the low heat conductivity of the thin skimmer walls near the orifice [23].

The geometry of the skimmer and its diameter also affect the ion transmission significantly. For example, the shape of the skimmer tip affects the shock structure formed inside the cone. It has been found, that a cylindrical skimmer tip can lead to more pronounced shock structures than conical shaped ones [43]. The skimmer geometry and surface may also affect polyatomic ion formation within the boundary layer formed at the cooler skimmer wall. These disturbances at the skimmer tip are considered the main processes responsible for the deviation of the ion behavior from the ideal case, described by Douglas [34]. As a result the ions motion downstream the skimmer orifice may also be described as a second expansion, originating inside the skimmer tip, leading to lower densities of all the species along the centerline than expected by the calculation of Douglas [34].

Thus, a steeper skimmer opening would reduce disturbance of the expanding plasma at the skimmer tip, but cause more pronounced interaction of the expansion with the inner surface. On the other hand, a flatter skimmer would allow locating the ion optics as close as possible to the skimmer tip allowing better control of the ion motion, but the shock structure at the skimmer orifice will be more pronounced.

#### 1.4.3. Space-charge Effects

During plasma expansion, space-charge effects occur due to the high ion density of the argon ions in the plasma and the mass-dependent ion kinetic energies. After the quasi-neutral plasma passes the skimmer orifice, the density of the beam drops rapidly. The electron temperature gets lower but stays in a range of 4000 – 8000 K [44]. Also the Debye length increases significantly and reaches approximately 0.5 mm as the electron density is reduced to about  $10^8 \text{ cm}^{-3}$ . This Debye length is already significant relative to the beam dimension and the dimensions of the ion optics, so electrons preferentially move out of the beam and are lost on the skimmer walls. The beam accumulates a net positive charge, causing repulsion between positively charged ions. Since the ion velocities are determined by the expanding carrier gas, and the extent of deflection depends on the respective ion kinetic energies, which makes space charge effects mass dependent. Light ions, carrying relatively low kinetic energy will be deflected more extensively than heavier ions [23].

It can be assumed that space-charge effects can lead to:

- a) Mass-dependent radial expansion of the ion trajectories.
- b) Limitation of the maximum current transmitted through a downstream aperture of finite size (the total current is not affected by space charge).
- c) Matrix effects, when components of the samples analyzed contribute significantly to the ion current but their relative contributions change.

Olivares and Houk were the first to suggest an important influence of space-charge effect on the performance of an ICPMS [32]. They estimated the ion current behind the skimmer without taking into account ion loss by collisions with walls and recombination. According to their calculations a 250

$\mu\text{A}$  ion current can be expected at the entrance of a 1.25 cm diameter lens 2.5 cm downstream from the skimmer tip. This current significantly exceeds the maximum ion current of  $1 \mu\text{A}$  that may be transferred through such a lens with negligible space charge effects.

Numerical simulation of ion trajectories in the presence of space-charge effects was carried out by Tanner [45]. Based on the theory of Douglas and French he assumed quasi-neutral plasma in front of the skimmer. He concluded that the major influence on electron diffusion is caused by the increase of the Debye length along the axis of the beam expansion due to the reduction of the ion density and thus a penetration of the electrostatic field from the first ion lens. The rate at which the plasma charges separate is a function of the plasma density (which is related to the gas density in the expanding beam) and electrostatic field gradients. Tanner assumed an exponential relationship between the net positive ion density and the axial distance downstream of the skimmer.

The influence of the space charge effect with Tanner's calculation is presented in the following figures:

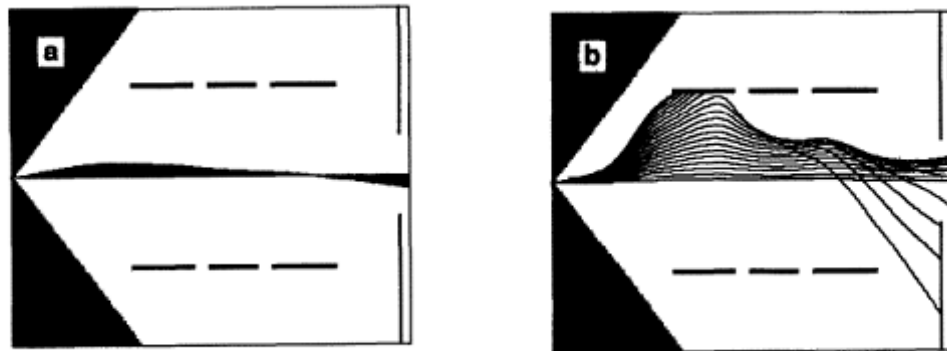


Figure 1.3. Calculated ion trajectories for  $^{40}\text{Ar}^+$  in the absence of the space-charge effect (a) and with the space-charge appropriate for a  $1.25\mu\text{A}$  total incident ion beam (b). [45].

Tanner considered the space-charge effect to be responsible for deviations in measured isotope ratios as a result of the different kinetic energies of light and heavy isotopes. This deviation is increasingly pronounced for elements of lower atomic mass. As the relative transmission of ions with higher kinetic energy increases, there is an opportunity to alleviate their influence by acceleration of the ions as soon as possible downstream of the skimmer aperture, while maintaining a narrow ion energy distribution. The space-charge effect can affect the optimal skimming distance according to Chambers, *et al.* [37], who investigated the optimal skimming position at different pressures and plasma operating conditions. They concluded that it depends not solely on the fluid dynamics of the beam expansion but also on electrostatic effects. According to their studies, the highest ion current through the ion optics can be established by lowering the ion flow through the skimmer orifice, which minimizes space charge effects in the low pressure region. Later, Chen and Houk made a basic

estimation of the space-charge effects in ICPMS [38]. They used a perveance  $P$  as a characteristic of an ion extraction system, where  $P$  is:

$$P = I / V^{3/2},$$

with

$I$  – the total ion current, A

$V$  – accelerating potential, V.

$P$  depends only on geometry of the extractor ( $D/L$ ) and the mass of the ion ( $m_{ion}$ ). For a beam of singly charged particles the space charge effect is negligible when

$$P < 10^{-8} (m_{ion}/m_e)^{-1/2}.$$

The maximum perveance for Ar ions without significant space charge effect ( $P_{max}$ ) is thus  $3.7 \cdot 10^{-11}$ . Downstream the skimmer where the ion current may reach a value of  $6 \mu\text{A}$  and at potential  $-10 \text{ V}$  the perveance is  $1.9 \cdot 10^{-7}$ , exceeding  $P_{max}$  by a factor of more than 5000.

Calculation of the maximum ion current that can be transmitted through an ion optics system with a beam diameter of 10 mm and 27 mm length and a mean lens potential of  $-50 \text{ V}$  result in a value of  $4.6 \mu\text{A}$ , which was in a good agreement with their measured value.

#### 1.4.4. Matrix effects

There are two regions in an ICPMS where chemical matrix effects can occur: in the ICP itself and during transport through the interface and ion optics. In the ICP, the number of analyte ions can be suppressed *e.g.* by high concentrations of easily ionized elements [46], while signal enhancement can also be observed depending on the analyte and the composition of the sample [47, 48], for example the increase of the sensitivity for As and Se in presence of carbon-containing species in an aqueous solution [49]. Most often suppression of analyte ion signal is observed, but some experiments have shown an increase of the analyte signal in presence of increasing matrix content [47].

The effects of a given matrix on the measured ion signal intensities is actually rather complex. One contribution is the change of the plasma temperature and electron density. When an aerosol of different matrix composition is introduced into the plasma, it can change the gas temperature and, thus, shift the optimum sampling distance. An ICPMS is usually optimized to reach maximum intensity, but the position of maximum ion density can vary slightly for different elements [50]. Generally, the matrix effect is dependent on the ICP operating conditions and can have positive or negative effect on the signal intensity: the change of the matrix composition can shift the conditions required to yield maximum signal intensities for the elements towards higher or lower temperatures.

As a result, signal increase or decrease might be observed. The plasma temperature is also affected by the matrix composition, as well as the aerosol particle size distributions entering the ICP. It may vary depending on the surface tension and to a lesser degree a viscosity of the solution nebulized, both characteristics being also dependent on the composition of the sample. These effects thus also change the transfer rate of the analyte into the ICP, the degree of ionization and the lateral diffusion of analyte ions within the ICP. Higher RF power and lower the carrier gas flow rates result in an upstream shift of the onset of vaporization due to the higher plasma temperature, and thus, lead to a greater radial diffusion of the ions [51].

Mass dependent matrix effects inside the ion optics region are rather a consequence of the space-charge effect. Heavier ions remain closer to the beam axis while lighter ones are deflected to a greater extent. Therefore in the presence of high concentrations of heavy elements in the sample, lighter analyte ions will be lost preferentially, compared to the situation, where the ion beam is dominated by Ar ions. Even if the total beam current through the skimmer is not increased appreciably by ions of the matrix element, the space charge model predicts that the spatial distribution of ions in the beam is altered by the presence of matrix ions, with a corresponding change (i.e. usually a decrease) in the signal at the detector [23].

The first connection between the space-charge and matrix effects downstream the skimmer orifice was made by Gillson, *et al.* in 1988 [52]. They studied the effect of different matrices (on the sensitivity of different ions ( $\text{Li}^+$ ,  $\text{Rb}^+$ ,  $\text{Th}^+$ ) at equimolar concentration. Their results show that heavy matrix elements lead to greater suppression of the analyte signal than light ones. For a given matrix, the suppression of low  $m/Q$  isotopes was greater than at high  $m/Q$ . Therefore the authors concluded that mass discrimination is an inherent part of a sampling process and heavy ions are transmitted more efficiently. They calculated an ion current of Ar and U ions before the skimmer and measured the actual one after the skimmer. The skimmer reduced the ion current from 1500  $\mu\text{A}$  before the skimmer to 6  $\mu\text{A}$  at its base when a blank solution was aspirated. With the addition of 0.04 M U, however, the increase of the total ion current after the sampler was 14  $\mu\text{A}$ , in good agreement to the ion current that would correspond to the added uranium ions. Later these conclusions were supported by numerous computer simulations [45], which have shown a greater deflection of the light elements in presence of heavy matrix element.

In order to decrease the matrix effect, for routine analysis fairly dilute solutions with solute levels below 0.1 % [23] are recommended, which also prevent deposition of material and potential clogging of sampler or skimmer cones. Nevertheless, higher concentration of some matrices can be tolerated. Internal standardization, isotope dilution, standard addition, and matrix matching are used to compensate, eliminate, or correct for such matrix effects.

## 1.5. Improving Ion Transmission of the conventional Vacuum Interface

Several attempts have been made to reduce space-charge effects in order to increase ion transmission or to minimize the mass dependency. A three-aperture interface was suggested by Ross and Hieftje in 1991 [53] and Tanner, *et al.* [54, 55] who additionally extracted the ions at an offset from the plasma axis. These approaches were based on the idea of reducing space-charge effects by lowering the total ion current. As a result, the fraction of ions that was transmitted further into the mass spectrometer would become less dependent on the composition of the ion beam. A limitation here was, however, that reducing the total ion current also affects the attainable analyte sensitivity. Praphairksit and Houk suggested a supplemental electron source behind the skimmer [56–58] in order to reduce charge separation and the corresponding electrostatic repulsion.

A different approach was used by Moussalami and Douglas [59] who employed quasi instantaneous ion acceleration to several thousand eV from the shock wave that occurs when the expanding plasma reached the differential pumping aperture positioned after the sampler cone instead of a skimmer in their set up. Sensitivities of up to 104 cps/ng/L have been achieved with this approach. It is however limited by the requirement for very high pumping capacity (working pressure is 32 Pa pressure instead of the more commonly used 1<sup>st</sup> stage pressure of ~ 500 Pa) and by the fact that the high kinetic energies of the resulting ion beam were not compatible with quadrupole mass analyzers. Sector field instruments could operate with these high energy ion beams, but such configurations have not been explored.

There were also other attempts to prevent charge separation at an early state of the expansion by modifying the ion optics [60, 61]. An offset ion lens system resulted in higher analyte sensitivity, but enhanced matrix effects when the ion optics were adjusted to positive potentials immediately downstream of the skimmer. When grounded however, the sensitivity was slightly reduced and matrix effects were also significantly reduced. Another more recent approach to improve ion transmission was realized with an ion optics arrangement using an “ion mirror” [62]. In this study the ion beam was deflected by 90° using a circular arrangement of ion optics elements. The expansion of the plasma jet occurred in an unrestricted region and neutral components of the beam were efficiently removed by the vacuum system since they were not reflected by the mirror. Additionally reactive or collision gases could be mixed into the expanding plasma via specially designed sampler and skimmer arrangements.

Thermalization of the expanding ion beam reduces the mass dependency of ion kinetic energies and should thus mitigate space charge influence on mass bias [63]. This approach has been initially utilized for sector field mass spectrometry [64] in a single focusing instrument, and subsequently transferred into quadrupole mass spectrometers as well by introducing a gas-filled multipole stage within the ion optics arrangement [65, 66]. In this arrangement, ion transmission can be enhanced by collisions with the background gas due to the reduced ion kinetic energies and their distribution. In the presence of reactive gas species, a manipulation of the beam composition can also be achieved by, for example attenuating the density of specific spectral interferences through charge or atom transfer reactions [66, 67].



In a broader sense, ion transmission in ICPMS instruments is mostly limited by the broad energy distribution after the supersonic expansion, its radial spread and the high and variable ion current occurring in the ion optics. They affect the fraction of analyte ions that can be efficiently transferred through the differential pumping stages towards the mass analyzer.

## 1.6. The Ion Funnel

In order to reduce ion loss at the differential pumping apertures of an electrospray ionization mass spectrometer (ESIMS), Shaffer, *et al.* introduced an electrodynamic “ion funnel” [68–70], which essentially represents a modified, stacked ring electrode trap [71] with successively reduced inner diameters. Radio frequency potentials of opposite polarity are applied to adjacent electrode rings, which result in a steep pseudo-potential near the electrode surfaces while the axis of the funnel is characterized by a fairly low radial gradient [72]. The effective potential inside the funnel is a function of the RF amplitude and frequency, the distance, thickness and diameter of the electrode rings [73] (Figure 1.4):

$$V^* \left( r, z \right) = \frac{z_i e \left| E_{rf}(r, z) \right|^2}{4m\omega^2}$$

where

$V^*$  - effective potential, Volts  
 $E_{rf}$  - amplitude of the local radio-frequency field  
 $z_i$  - ion charge state  
 $e$  - elementary charge  
 $m$  - ion mass (SI units)  
 $\omega$  - rf frequency  $f$  in angular units,  $\omega = 2\pi f$   
 $r$  - radial position  
 $z$  - axial position

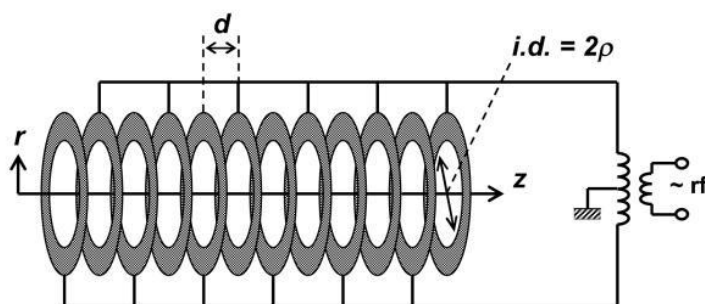


Figure 1.4. Sketch of a stacked ring rf ion guide [74].

The maximum value of effective potential  $V_{\max}$  is achieved at the inner walls of the funnel between the electrodes ( $r = \rho, z = d(i+1/2)$ ):

$$V_{\max} = \frac{z_i e V_{rf}^2}{4m\omega^2 \delta^2}$$

with:

$V_{rf}$  - one half of the peak-to-peak RF amplitude

$\delta = d/\pi$

The well depth along the axis or so-called “trapping potential” is related to the maximum value of effective potential:

$$V_{trap} = \frac{V_{\max}}{I_0^2(\rho / \delta)}$$

where  $I_0$  is the zero order modified Bessel function.

The RF field creates an effective electric field  $E_{eff}$ , which repels charged particles towards the funnel axis transversely to the funnel walls. An additional DC gradient  $E_{DC}$  applied along the funnel is widely used to drag ions towards the funnel outlet (Figure 1.5).

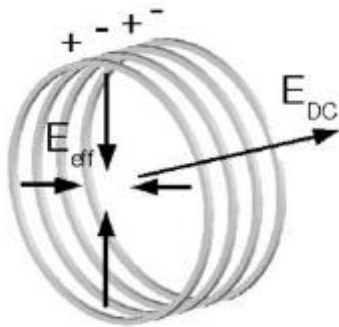


Figure 1.5. The schematic view of the electric fields in the ion funnel:  $E_{eff}$  generated by the RF field effectively confines ions by repelling them towards the funnel axis and  $E_{DC}$  formed by DC gradient drives ions towards the funnel exit [75].

The effective focusing of ions by the applied RF field is presented in figure 1.6. Ions move towards the centerline of the funnel into the weak field region and are driven by the superimposed DC field towards the ion exit. The ions moving axially are almost not affected by the RF field, while ions in the vicinity of electrodes have the oscillatory trajectories due to the form of the effective potential field. The confinement is further assisted by operating the ion funnel in a region of elevated pressure of an inert gas. The remaining kinetic energy is then determined by the gas pressure but also the acceleration by the DC gradient and eventually excitation in the RF-field of the funnel.

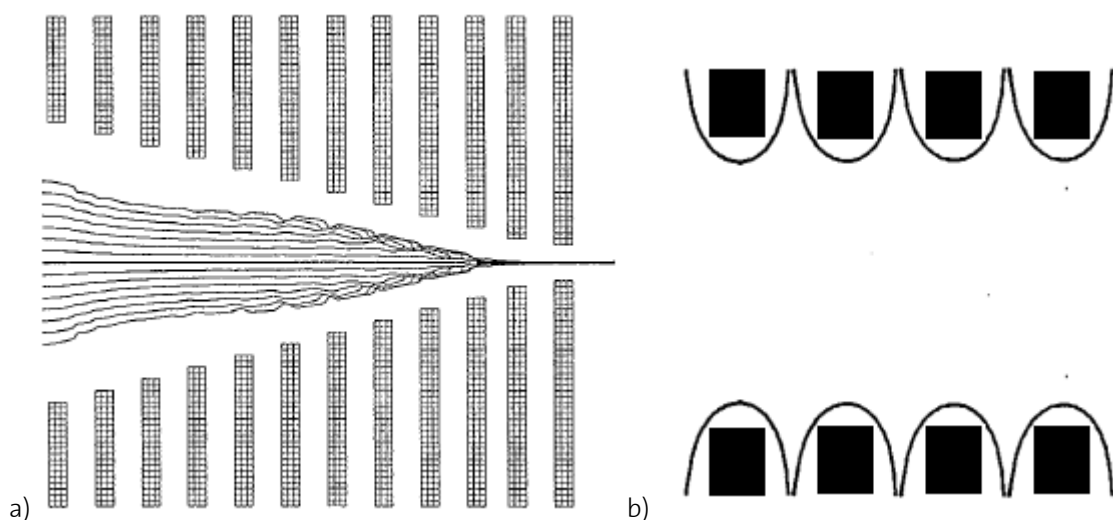


Figure 1.6. a) Simulation of the ion paths for  $m/Q$  18 at 1 MHz and 133 Pa damping pressure with an initial ion energy of 10 eV at RF amplitude of 100 Volts [68].

b) Equipotential lines at the ring electrodes and the actual shape of the electrodes marked in black [71].

In contrast to linear RF-only multipoles, which are also able to be operated in the pressure regimes of about 1 Pa, the ion funnel provides a comparably simple way to effectively reduce the diameter of an ion beam by the geometric dimensions of its apertures. The geometry of the ion funnel allows to combine the large acceptance area and effective focusing to a narrow conductance-limiting aperture [68]. As a result, such a funnel can be operated over a wide pressure range (10 – 4000 Pa) [73] allowing for efficient damping of the ion kinetic energies.

This has been shown to achieve an efficient transfer of ions through the terminal aperture before the mass analyzer [73]. Thus ion transmission in an ion funnel should not be as sensitive to the energy spread as in an electrostatic ion lens system. The loss of axial energy by collisions on the other hand may cause the ions to be stopped inside the funnel where they ultimately can be lost due to scattering. Therefore, an additional axial DC potential may be applied to accelerate the ions towards the funnel exit [68–70,72–74].

Such an ion funnel was successfully implemented as a differential pumping interface for an electrospray ion source (ESI) [68–70,72–74,76,77], resulting in a 10-fold gain in ion transmission when compared to an unmodified instrument. Further modifications, such as increasing the number of funnel electrodes, decreasing electrode thickness and spacing achieved the lowest detection limit reported. For the  $m/Q$  range between 118 and 2121 the transmission achieved was up to 100%, depending on the RF field applied [73]. Other applications include the use in ion mobility spectrometry [78,79] or novel electrospray techniques as secondary electrospray ionization (SESI) [80] and extractive

electrospray ionization (ESI) [81], where the installation of an ion funnel resulted in up to 3 orders of magnitude signal enhancement.

These promising results led to the studies reported here, where this type of interface was investigated for use with ICPMS instrumentation. In contrast to an ESI ion source however, the plasma source of an ICPMS instrument creates a significantly higher ion flux (~ mA at the sampler orifice [23] vs. fA range for ESI) and operates at a much higher temperature, which obviously affects the operating conditions. Furthermore the  $m/Q$  range required for elemental analysis is much lower than those typically measured by ESIMS where transmissions of ions with  $m/Q < 118$  could not be significantly improved.

## 2. Characteristics of an ion funnel coupled to the vacuum interface of an ICP MS

### 2.1. Experimental

The first part of these studies focused on the use of an ion funnel as ion guide in an otherwise conventional ELAN 6000 ICPMS instrument (PE/Sciex, Ontario, Canada). Examination of the ion funnel's influence on the signal intensity was carried out and compared to the original configuration. Though an ion funnel placed in the ELAN 6000 interface operates in a pressure regime, which is significantly lower than considered optimum [74], it can serve as an initial estimation of the ion transmission attainable when using an ion funnel.

#### 2.1.1. Instrumentation

All experiments were carried out using an ion funnel, which was developed and built in the workshop of ETH and installed in a conventional quadrupole ICPMS (ELAN 6000, PE/Sciex, Ontario, Ca) instrument after removing the ion lens assembly (Figure 2.1).

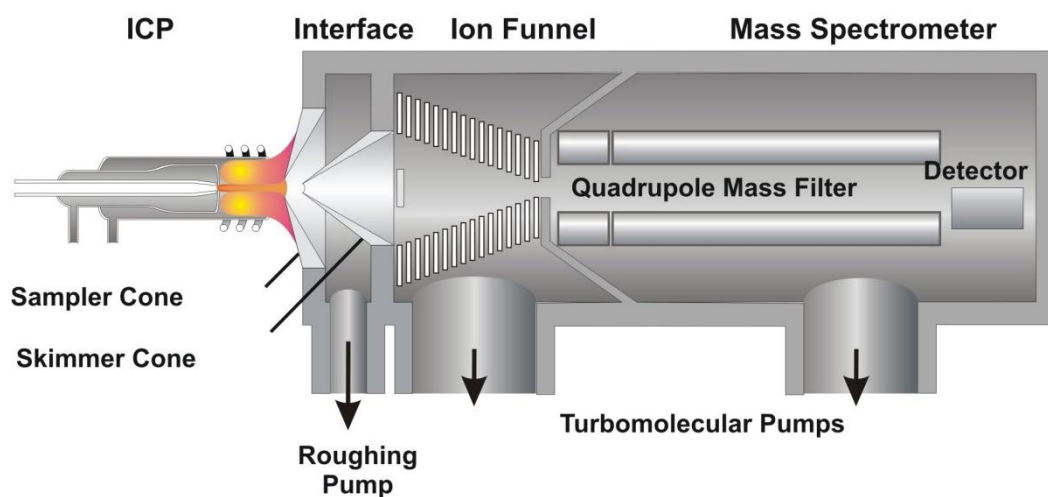
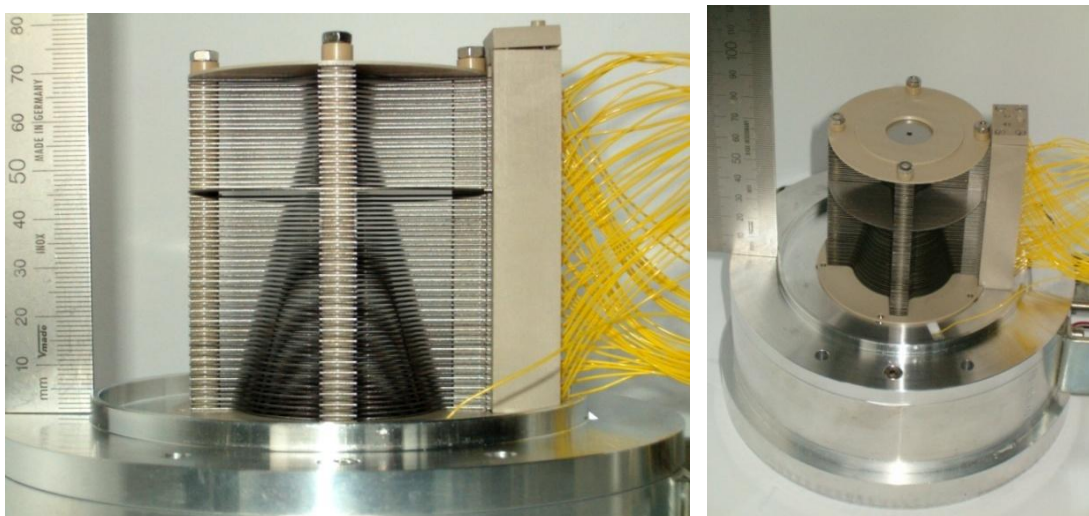


Figure 2.1. Sketch of an ELAN 6000 with standard ion lens replaced by an ion funnel.

#### 2.1.2. Ion Funnel

The ion funnel (Figure 2.2) consisted of 54 ring electrodes with 0.5 mm thickness and 0.5 mm spacing in between the electrodes. The electrodes' apertures were of circular shape with continually decreasing inner diameters from 35mm at the funnel entrance to 2mm at the exit. The electrodes were mounted on 4 PEEK rods using metal strips and isolated using 0.5mm PEEK rings. One of the four strips additionally served as an electrical connection to the power supply. The third funnel electrode was additionally equipped with a photon stop of 3mm diameter, positioned on the axis of the ion funnel, similar to the original ion optical system of the ELAN 6000. All electrodes were machined from stainless steel sheets by laser cutting. The funnel exit aperture was fixed on a PEEK™ plate and served as the differential pumping aperture before the quadrupole mass analyzer chamber. The PEEK™ plate has a thicker central part in order to precisely fit into the region of the original 2 mm pumping aperture of the ELAN 6000.



*Figure 2.2. Photograph of the ion funnel used in these studies. The ion funnel was installed in the second differential pump stage. Each funnel electrode was independently connected to the power supply with the yellow wires.*

All potentials were supplied to the funnel electrodes from an in-house built symmetrical RF amplifier coupled to a tunable, resonant LC circuit, which delivered two mirrored RF channels of up to 250V amplitude peak to peak. The feed RF voltage was provided by an adjustable commercial function generator (SFG-2110, GW Instek, Taiwan). The amplifier was combined in a case together with a power supply for the DC-gradient along the funnel axis. The DC potential was fed through a serial resistor chain from the first to the last funnel plate with 0.51M $\Omega$  metal film resistors. Each funnel electrode was additionally connected through a separate 0.01 $\mu$ F metal film capacitor (WIMA, Germany) to the 0° phase (even numbers) or 180° phase (odd numbers) RF channels. Electrical contact to the funnel electrodes was achieved through an in-house built mechanical connector (PEEK, stainless steel) without soldering because of the thermal load of the soldering potentially could have distorted the funnel electrode and their positions. The RF frequency was variable in the range of 600–2000 kHz while the LC circuit was optimized for resonance by fine tuning the tapping position on the load.

The RF frequency and amplitude were monitored using a digital oscilloscope (DPO 4054, Tektronix, USA) with  $1\text{M}\Omega$  termination directly at the funnel feed connections. Unless specified in the text, the default RF frequency was 600 kHz. In contrast to the standard lens configuration of the ELAN 6000, where a positive potential is applied to the lens at the skimmer base, the entrance electrode of the ion funnel was always set to 0V DC and the potential slope along the funnel axis adjusted by varying the voltage applied to the funnel exit electrode. In order to maintain acceleration towards the mass analyzer, the quadrupole and pre-filter bias voltages were biased relative to the last ion funnel plate by an additional electric circuit. An additional voltage was controlled in the instrument control software. The pressure inside the ion funnel was not measured directly. It should however be expected that it was significantly higher than in the ion optics region of the standard Elan 6000. Tolmachev, *et al.* estimated the pressure inside an early version of their ion funnel to be about three times higher than in the surrounding chamber [74]. Compared to their configuration, however, the funnel used in this study has a smaller effective pump area (27 mm vs. 45mm total length of the between electrode spacing), and thus the pressure inside the in funnel can be expected to be about 5 times higher than in the surrounding chamber.

### 2.1.3. Gas Addition

In order to investigate the influence of an additional gas supplied to the funnel to modify the background pressure and chemical environment, the terminal part of the funnel could be enclosed with a cylindrical cover reaching from the 27<sup>th</sup> electrode, to the terminal PEEK plate. Gas was added to the enclosed region through two 6 mm i. d. gas inlets at the front part, and the gas flow was adjusted using a needle valve. The gas flow into this enclosed region was set to the maximum rate that allowed operation of the quadrupole mass analyzer. Typical pressures in the MS chamber, as recorded by the Bayert-Alpert gauge, were  $8.9 \cdot 10^{-4}$  Pa without gas addition,  $1 \cdot 10^{-2}$  Pa with  $\text{H}_2$ , and  $7.5 \cdot 10^{-3}$  Pa with  $\text{N}_2$ , respectively.

### 2.1.4. ICPMS Operation

Other than the modifications required to implement the ion funnel, the ICPMS was operated using typical conditions, using a quartz concentric nebulizer with a cyclonic spray chamber. A calibration solution containing 10  $\mu\text{g/L}$  of B, Mg, Co, Rh, Ce, Pb, and U in 1%  $\text{HNO}_3$  was introduced via a peristaltic pump at a rate of 0.8 mL/min, yielding an aerosol load of 29  $\mu\text{L/min}$ . Typical operating conditions are listed in Table 2.1. Data acquisition was carried out by scanning the quadrupole mass spectrometer over selected  $m/Q$  ranges and exporting the data to Excel™ for further evaluation of signal intensities and peak shapes. The mass scans were performed with a step size of 0.05 amu and an integration time of 25 ms per step. In the optimization experiments the integrated ion signal intensities had been evaluated as a summed signal (cps) values for 13 points around the peak maximum. These measurements were carried out on different days and with different configurations,

which required slight adjustments of the ICP operating conditions to achieve highest sensitivity (i.e. x–y torch position, and carrier gas flow rate).

Based on replicate measurements, the absolute intensities were reproducible to approximately 20% between days. Within day reproducibility was significantly better and was usually less than 5%.

*Table 2.1. Instrumental parameters.*

ICP:	
ICP power	1350 Watt
Plasma gas flow	15 L/min
Auxiliary gas flow	1 L/min
Nebulizer gas flow	1 L/min
Sampler:	1.1 mm, platinum, ELAN type
Skimmer:	0.9 mm, nickel, ELAN type
Mass spectrometer:	
AC Rod Offset	-6 V relative to funnel exit
Quadrupole Rod Offset	0 V relative to funnel exit
Scan interval, a.m.u.	5 – 11, 22 – 26, 35 – 37, 54 – 60, 77 – 81, 100 – 105, 139 – 158, 205 – 239

## 2.2. Results and Discussion.

### 2.2.1. DC Gradient Influence

Figure 2.3 shows ion signal intensities as a function of the DC-potential applied to the funnel exit. No RF field was applied in these experiments to study the effect of ion acceleration along the funnel axis alone. Together with the DC gradient, the quadrupole pre-filter (AC rod offset, table 2.1) and analyzer bias (quadrupole rod offset, table 2.1) were adjusted in parallel (see table 2.1).



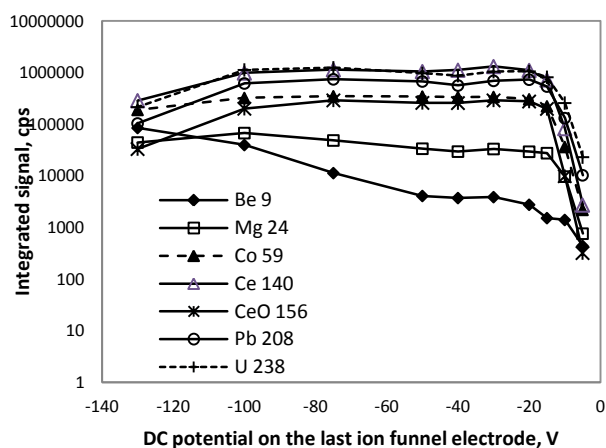


Figure 2.3. Dependence of the ion signal intensities on the DC gradient in the ion funnel with no RF field applied.

When increasingly negative voltage was applied at the funnel exit, an increase in transmission was observed for relatively low potentials. When the potential was less negative than  $-10\text{V}$  the ion signals were very low but showed a fairly steep increase with more negative values. The magnitude of the increase was dependent on  $m/Q$  with a greater increase for low  $m/Q$ . Also the setting yielding the highest ion signals was dependent on  $m/Q$  with lower  $m/Q$  typically showing the highest signal intensities at a more negative potential. The variability of signal intensities was in the range of 10% for potential gradients between  $-25$  and  $-75\text{V}$  at higher  $m/Q$  ( $>59$ ). For settings more negative than  $-100\text{V}$ , the ion signals of all isotopes except  ${}^9\text{Be}^+$  showed a substantial decline.

The DC gradient causes axial acceleration, driving the ions towards the ion funnel exit aperture. This explains the increase of the ion signals with the gradient present relative to field-free situation. The acceleration partly compensates for the scattering losses occurring from collisions with the background gas. The lower intensity for settings below  $-100\text{V}$ , however, indicates that an increasing fraction of the ions were accelerated towards the electrodes directly due to the absence of a confining RF-field. Additionally the mass resolution of the quadrupole mass analyzer was found to degrade with settings below  $-40\text{V}$  (Figure 2.4), indicating that either fringe-fields at the funnel exit affect the ion energy spread or that the ions were entering the quadrupole with too high of a kinetic energy to be sufficiently resolved. This lack of mass resolving power also affects the low  $m/Q$  background intensities that become apparent in the continuous increase of the signals at  $m/Q$  9. A significantly higher abundance of  $\text{CeO}^+$  was observed in all experiments. In the standard configuration of the ELAN 6000 the  $\text{CeO}^+/\text{Ce}^+$  is typically  $<3\%$ , while with the ion funnel installed, it was never less than 10%, which is considered to be a result of the higher pressure inside the ion funnel. Reactive collisions with oxygen and water vapor introduced with the plasma are likely responsible for the increase of the  $\text{CeO}^+$ -abundance with the ion funnel installed.

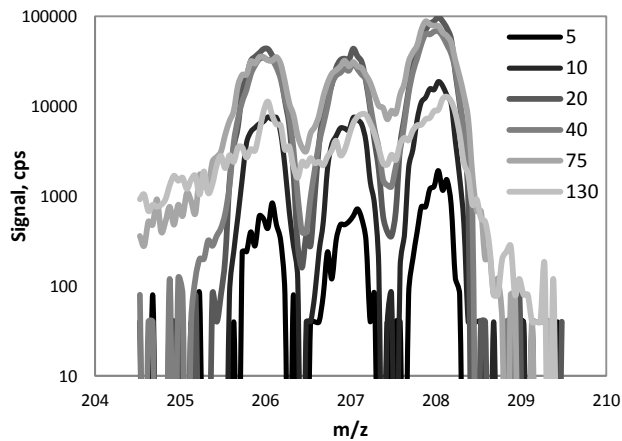


Figure 2.4. Mass spectra of the major Pb isotopes for different DC gradients (no RF field). Data acquired in a single scan.

### 2.2.2. RF Field.

Ion confinement to the funnel axis resulted in an increase of transmission towards the mass spectrometer when the RF field was applied to the funnel electrodes. Figure 2.5 shows this effect for an RF frequency of 600 kHz with increasing amplitude. The potential at the funnel exit was fixed at  $-20$  V in these studies.

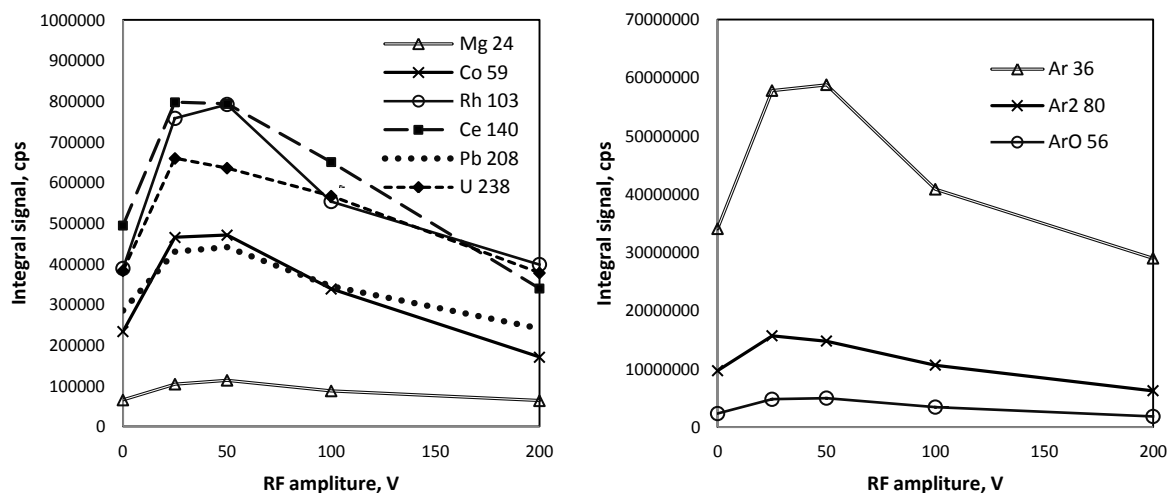


Figure 2.5. Dependence of integrated ion signal intensities on RF amplitude for selected elements with different  $m/Q$ . RF frequency: 600 kHz, funnel exit:  $-20$  V DC.

For a fixed RF frequency, the ion signals initially increase with increasing RF amplitude due to the increasing potential near the electrodes. For an RF frequency of 600 kHz, the optimum amplitude was between 25 and 50  $V_{pp}$  for most  $m/Q$  investigated while higher values lead to a loss in

transmission. The latter effect was most likely a result of an inter-electrode potential well (“trapping potential” [66] which can effectively capture slow ions in a local potential minimum, where they ultimately were discharged at an electrode. The increase in sensitivity with additional RF-field however depended on the  $m/Q$ . High  $m/Q$  such as U or Pb only showed about 50% increase while intermediate  $m/Q$  such as Rh or Ce exhibited an increase of a factor of 2. Low  $m/Q$  isotopes such as Mg, on the other hand, show an enhancement of only 50% for these settings. In accordance with theoretical considerations [71], confinement by the repulsive potential and losses in the potential wells occurs to a different extent at different  $m/Q$  for a given combination of operating conditions. As observed in figure 2.6, low  $m/Q$  show highest transmission at higher frequency than higher  $m/Q$ . The optimum for  $^{24}\text{Mg}^+$  occurs at 1.2 MHz RF and 25 V RF amplitude, while  $^{103}\text{Rh}^+$  intensity maximized around 800 kHz, between 25 V and 50V.  $^{208}\text{Pb}^+$  intensities maximize at frequencies <600 kHz. The RF amplitude on the other hand appears to be less critical and highest ion signals were observed for amplitudes between 25 and 50V<sub>pp</sub>.

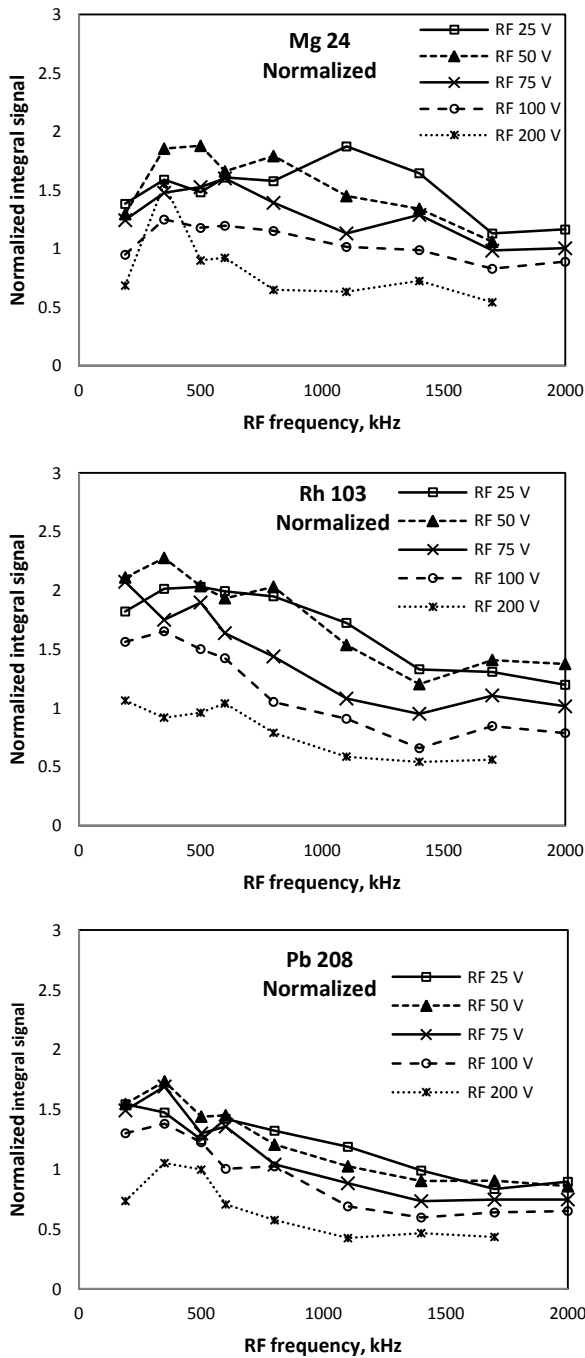


Figure 2.6. Influence of RF frequency on the signal intensities of different  $m/Q$ . Data normalized to the mean signal at 0V RF amplitude. Funnel exit:  $-20V$  DC. Uncertainty of the intensities, based on repeat measurements at 0V RF amplitude, is  $\approx 10\%$ .

As the RF amplitude exceeds a critical value, depending on frequency and  $m/Q$ , the ions are supposed to be increasingly trapped inside the funnel and transmission can decrease to values even lower than in absence of the RF field. Additionally, the attainable mass resolution gets poorer when the RF amplitude exceeds  $50V_{pp}$  (Figure 2.7). This was attributed to a result of fringe-fields between the funnel exit electrode and the RF-only pre-filter of the quadrupole. The same effect was considered

to be responsible for the increase of the  $^{36}\text{Ar}^+$  ion signal intensities (Figure 2.8), with increasing RF frequency as a result of more pronounced tailing of the  $^{40}\text{Ar}^+$  peak to lower  $m/Q$ .

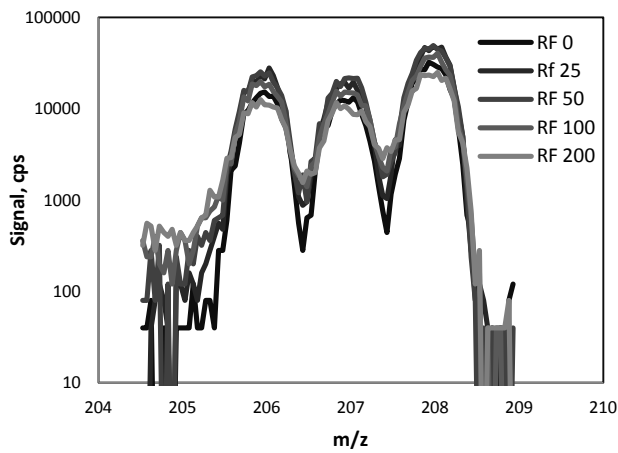


Figure 2.7. Mass spectra for major Pb isotopes at different RF amplitudes. RF frequency 600 kHz, funnel exit: -20 V DC

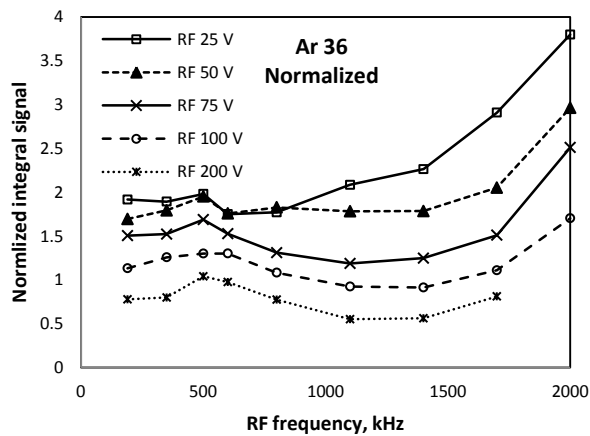


Figure 2.8. Influence of RF frequency on the signal intensities of  $^{36}\text{Ar}^+$ . Data normalized to the mean signal at 0 V RF amplitude. Funnel exit: -20 V DC.

### 2.2.3. Gas Addition

As observed in the previous study, higher gas pressure and reactive collisions can alter the composition of the ion beam. To explore this further, the terminal part of the ion funnel was enclosed and  $\text{N}_2$  or  $\text{H}_2$  was fed to the internal volume as additional gas directly from the supply without further attempts for purification using, for example, a getter. The dependency of ion signals on DC voltage and RF amplitude was investigated, but the optimum conditions were found to be similar to the open configuration. The effect of the different gases is presented in Figure 2.9.

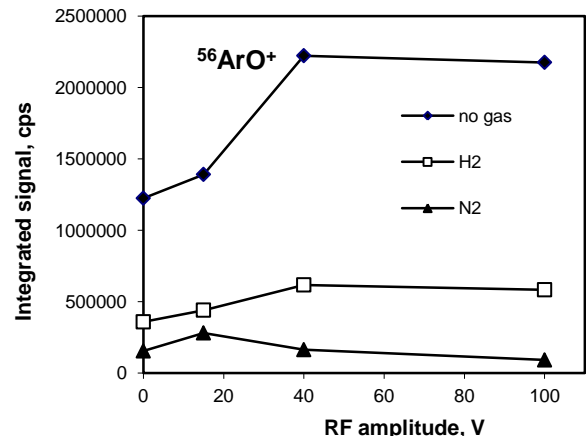
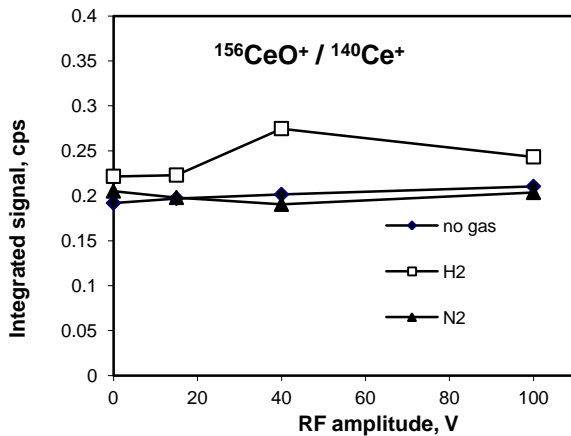
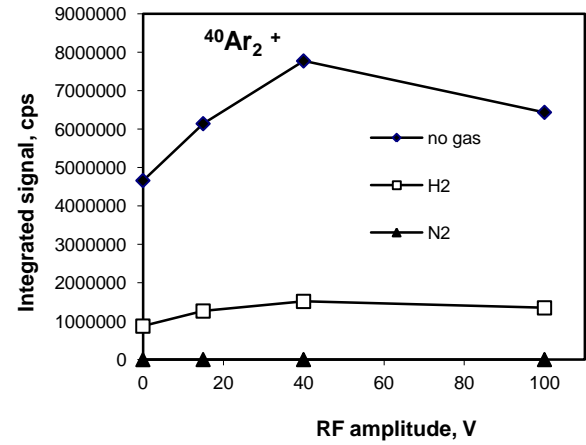
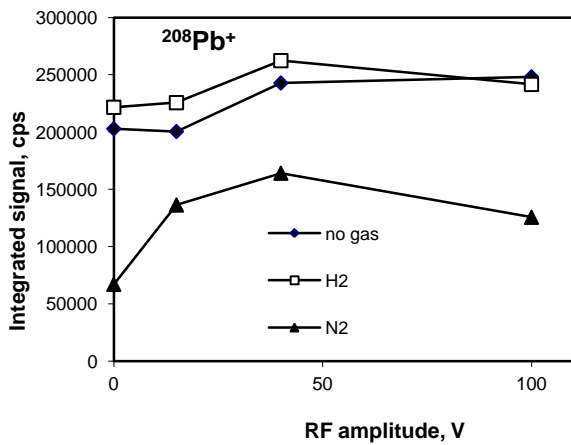
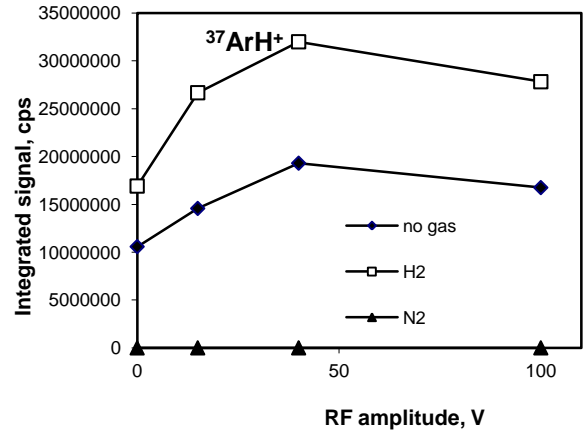
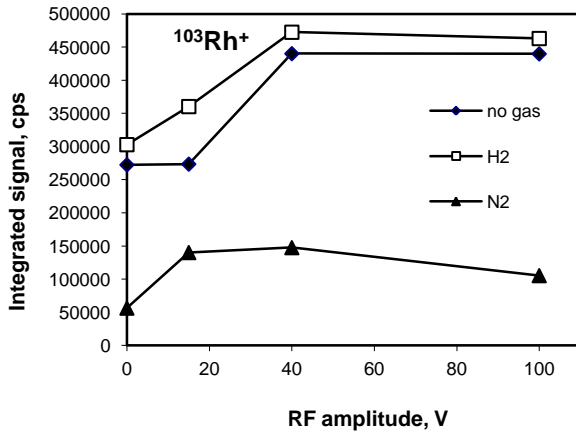
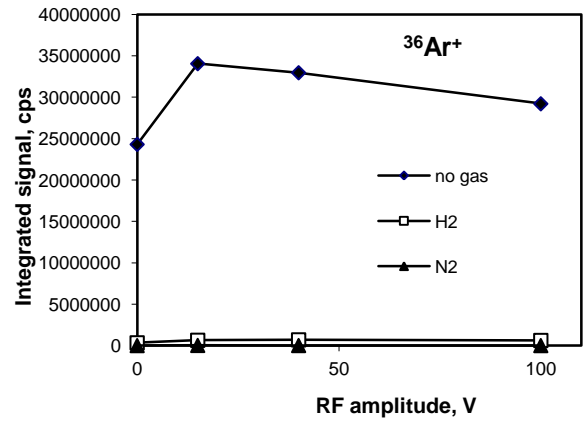
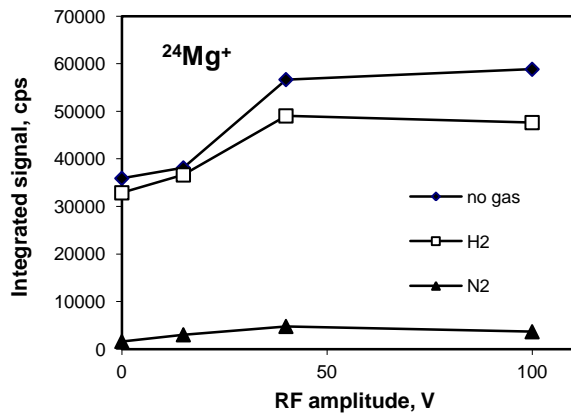


Figure 2.9. Influence of gas addition to the enclosed ion funnel part. Funnel exit:  $-20\text{V DC}$ ,  $600\text{ kHz}$  RF frequency. "No gas" refers to the configuration with the gas chamber installed at the end of the funnel, with no reactant gas added.

Enclosing the terminal part of the funnel induce a suppression of the recorded ion signal intensities by almost 50% compared to the open configuration. Since optimization was carried out in the usual way and manipulation of the ion funnel never resulted in sensitivity changes larger than 20% for a given setup, this was considered to result from the higher pressure inside the funnel as a result of the low pumping capacity. The effect of the gas fed into this region is highly dependent on the gas used and the ion species. The most dramatic effect on signal intensities was observed for Ar-based background ions ( $\text{Ar}^+$ ,  $\text{ArH}^+$ ,  $\text{ArO}^+$ ,  $\text{Ar}_2^+$ ), which can react by charge or atom exchange with  $\text{H}_2$  or  $\text{N}_2$  [82] or collision induced dissociation with  $\text{N}_2$ . Analyte ions as Mg, Rh, or Pb, which are presumed to be non-reactive with either  $\text{H}_2$  or  $\text{N}_2$  show indications for scattering effects. Low  $m/Q$  ions are significantly suppressed ( $> 90\%$ ) with  $\text{N}_2$ , while high  $m/Q$  only show 50% signal loss in this case.  $\text{H}_2$  shows practically no effect on transmission of Rh or Pb, while Mg was suppressed by less than 10%. The  $\text{CeO}^+/\text{Ce}^+$  ratio increased two fold by enclosing the funnel, but remained practically unaffected by the RF amplitude or the addition of  $\text{N}_2$ . Addition of  $\text{H}_2$  leads to a slight increase in the signal without a significant dependence on RF amplitude.

#### 2.2.4. Comparison With the Original ELAN 6000 Configuration.

Table 2.2 lists the signal intensities obtained for the instrument operating with the ion funnel in place in comparison to the original configuration with the single cylindrical ion lens. These data represent operating conditions that are considered analytically reasonable, i.e. those retaining the initial mass resolving power and abundance sensitivity. Plasma background ion signals are listed for conditions representing those optimized for elemental ions close in  $m/Q$ . For all settings shown, the instrumental background at  $m/Q$  220 was less than 10 cps. The ion current with the ion funnel in its present configuration was 3 – 6 times lower than with the conventional ion optics for most of the elements. The difference was greater for the heavy ions (for  $^{238}\text{U}$  5.6 times lower).  $\text{CeO}^+/\text{Ce}^+$  ratios were significantly increased in all configurations while Ar-based background ions usually showed a more pronounced suppression.

Table 2.2. Comparison of sensitivities (cps/mg/L) and background ion signal intensities (cps) for the unmodified instrument with the different ion funnel configurations. All data refer to the sensitivity at the peak maximum in cps. “dc”, RF and kHz data refer to the funnel exit potential, RF amplitude (both in Volts) and frequency applied to the ion funnel.

Isotope	Standard ELAN 6000	“Open” funnel	Enclosed, no gas	Enclosed, H <sub>2</sub>	Enclosed, N <sub>2</sub>
<sup>9</sup> Be <sup>+</sup>	9.0•10 <sup>5</sup>	1.2•10 <sup>5</sup> dc 20, RF 50 1700kHz	1.1•10 <sup>5</sup> dc 40, RF 40 600kHz	7•10 <sup>4</sup> dc 40, RF 40 600kHz	1•10 <sup>4</sup> dc 40, RF 40 600kHz
<sup>24</sup> Mg <sup>+</sup>	6.5•10 <sup>6</sup>	1.2•10 <sup>6</sup> dc 20, RF 25 1100kHz	5. •10 <sup>5</sup> dc 20, RF 40 600kHz	4.9•10 <sup>5</sup> dc 20, RF 40 600kHz	6.0•10 <sup>3</sup> dc 40, RF 40 600kHz 2
<sup>59</sup> Co <sup>+</sup>	1.5•10 <sup>7</sup>	5.2•10 <sup>6</sup> dc 20, RF 25 1100kHz	1.0•10 <sup>6</sup> dc 20, RF 40 600kHz	1.1•10 <sup>6</sup> dc 20, RF 40 600kHz	5.0•10 <sup>4</sup> dc 10, RF 15 600kHz
<sup>103</sup> Rh <sup>+</sup>	3.3•10 <sup>7</sup>	8.9•10 <sup>6</sup> dc 20, RF 50 350kHz	4.4•10 <sup>6</sup> dc 20, RF 40 600kHz	4.7•10 <sup>6</sup> dc 20, RF 40 600kHz	3.5•10 <sup>6</sup> dc 40, RF 40 600kHz
<sup>140</sup> Ce <sup>+</sup>	4.6•10 <sup>7</sup>	9.1•10 <sup>6</sup> dc 20, RF 25 800kHz	4.4•10 <sup>6</sup> dc 20, RF 40 600kHz	4.7•10 <sup>6</sup> dc 20, RF 40 600kHz	4.5•10 <sup>6</sup> dc 40, RF 40 600kHz
<sup>208</sup> Pb <sup>+</sup>	2.4•10 <sup>7</sup>	4.3•10 <sup>6</sup> dc 20, RF 50 350kHz	2.4•10 <sup>6</sup> dc 20, RF 40 600kHz	2.6•10 <sup>6</sup> dc 20, RF 40 600kHz	2.2•10 <sup>6</sup> dc 40, RF 40 600kHz
<sup>238</sup> U <sup>+</sup>	4.5•10 <sup>7</sup>	6.7•10 <sup>6</sup> dc 20, RF 50 350kHz	3.5•10 <sup>6</sup> dc 20, RF 40 600kHz	3.7•10 <sup>6</sup> dc 20, RF 40 600kHz	3.5•10 <sup>6</sup> dc 40, RF 40 600kHz
<sup>140</sup> Ce <sup>16</sup> O <sup>+</sup> / <sup>140</sup> Ce <sup>+</sup>	2.1%	18% dc 20, RF 25 800kHz	20% dc 20, RF 40 600kHz	27% dc 20, RF 40 600kHz	24% dc 40, RF 40 600kHz
<sup>36</sup> Ar <sup>+</sup>	9.3•10 <sup>8a</sup>	7.1•10 <sup>8</sup> dc 20, RF 50 600kHz	6.7•10 <sup>8</sup> dc 40, RF 40 600kHz	3.7•10 <sup>7</sup> dc 40, RF 40 600kHz	1.1•10 <sup>6</sup> dc 40, RF 40 600kHz
<sup>40</sup> Ar <sup>16</sup> O <sup>+</sup>	1.2•10 <sup>8a</sup>	5.4•10 <sup>7</sup> dc 20, RF 25 800kHz	2.0 •10 <sup>7</sup> dc 20, RF 40 600kHz	6.4•10 <sup>6</sup> dc 40, RF 40 600kHz	2.8•10 <sup>6</sup> dc 20, RF 15 600kHz
<sup>40</sup> Ar <sub>2</sub> <sup>+</sup>	4.7•10 <sup>8a</sup>	2.0•10 <sup>8</sup> dc 20, RF 25 800kHz	3.8•10 <sup>7</sup> dc 20, RF 40 600kHz	2.6•10 <sup>7</sup> dc 40, RF 40 600kHz	2.5•10 <sup>4</sup> dc 20, RF 40 600kHz

a : cps.



### 2.3. Conclusions

An ion funnel has been adapted as an ion guide between the standard sampler-skimmer vacuum interface and the MS region of a commercial ICPMS. Ion transmission of the configuration developed here was however generally lower than in the original ICPMS configuration with a single cylindrical lens. At optimum conditions, ion transmission was on average lower by one order of magnitude compared with the conventional setup. The optimum pressure regime for the ion funnel is supposed to be in range 10 – 100 Pa, while the pressure in the 2<sup>nd</sup> vacuum stage according to the manufacturer should be around 0.1 Pa. The pressure inside the funnel was estimated to be approximately 5 times higher than outside the funnel. Hence, the mean free path of ions should be about 10 cm, which is larger than the dimensions of the ion funnel but greatly exceeds the electrode spacing. Under these conditions the basic working principle of collisional focusing within the funnel was not working efficiently. Nonetheless it could be shown that even low  $m/Q$  ions can be transported through the ion funnel under optimized DC and RF potential and frequency.

Most isotopes showed the highest transmission for RF frequencies in the range between 200 and 600 kHz, RF amplitudes of 40–50  $V_{pp}$  and a DC gradient along the funnel axis of 20 – 40V. Lower  $m/Q$  were found to optimize at higher RF frequencies, which is in agreement with the theoretical transmission properties of a stacked ring electrode guide. Higher values of DC gradient and RF amplitude however, usually, deteriorated the mass resolving power of the quadrupole MS, most likely due to fringe fields or too high ion energy spread at the funnel exit. When enclosed and fed with an additional gas, the ion funnel can also be used to initiate ion-molecule reactions. Especially the abundance of  $Ar^+$  and Ar-based polyatomic ions can be substantially reduced by the addition of  $N_2$  or  $H_2$ . The latter would be rather favorable in this context as it would not affect the transmission of low  $m/Q$  analyte ions to a great extent. Ultimately, the configuration of the ion funnel used in this study does not bring a benefit in the performance of the ICPMS. This was most likely the consequence of several aspects of the ion source. First of all, it could be the case that the high ion current caused by the plasma itself is limiting the ion transmission inside the ion funnels due to space charge effects, which are more severe when the ion kinetic energies are damped by the collisions with the background gas. Addition of  $H_2$  was expected to mitigate this effect to some extent because it would cause the fraction of the ion current carried by  $Ar^+$  and Ar-based ions to an ion of lower  $m/Q$  ( $H^+$ ,  $H_3^+$ , or  $H_2O^+$ ) that are more likely repelled from the ion cloud than analyte ions. A further increase in the density of  $H_2$  inside the ion funnel however was not possible in the current configuration due to constraints on the pumping speed in the mass spectrometer chamber. Another apparent disadvantage would be the increase of metal-oxide ions and the concurrent increase in spectral interferences. It is thus apparent that the present configuration of an ion funnel is far from optimum as ion transfer device. Further studies are thus needed to investigate the influence of the total ion current inside the ion funnel on transmission of different  $m/Q$  and plasma background species in order to improve overall sensitivity.

### 3. Directly Coupled Ion Funnel

---

Previous studies have shown that ion funnel configurations yield the greatest advantage when operating in the range of 10 – 1000 Pa with slow ions [65]. Installation of the ion funnel downstream the skimmer cone of a conventional ICPMS is therefore not providing the optimum operating conditions for the ion funnel to confine the ion beam. Therefore the properties of the ion funnel installed directly in the region of the expanding plasma after the sampler cone were investigated in the following sections.

#### 3.1. Experimental

The plasma source the RF-generator, controller and the torch box of the ELAN 6000 ICPMS used in the previous study were mounted on an external supporting frame and a custom made vacuum recipient was constructed. The recipient was milled from an aluminum block and consisted of two chambers (Figure 3.1): the first chamber holding the ion funnel, while the second chamber could be equipped with different detector systems for current measurement. The top of the system was covered with a glass plate (1 cm thickness) to allow visual observation of both, funnel and detector chambers when the system was under vacuum.

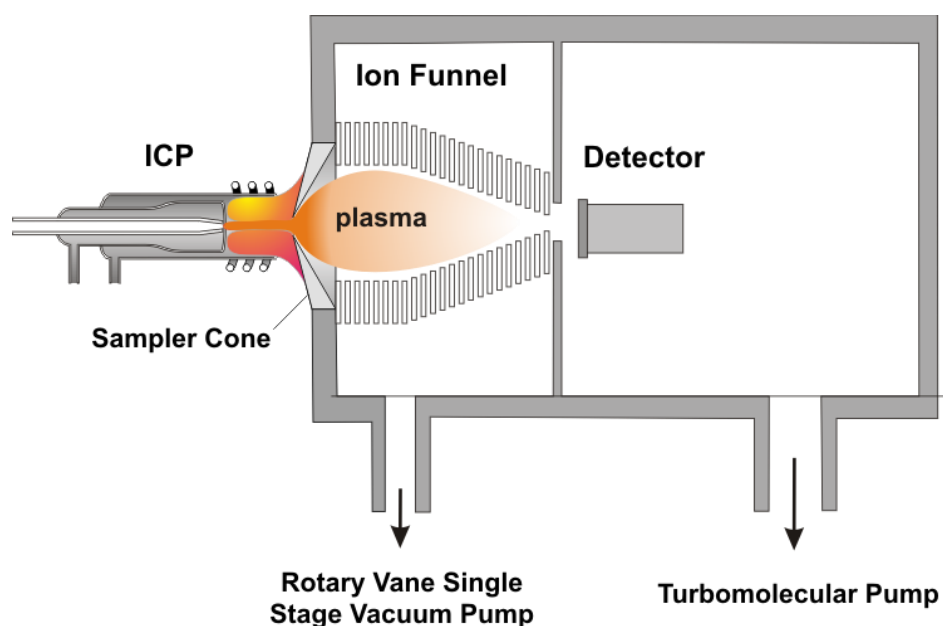


Figure 3.1. Schematic view of the instrument with the ion funnel placed directly after the sampler. The sampler is installed in a water cooled copper plate at the front of the first chamber.

The first vacuum chamber had a quadratic cross-section of 173 mm width and was 73 mm deep. All surface connections were sealed by VITON® (DuPont™ Dow Elastomers, Geneva, Switzerland) O-rings. The first vacuum chamber was separated from the second chamber by a 9 mm thick wall with circular opening for installation of the ion funnel. The funnel was mounted on the same MACOR® (Corning, USA, New York) base-plate, used in the previous study. The second chamber was 173 mm wide and 149 mm long. Vacuum feed throughs provided electric connections to the funnel electrodes and detection systems.

The ion funnel chamber was evacuated by a Leybold S25B Trivac Rotary Vane Single Stage Vacuum Pump (Oerlikon Leybold Vacuum GmbH, Köln, Germany). This rotary vane pump was also used as a backing pump for the turbomolecular pump (TurboVac 361 Vacuum Pump, Oerlikon Leybold Vacuum GmbH, Köln, Germany) evacuating the detector chamber.

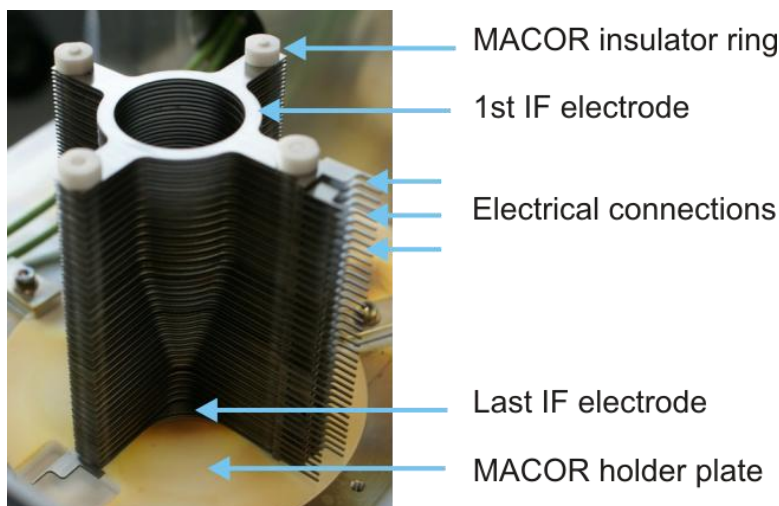


Figure 3.2. The ion funnel (IF), mounted on the MACOR plate.

The ion funnel was modified from the previous arrangement and contained 74 additional ring electrodes in the front part (Figure 3.2). The entrance of the funnel consisted now of 25 electrodes with 24 mm inner diameter. The following electrodes were of linearly decreasing inner diameter until the terminal electrode with orifice with 2 mm diameter as used in the previous study. The thickness of the electrodes and the spacing were 0.5 mm. All funnel electrodes had a 1 mm pin, through which they could be independently connected to the resistor chain / capacitor board fed by the power supply as in the previous study.

Initially all the funnel electrodes were mounted on four MACOR<sup>®</sup> rods, but later, due to their fragility, the rods were changed to aluminum rods, anodized for insulation. MACOR<sup>®</sup> rings were placed between all adjacent electrodes for insulation.

The RF and DC power supplies used were as described in the previous chapter. If not stated specifically, the RF frequency was set to 600 kHz for all experiments presented here because that yielded the highest ion transmission in the previous set up. In contrast to the configuration described previously, the DC-gradient was determined by the potential applied to the 2<sup>nd</sup> last funnel electrode, while the terminal electrodes' DC offset could be adjusted independently. In all series presented in this chapter however, both electrodes were set to equal potentials. The 1<sup>st</sup> ion funnel electrode was usually set to ground potential.

Since the pressure inside the second chamber has been above the pressure suitable for mass spectrometric ion detection, an L-shaped stainless steel strip was used as a probe ("strip detector") to measure the electric current downstream of the ion funnel. The width of the strip was 1 cm and the part reaching across the funnel axis was 4 cm long. It was positioned on a support frame in a way that the bent part was located vertically and in parallel to the funnel exit aperture at a distance of 2 cm. The detector was connected to a power supply to adjust the potential offset and to an ammeter for the current measurements.

Depending on the experiment, the detector potential was either adjusted independently or with a fixed bias relative to the last funnel electrode. All the potentials are given as absolute values, relative to ground potential.

Default system parameters are listed in table 3.1. If not mentioned otherwise, these parameters were used.

*Table 3.1. Instrumental parameters.*

<b>ICP:</b>	
ICP power	1350 Watt
Plasma gas flow	15 L/min
Auxiliary gas flow	1 L/min
Nebulizer gas flow	1 L/min
Sampler	1.1 mm, platinum, ELAN type
Plasma	Dry Ar, peristaltic pump switched off
Blank solution	1% HNO <sub>3</sub>
Detector	Strip type
<b>Ion funnel:</b>	
1 <sup>st</sup> electrode	Grounded
last electrode  (DC gradient)	relative to the 1 <sup>st</sup> ion funnel electrode

Most experiments were carried out with dry argon-only plasma conditions. In some experiments however aspiration of a blank solution (1% HNO<sub>3</sub>) was carried out in the same way as described in the previous section. Switching back to dry argon-only plasma however required extended drying periods of the entire sample introduction system, as indicated by the drift in the currents measured for otherwise identical conditions. If not dried by external heating, 10 days were needed to reach the conditions for the dry plasma.

All the experiments described in this chapter have been performed with the strip detector. Thus, the ion and currents cannot be determined directly because the measured value will depend on the respective flux of positively charged ions and electrons, which are discharged at its surface (the abundance of negatively charged ions from the ICP is considered negligible in this context) and potentially occurring secondary electrons or ions leaving the surface due to thermal or Schottky emission. An indirect description can however be made based on the variation of the measured current with the potential applied to the detector. When set above source potential, positively charged ions are stopped. Electrons, present near the funnel exit on the other hand are accelerated towards the strip and discharged, leading to a net negative current measured. Successively lower

potentials will allow an increasing ion current to reach the detector, shifting the current towards positive as well. The transition between the regimes occurs at the potential characteristic for the source. Further lowering the potential at the detector discriminates against electrons exiting the ion funnel but may give rise to electron emission, especially in cases where the hot plasma can penetrate the funnel and heat the metal strip. However, within the pressure regime and potentials used in this work, a contribution by Schottky emission was estimated to be about 2  $\mu\text{A}$  for the ion funnel with an inner surface area of 29.5  $\text{cm}^2$  at a temperature of 500°C, where the steel plates begin to glow and a DC potential of several 10 V used between the funnel and the detectors. The range of ion currents measured with negative detector bias however significantly exceed this value and Schottky emission is considered to be negligible.

### 3.2. Plasma Expansion

The expansion of the plasma jet was investigated visually while successively inserting the ion funnel components. The expansion after the sampler cone into a vacuum region at 280 Pa is shown in figure 3.3. In this case, the plasma jet expansion remains fairly stable and passes through the entire vacuum chamber with only a slight radial expansion (Figure 3.3.). The diameter of the plasma beam near the supersonic structure was about 1 cm and at the end of the box spread up to approximately 4 cm. The barrel shock region and 1<sup>st</sup> Mach disk were clearly visible near the sampler cone followed by a second, less clearly defined supersonic region after which the expansion appears to convert into a diffuse beam.

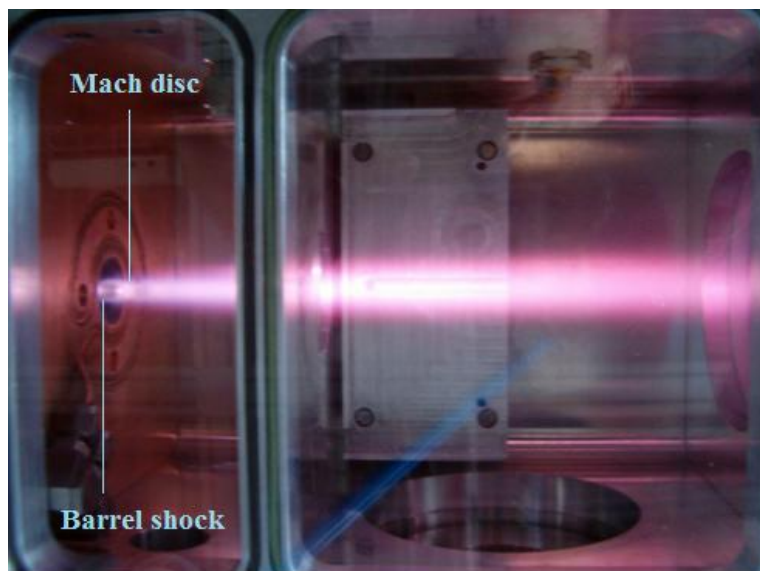
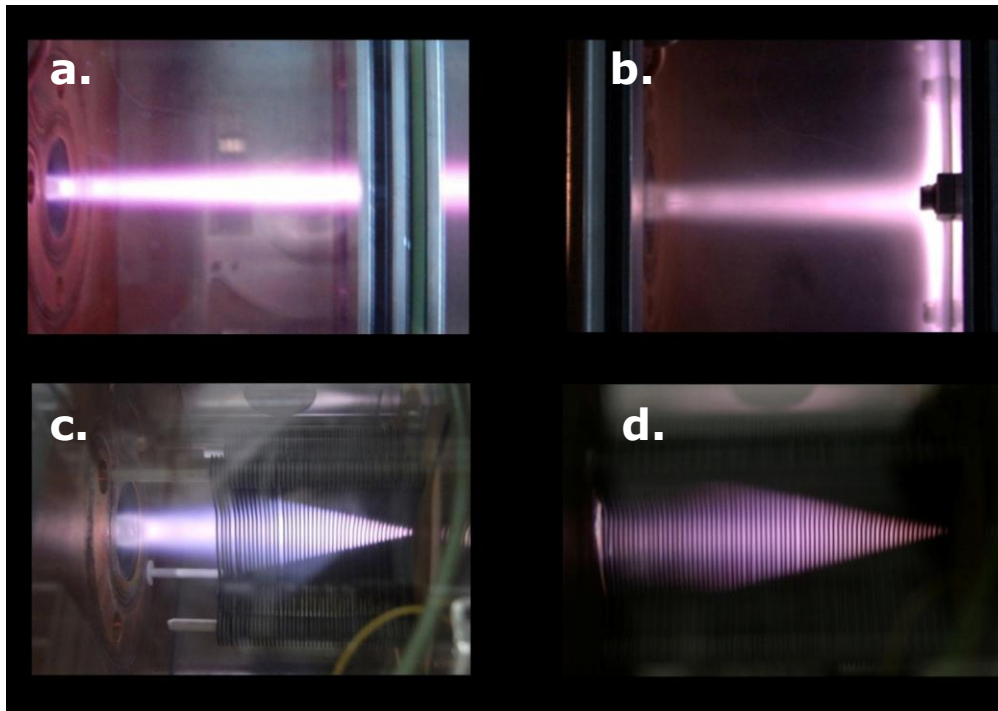


Figure 3.3. Photograph of the plasma expansion into the vacuum chamber at a pressure of 280 Pa.

In figure 3.4 the plasma beam dissipation is shown when an increasing number of the funnel electrodes is installed in the expansion region. The free expansion of the plasma jet (a) is interrupted

at the terminal funnel orifice forming a stagnation layer along the wall (b). Collision of the hot plasma with further electrodes leads to increasing dissipation within the funnel (c). The initial expansion however remains relatively stable even with the full funnel installed and the Mach disc is still apparent through the funnel electrodes (d).



*Figure 3.4. Photographs of the plasma expansion in the first vacuum chamber with different lengths of the ion funnel. No ion funnel (a), only the funnel exit aperture installed (b), the first 50 rings of the ion funnel (c), and the complete ion funnel with 72 electrodes (d).*

### **3.3. DC Influence**

Figure 3.5. shows the current measured downstream the ion funnel with increasing funnel electrodes installed.

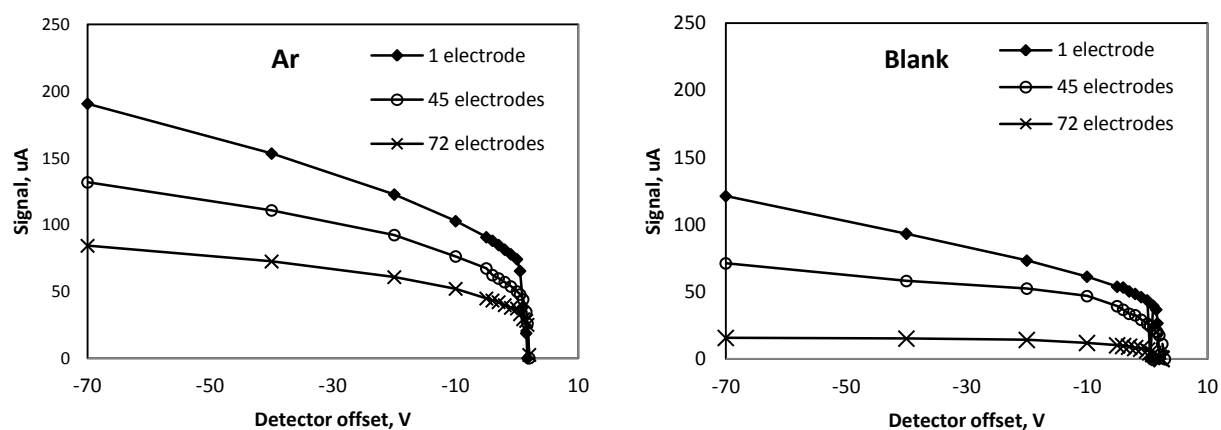


Figure 3.5. Dependence of the current measured on the strip detector on the detector potential for different numbers of funnel electrodes with an Ar-only ICP (left) and with addition of a blank aerosol (right). All funnel electrodes were grounded.

The measured current showed a similar trend when lowering the detector potential. A steep increase is observed for voltages near the source potential (2 – 5 V) in all cases, followed by a further gradual increase when biasing the detector by more than -10 V negative. Increasing the number of funnel electrodes reduces the terminal current and this reduction is significantly more pronounced with the addition of the aqueous aerosol to the ICP. For – 70 V detector bias the current reached a value of more than 180  $\mu$ A with only the exit aperture of the funnel installed and the dry, Ar-only ICP. With the entire ion funnel installed, the currents dropped to about 50% for the dry plasma, while only 15% remained with introduction of the aerosol.

Since the pump speed applied to evacuate the funnel chamber was the same in all experiments, it is safe to assume that the pressure within the expansion region increases when the funnel is installed. This higher gas density leads to more scattering of the ion motion and the proximity of the grounded funnel electrodes causes a greater loss of ions inside the funnel when compared to the open configuration. The lower current observed with the aerosol introduced to the ICP is most likely caused by the lower initial kinetic energy of the ions leading to even greater scattering losses.



### 3.4. RF Influence

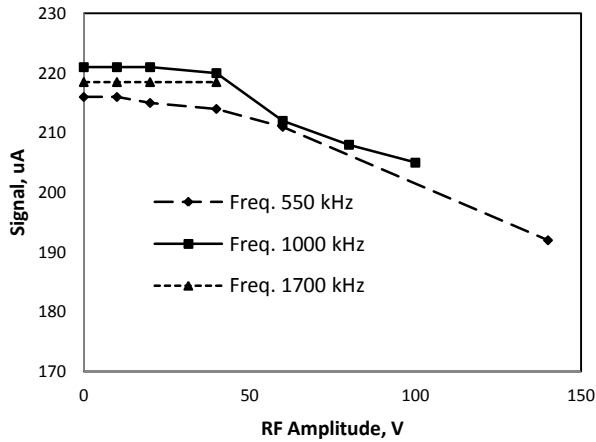


Figure 3.6. Dependence of the measured current after the funnel exit on the RF amplitude and frequency applied. Ar-ony ICP, 1<sup>st</sup> ion funnel electrode = -15V, last ion funnel electrode = -15 V, detector = -15 V

To investigate the effect of the RF-field in this configuration, the current was measured for different RF amplitude and frequency while detector bias and an ion funnel offset were fixed to potentials of -15 V each (Figure 3.6). The measured current however could not be improved with the RF field applied. At all frequencies the current remains rather constant for RF amplitudes between 0 and 20 or 40 V and then continuously decreased for higher RF amplitudes when using frequencies of 550 kHz and 1000 kHz. For an RF frequency of 1700 kHz, amplitudes greater than 40 V could not be applied, which is most likely the result of electrical shorting by the electrically conductive plasma inside the funnel. The signal decrease for higher amplitudes is most probably the consequence of an increasing effective potential near the funnel electrodes. Especially at the terminal electrodes with smallest diameter, the additional RF field reduces the effective area where the potential is sufficiently low to allow the ions to pass. Increasing the RF-frequency (i.e. lowering the effective potential for the same RF amplitude) leads to a broader region of transmission as has been observed in the experiments.

### 3.5. Summary

The observed behavior of the measured current on the potentials applied on the funnel and detector indicates that the beam inside the ion funnel remains electrically conductive plasma, which connects the source with the funnel electrodes and causes electric shorting also between the electrodes when the potential difference exceeds a critical value. This is supported by the fact that the potential

applied to the detector, where the measured current was equal to zero, does not depend significantly on the potentials applied to the ion funnel, and was similar to that reported for the plasma potential of an ICP source of the type used here [83]. Furthermore, the RF amplitude could only be adjusted to a maximum value, which depended on the RF frequency. Higher amplitudes led to electrical shorting inside the funnel. Ultimately however, the presence of the RF field caused no improvement in the ion transmission, but rather caused the signal to decrease. It cannot be determined whether there was actually no focusing effect, but especially the higher effective potential at the funnel exit effectively narrowed the funnel exit aperture, reducing the number of ions transmitted to the next stage. These ions are then trapped in the potential wells, formed by the RF field between the electrodes and ultimately discharged. Additionally the electrical flux into the funnel in these experiments was significantly higher than in the experiments using ESI sources [72] where ion currents of several 10 nA were applied. Thus the more than 1000 times higher currents observed here after the funnel and the collisions inside the funnel region may amplify space effects significantly.

It may be summarized that the density of the plasma inside the funnel was too high, so that the confining effective potential was not sufficient to improve ion transmission while at too high amplitude ions were trapped within the funnel exit region. The ion movement was thus primarily affected by the gas dynamics. In order to be able to use the ion funnel to actually confine an ion beam, the plasma density needs to be reduced.

There are several ways to lower the plasma density inside the funnel. One possibility would be to decrease the sampler orifice diameter. This configuration was considered for the initial ICPMS instruments and had shown significant limitations due to cone clogging and orifice deterioration [21]. The other approach would be a modified 2-stage interface, similar to the sampler-skimmer arrangement, which will be employed in the further experiments.

## 4. Additional Extraction Interface

---

### 4.1. Introduction

In order to reduce the plasma density in the ion funnel region a two stage interface was added to the set up. The interface was based on a design initially proposed by Moussalami *et al.* [59], where the plasma beam expands freely into the 1<sup>st</sup> pressure stage, and then passes the aperture in a plate located ~32 mm downstream from the sampler so near the shock wave of the expanding plasma in their set up. The modifications made also allowed an easy change of electrodes and apertures to enable studying a wide range of operating conditions of interface and ion funnel. Additionally, numerical simulations of the ion trajectories were carried out using Simion 8 (Scientific Instrument Services Inc. NJ, USA) in order to estimate promising configurations.

### 4.2. Experimental

The instrument described in previous chapter had been modified by the addition of an in-house built interface, which was mounted in front of the ion funnel chamber. It consisted of an additional round chamber, which was attached using screws to the copper plate in front of the aluminum housing containing the funnel chamber and the detector chambers. It was 171 mm in diameter and 66.5 mm in depth. It was water cooled and evacuated via a standard CF25 flange and the pressure could be adjusted by a throttling valve. The extraction of the ion beam into the ion funnel was carried out using a two-electrode pressure reducing stage (Figure 4.1), where apertures of different inner diameter could be inserted. Additionally a cylindrical electrode made from stainless steel mesh could be installed before the extraction electrodes. The extraction electrodes were 0.5 and 0.3 mm thick and various aperture sizes, all chamfered to 45° at the outlet, were tested. Separation of the electrodes was 0.5 mm. All three electrodes could be mounted in a single MACOR® holder and individually connected to their power supplies. The plasma was sampled using a standard platinum sampler cone as used with ELAN 6000 type ICPMS instruments, which had a 1.1 mm orifice diameter.

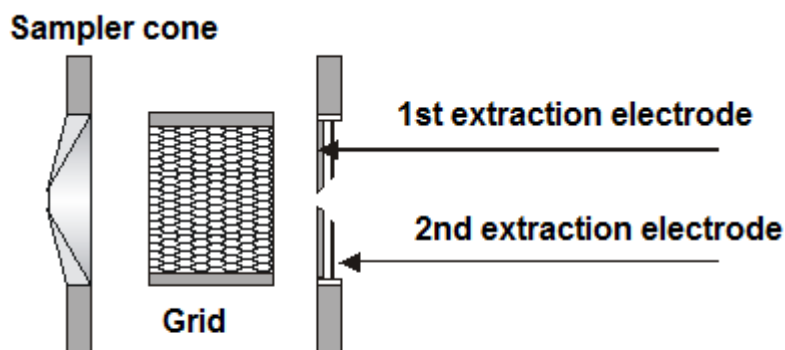
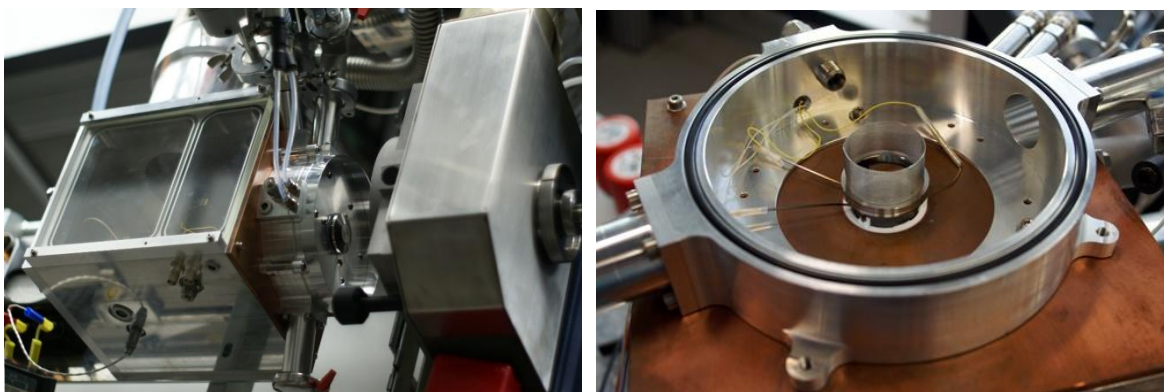


Figure 4.1. Sketch of the active components in the extraction interface.

A photograph of the extraction interface interior and mounted to the ion funnel chamber is shown in figure 4.2.



A

B

Figure 4.2.

A. - The instrument with the extraction interface chamber and top glass plate installed.

B. - The extraction interface without the front plate with the installed extraction electrodes and the grid.

The 1<sup>st</sup> interface stage was pumped by a 2<sup>nd</sup> stage rotary vane pump. The typical pressure in the 1<sup>st</sup> chamber in the working regime was approximately 520 Pa and the pressure could be increased via the throttling valve mounted between the chamber and the pump. The ion funnel stage was evacuated using a single stage rotary vane pump. This pump was also used as a backing pump for the turbomolecular pump, which evacuated the detector chamber. The pressure in the 2<sup>nd</sup> chamber could also be adjusted via a throttling valve. The pressures in the 1<sup>st</sup> and 2<sup>nd</sup> chambers were measured using a

Baratron® (MKS 626A 10 Torr Baratron® Absolute Capacitance Manometer, MKS Instruments, Germany) for pressures between 1 and 1000 Pa. Lower pressure in the detector chamber was monitored using a magnetron (AIM-S-NW25, Edwards®, Manor Royal, Crawley, West Sussex). Details of the pumping system and typical pressures are given in table 4.1.

*Table 4.1. The pumps and typical pressures in the different stages of the instrument with the additional extraction chamber installed.*

Stage	Pump	Typical pressure, Pa
1 <sup>st</sup> stage (extraction interface region)	Leybold S25B Trivac Rotary Vane Single Stage Vacuum Pump  Oerlikon Leybold Vacuum GmbH, Köln, Germany	520 Pa
2 <sup>nd</sup> stage (ion funnel region)	40 BOC E2M40 2 stage rotary vane pump  Edwards High Vacuum Int., England	50 Pa
3 <sup>rd</sup> stage (detector region)	TurboVac 361 Vacuum Pump  Oerlikon Leybold Vacuum GmbH, Köln, Germany	1·10 <sup>-2</sup> Pa

#### 4.2.1. Simulations

A series of simulations have been carried out using Simlon software prior to executing experiments. Two systems were investigated with 2 or 3 extraction electrodes, but there was no significant difference in the ion motion between the two configurations. Thus most of the simulations were performed with 2 electrodes. The 1<sup>st</sup> electrode, which is supposed to be in direct contact with the plasma, was always set to +3 V, while the potential of the 2<sup>nd</sup> electrode was varied. The edges of the electrode apertures were defined with 90°, 45°, and 35° exit angle. Electrode thickness was 0.5 or 0.3 mm and the spacing in between was 0.5 mm. The simulation of the ion motion a set of 101 ions with a mass of 40 a.m.u. and a charge +1 have was used. Initial ion kinetic energy was set to +5 eV, which corresponds to the approximate plasma potential. To model the space-charge effect, the Coulomb repulsion in a range 1·10<sup>-10</sup> C - 1·10<sup>-14</sup> C was added. To estimate the collisional damping, a damping factor was added in some simulations to the model, which was either a constant value of 0.5 for every iteration or a decreasing damping factor from 0.5 at the initial point to 0 at the end of the ion path. The

damping factor was applied to the ion velocity at every iteration. The number of the collisions was calculated based on the mean free path (0.15 mm) of the Ar ions at a pressure of 100 Pa. The collisional model assumed a random change of the three velocity components at the distance of free length path of ions.

It was found that electrodes with 45° exit angle of the orifices provided the best confinement of the ions with all other variables being equal. With a -100 V potential on the 2<sup>nd</sup> extraction electrode the angular spread of the ions could be significantly reduced. A further decrease of the 2<sup>nd</sup> electrode offset into a negative range provided for a more confined beam, but this improvement was relatively small.

The simulation of the focusing effect of the extraction electrodes is presented in figure 4.3.

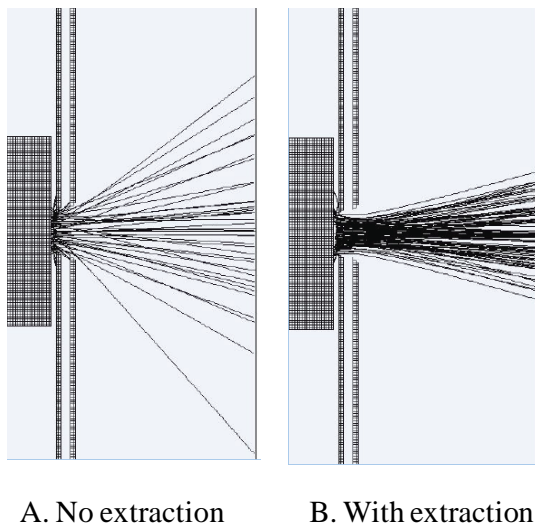


Figure 4.3. Extraction interface with grounded 2<sup>nd</sup> electrode (A) and -100 V on the second plate (B). The first electrode in both cases had potential of +5 V.

The most suitable design included:

- two metal plates (0.5 mm thickness – 1<sup>st</sup> plate and 0.3 mm – 2<sup>nd</sup> one)
- 0.3 mm insulator ring between two plates
- diameter of the first plate orifice = 1.5 mm
- diameter of the 2<sup>nd</sup> plate orifice = 2 mm
- apertures in plates to be made with a 45° exit angle

Three configurations were investigated in these experiments (Figure 4.4): (a) additional interface without ion funnel installed, (b) with the ion funnel placed in the 2<sup>nd</sup> chamber and (c) with extraction interface, and ion funnel, and detector for angular resolved current measurement. The ICP operating conditions were the same as described in chapter 3.

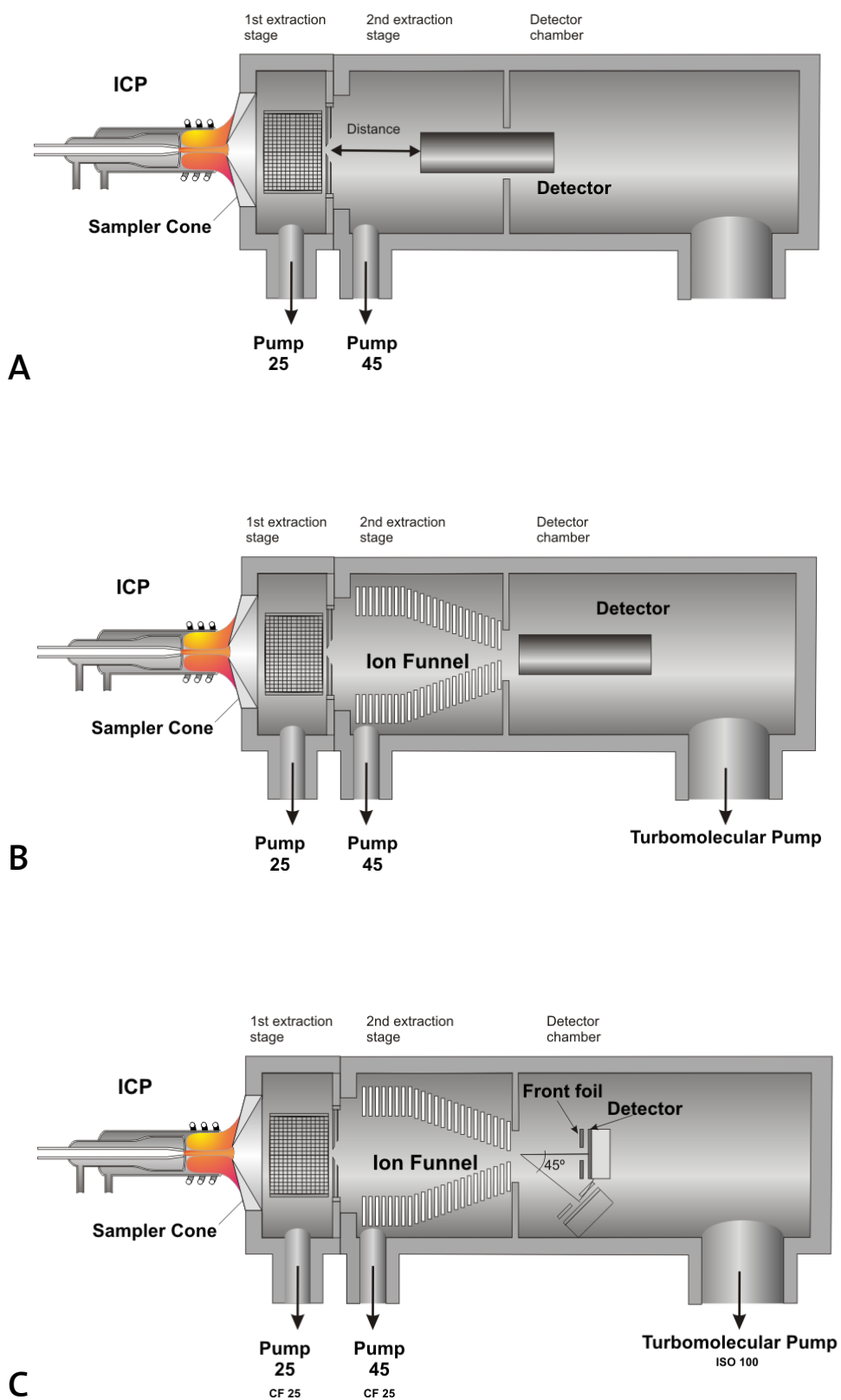


Figure 4.4. The scheme of the instrument with the additional extraction interface:

A: Extraction interface installed no ion funnel, distance between interface exit aperture and detector could be varied, no aperture separating the 2<sup>nd</sup> and the 3<sup>rd</sup> chambers. Turbomolecular pump off.

B: The extraction interface and the ion funnel installed. The cylindrical detector located 1 cm downstream the ion funnel outlet in the 3<sup>rd</sup> stage. Turbomolecular pump on.

C: The extraction interface and the ion funnel installed. Detector for angular resolved measurements in the 3<sup>rd</sup> stage. Turbomolecular pump on.

#### 4.2.2. Detectors.

Measurement of the current downstream the extraction interface directly (Figure 4.4, a) was carried out with either the strip detector used in the experiments describe in chapter 3 or via a distance-variable stainless cylinder of 2 cm diameter. The cylindrical detector could be adjusted at variable distance (between 1 and 8 cm) from the exit aperture of the extraction interface allowed axially resolved detection of the current. The detector was held in a PEEK block for electrical insulation. For most of the studies in this chapter the cylindrical detector potential was biased relative to the 2<sup>nd</sup> extraction plate. In order to determine the angular distribution of the ions exiting the ion funnel, a specific detector was designed (Figure 4.5).

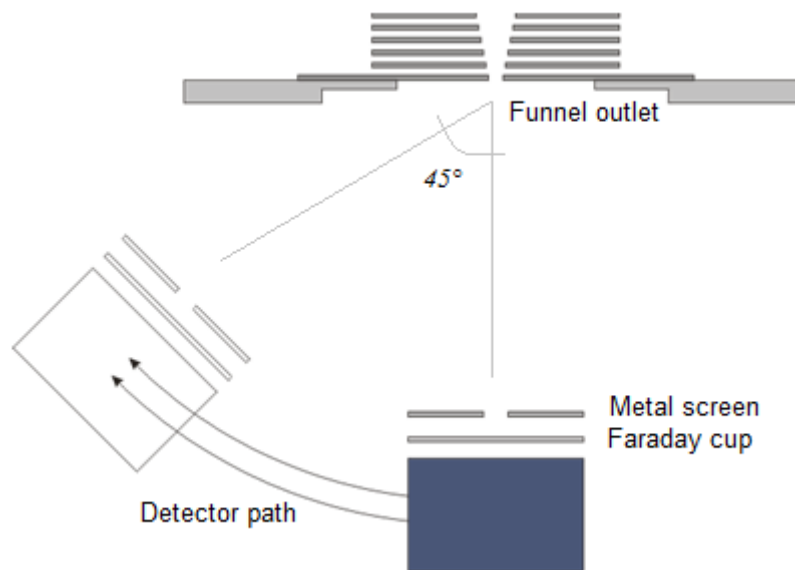


Figure 4.5. The scheme of the detector system for angular resolved current measurement. The 0° position corresponds to the location of the detector along the axis. From this point the detector could be rotated about 45° at a constant distance to the funnel exit aperture.

This detector system consisted of a Faraday cup for charge collection located behind an isolated 0.1 mm stainless steel “screen” with an aperture of either 4x4 mm<sup>2</sup>, defining the angular resolution of the measurement. This arrangement was mounted in an isolated holder with grooves, defining a path



over 1/8 of a circle at a constant radius of 39.2 mm between the ion funnel exit and the screen's aperture, thus integrating over a solid angle of 5.84°. A stepper motor with a linear actuator (LP2515, Nanotec Electronic GmbH & Co. KG, Landsham, Germany) and in-house built multi-controller was used to rotate the detector about the funnel exit with a resolution of 1°. The potentials applied to the screen and Faraday cup could be individually adjusted by external power supplies. The Faraday detector was generally set to 10 V more negative than the screen. The term "Delta potential" is used hereinafter as the potential difference between the last funnel electrode and the metal screen in front of the detector. The ion current was measured using an analog ampere meter (Picoamperometer 414S, Keithley Instruments Inc., Ohio, US). The signal was taken as the mean of the values during 1 to 5 seconds, depending on stability of the signal. In these experiments the two terminal ion funnel electrodes were set to the same potential, so the term DC gradient refers to the potential difference between the 1<sup>st</sup> and last funnel electrodes. The potentials along the ion funnel were chosen to create either a plane potential field or the slope to negative values in order to accelerate ions towards the detector. Thus the DC value refers to this difference and does not reflect the negative or positive is an offset of the last funnel electrode. The 1<sup>st</sup> funnel electrode was always set to ground potential.

#### **4.2.3. Extraction interface orifice diameter**

Before the final version of the extraction interface designed was finished, a series of studies with a single exit aperture (0.5 mm thickness) were performed. The plate had the same diameter as the ELAN sampler and was held in the slot between the 1<sup>st</sup> and 2<sup>nd</sup> chambers by the pressure difference. There was no insulator ring between the separator plate and the copper plate, so for these studies it was grounded.

Six plates were prepared with orifices of 1 mm, 1.5 mm, 2 mm, 2.5 mm, 3 mm, and 4 mm inner diameter. To investigate the beam expansion dependence on the separator plate orifice diameter, the ion funnel was removed to measure precisely the pressure in the chamber and be able to observe the plasma emission. ICP operating conditions were kept constant for all the studies. The lowest pressure achieved under these conditions was 520 Pa in the extraction interface, which is similar to the typical pressure regime of the 1<sup>st</sup> stage of a standard ICPMS instrument (ELAN 6000). The pressure in the 3<sup>rd</sup> chamber when separated by the exit aperture of the ion funnel installed, could be reduced to approximately 2 Pa using the turbomolecular pump.

First, at a fixed 1<sup>st</sup> stage pressure, the pressure of the 2<sup>nd</sup> stage, evacuated at full pump speed, was measured for different aperture sizes in the exit plate (Figure 4.6).

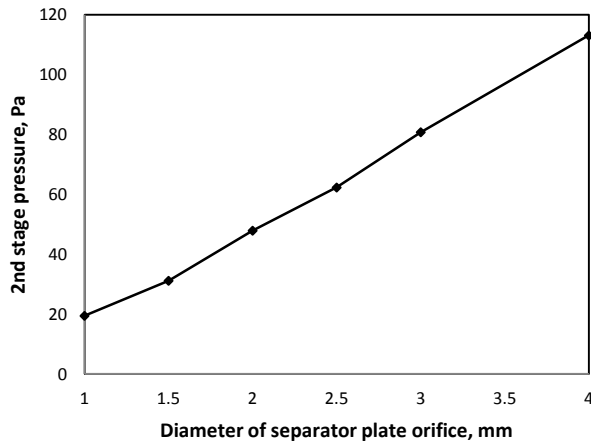


Figure 4.6. Pressure dependence on the aperture size of the extraction interface exit plate. 1<sup>st</sup> stage pressure – 550 Pa. Dry Ar plasma. 1<sup>st</sup> and 2<sup>nd</sup> stage pumps on.

The pressure in the 2<sup>nd</sup> chamber showed an apparently linear dependence on the diameter of the orifice between the 1<sup>st</sup> and the 2<sup>nd</sup> pressure stages, indicating that the density of the plasma before the exit was radially not homogeneous but decreases rapidly. Considering that the aperture is located close to the Mach disk of the expanding plasma it would have been expected that the pressure were fairly similar in this region. Nonetheless, this linear dependence would allow the use of a wide range of the orifice sizes without a exceeding the typical operating pressure of the ion funnel of 10 – 1300 Pa [74].

The same dependence, but for the measured current, looks different (Figure 4.7). Again, the pressure in the 1<sup>st</sup> chamber was fixed at 550 Pa (minimum possible pressure at the applied conditions). The strip type detector was located 20 mm downstream the exit aperture in the 3<sup>rd</sup> chamber and biased to -37 V. The pumps of the 1<sup>st</sup> and 2<sup>nd</sup> stages were on, while the turbomolecular pump of the 3<sup>rd</sup> chamber was off.

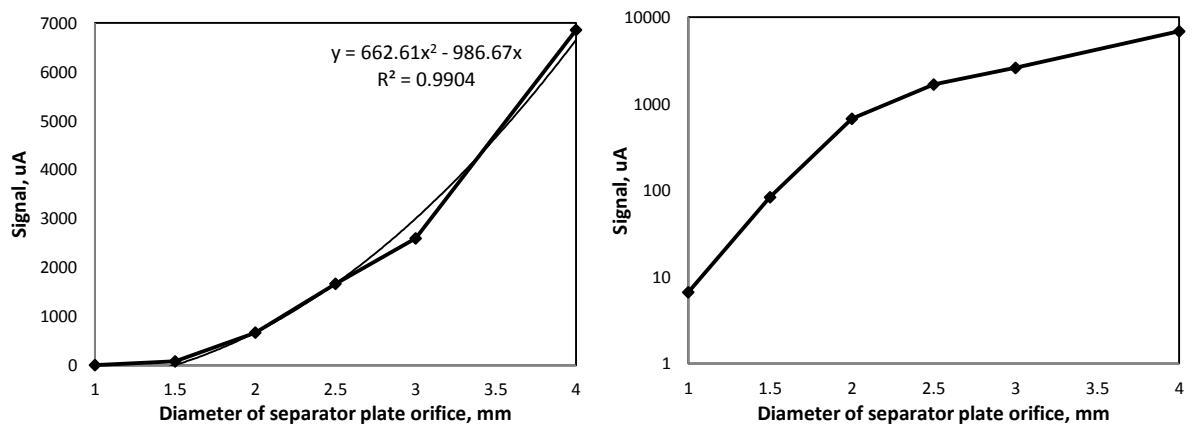


Figure 4.7. Dependence of the measured current on the diameter of the plate between the 1<sup>st</sup> and the 2<sup>nd</sup> pressure stages. Left: linear intensity scale, right: log signal shown. No ion funnel installed, turbo pump off, dry Ar plasma, Detector voltage: -37 V. 1<sup>st</sup> stage pressure 550 Pa.

The dependence of the measured signal on the orifice diameter of the separator plate can be reasonably well approximated by a second order polynomial ( $R^2 = 0.99$ ). On a logarithmic scale (Figure 4.7, right) the most substantial relative increase occurs at the smaller orifices: every 0.5 mm increase of the orifice diameter in the range of 1 mm – 1.5 mm – 2 mm resulted in about 10-fold higher measured signal, while at the larger apertures of the separator plate the signal increase was only 2 – 3 times. It seems surprising that the measured current exhibits such a different trend than the pressure since the ion fraction of ions in the expansion is usually assumed not to vary so substantially across the expanding plasma. It is however rather a result of the gas dynamics of the expansion into the second stage. As can be seen from the photographs in figure 4.8 the visible plasma extends much further into the 2<sup>nd</sup> stage as the aperture size increases.

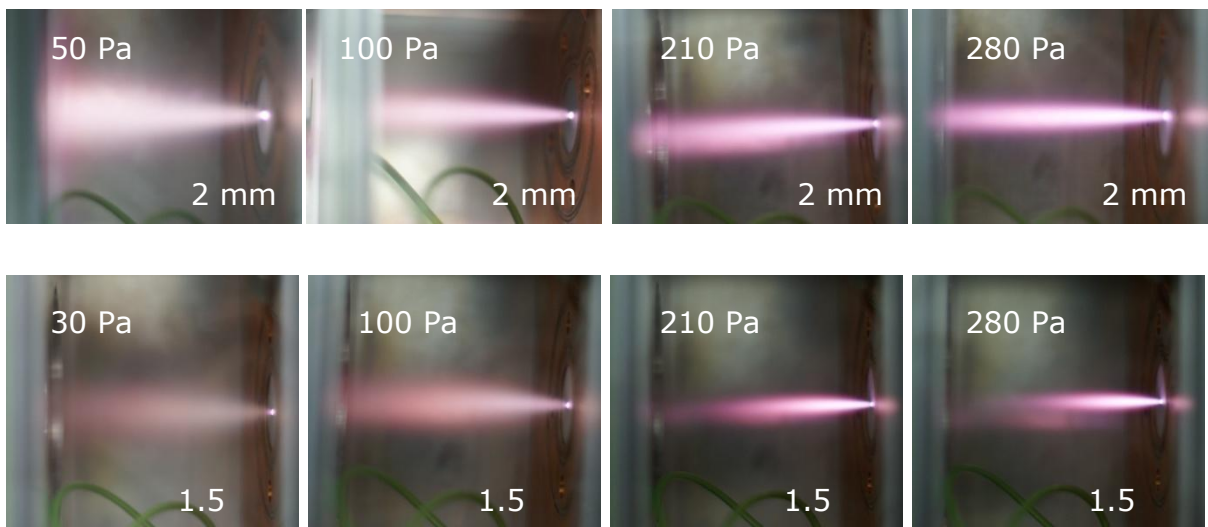


Figure 4.8. Photographs of the plasma beam expansion into the 2<sup>nd</sup> stage at different pressures for exit apertures of 1.5 mm (bottom) and 2.0 mm (top). 1<sup>st</sup> stage pressure 830 Pa.

Similarly, the current measured decreases with increasing pressure in the 2<sup>nd</sup> stage (Figure 4.9) as the plasma appears to remain more confined within higher pressure (Figure 4.10).

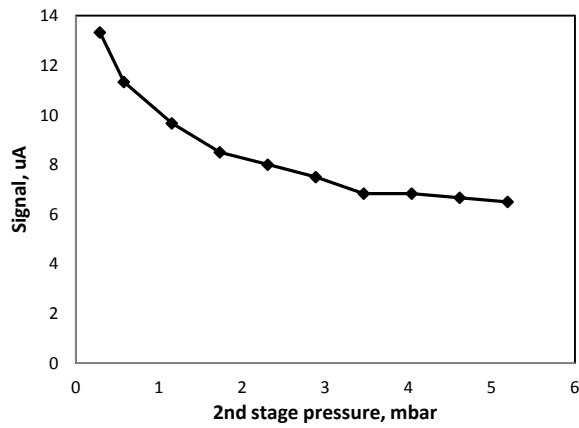


Figure 4.9. Dependence of the measured current on the pressure in the 2<sup>nd</sup> stage with an exit aperture diameter of 1.5 mm. 1<sup>st</sup> stage pressure is fixed at 520 Pa.

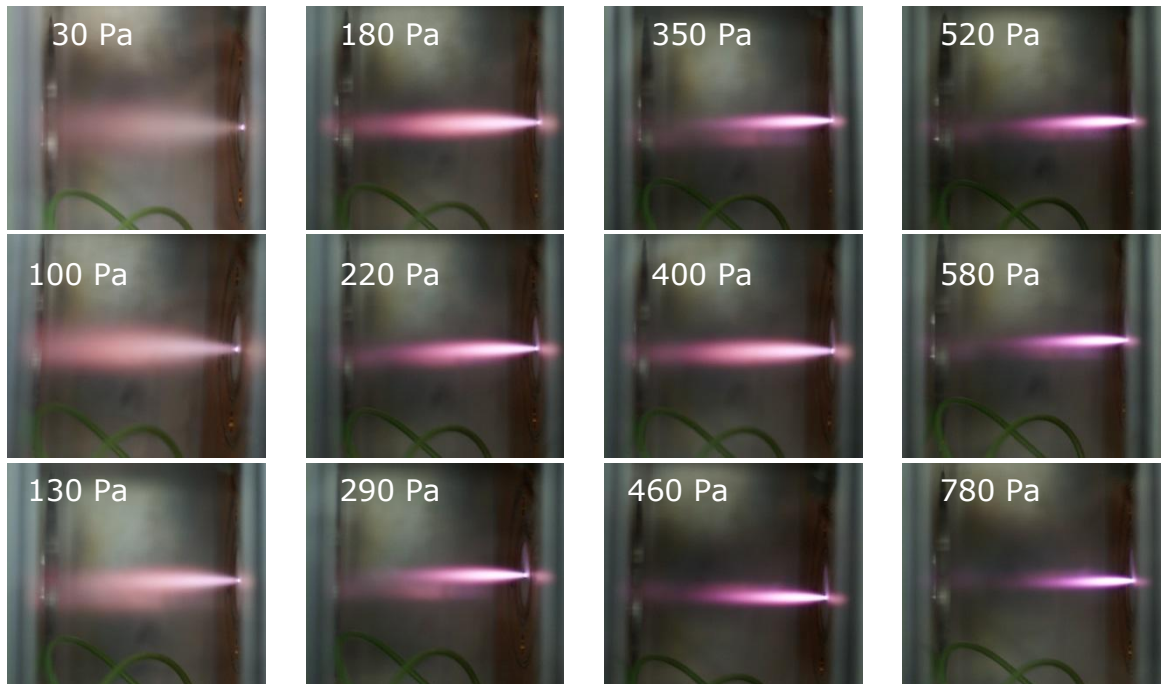


Figure 4.10. Photographs of the plasma expansion in the 2<sup>nd</sup> stage for varying the pressure 1<sup>st</sup> chamber pressure – 830 Pa. Exit plate aperture diameter - 1.5 mm.

Since the pump speed applied in the extraction interface was kept constant in these experiments, a higher pressure inside the 2<sup>nd</sup> chamber reduces the flow through the exit aperture and thus the pressure in the extraction interface increases at the same time. This leads to a compression of the supersonic expansion. As only the pressure in one vacuum chamber could be monitored at a time, it is not possible to quantify this effect. It seems however not to affect the ion current measured in the 2<sup>nd</sup> chamber in the same way as shown in figure 4.9, because increasing the pressure in the extraction

interface (and thus higher pressure in the 2<sup>nd</sup> chamber) leads to increasing currents instead (Figure 4.11). At > 800 Pa pressure in the 1<sup>st</sup> stage, the plasma emission was extending until the detector surface, which is accompanied by significantly more pronounced increase in current.

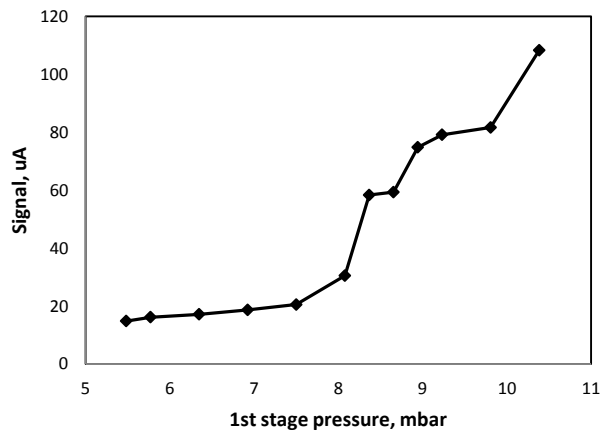


Figure 4.11. Dependence of the measured current on the pressure in the 1<sup>st</sup> stage with 1.5 mm diameter exit plate aperture.

The dependency of current measured with the strip detector far downstream the exit aperture is thus resulting from a convolution of several effects including plasma flow from extraction interface into the 2<sup>nd</sup> chamber, confinement of the plasma inside the 2<sup>nd</sup> chamber due to the pressure in this region and position and potential applied to the detector. High pressure inside the 1<sup>st</sup> stage leads to further penetration of the plasma into the 2<sup>nd</sup> chamber but also higher pressures, which leads to non-proportional increase in current. Reduced pressure in the 2<sup>nd</sup> chamber on the other hand increases the penetration of the plasma and the inflow from the extraction interface and increases the measured current.

### 4.3. Results and Discussions

#### 4.3.1. Influence of Extraction Electrode Potentials without the Ion Funnel

For the extraction interface the orifice diameter chosen should be the one which provides a suitable pressure and a sufficient reduction of the plasma inflow. Based on the current study, the 1.5 mm orifice was chosen as most suitable for the extraction interface. It provided sufficient ion current (10 times higher than the 1 mm orifice) but maintained a dissipated plasma beam in the funnel at a pressure regime which is supposed to be in range of the ion funnel operating pressure.

With the extraction electrodes installed the dependence of current was investigated in dependence on the potential applied the 2<sup>nd</sup> electrode and distance to the exit aperture using the cylindrical detector. The 1<sup>st</sup> extraction electrode, in contact with the expanding plasma was fixed at 5 V.

The detector was positioned at distances between 1 and 8 cm from the exit aperture and then the ion current was measured at different potentials of the 2<sup>nd</sup> extraction plate, while keeping potentials on the front extraction plate (5 V) and the grid (0 V) fixed (Figure 4.12). In these experiments the voltage applied at the detector was varied together with that of the 2<sup>nd</sup> extraction electrode to maintain a potential difference of -70 V in all cases. The current decreased almost monotonously with distance and did not show remarkable dependency on the voltage applied to the 2<sup>nd</sup> extraction electrode. The higher values observed when compared to the previous experiments are the result of the larger detector surface. The major difference is observed when the detector is placed closest to the electrode, where a more negative voltage on the electrode leads to decreasing current, while the slightly higher currents were obtained at greater distance and more negative potential. Especially when the electrode potential was set to less than -60 V however, the profiles for distances > 2 cm are practically identical. More negative values lead to slightly higher currents measured.

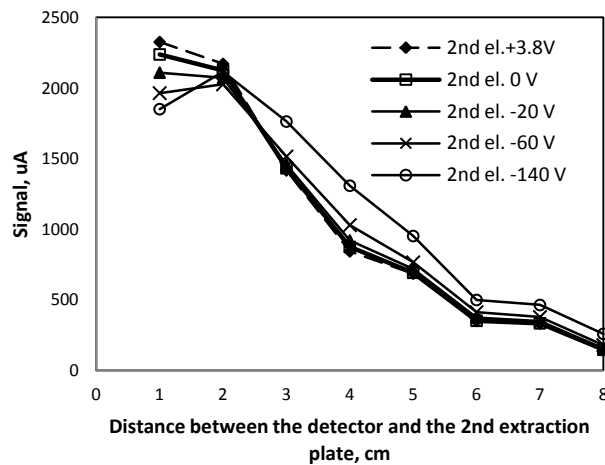


Figure 4.12. The dependence of the measured current on the distance between the extraction interface and the detector for different potentials applied to the 2<sup>nd</sup> extraction electrode. 1<sup>st</sup> stage pressure 550 P, Grid offset: 0 V, 1<sup>st</sup> extraction plate offset: +5 V

The dependence current on the extraction potential for a fixed detector position (Figure 4.13) also suggests that the current measured for 1 and 2 cm is not a simple function of the potentials applied. While at larger distance the current monotonously increases with extraction potential, as suggested by the simulations, an additional effect must occur that leads to higher currents at lower extraction potential when the distance is reduced. It is most likely a combination of lower dispersion of the plasma and reduced ion loss at the extraction electrode, when its voltage is less negative.

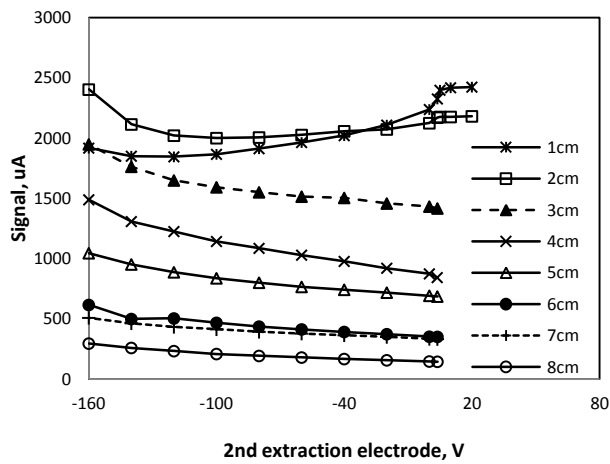


Figure 4.13. The dependence of the measured current on 2<sup>nd</sup> extraction electrode potential for varying distance between extraction interface and detector for. No ion funnel installed, 1<sup>st</sup> stage pressure 550 Pa, Grid offset: 0 V, 1<sup>st</sup> extraction plate offset: +5 V.

#### 4.3.2. Potential on the Electrodes in Expanding Plasma

It was interesting to note that the plasma expansion causes the individual electrodes to assume specific potentials that alternate around 1 V, i.e. close to the assumed plasma potential. With all other electrodes floating, the potential on the first electrode (cylindrical grid) and 2<sup>nd</sup> extraction electrode was below (0.45 V and 0.36 V respectively), while the 1<sup>st</sup> extraction electrodes and detector were above the plasma potential (1.6 and 1.9 V respectively, figure 4.14).

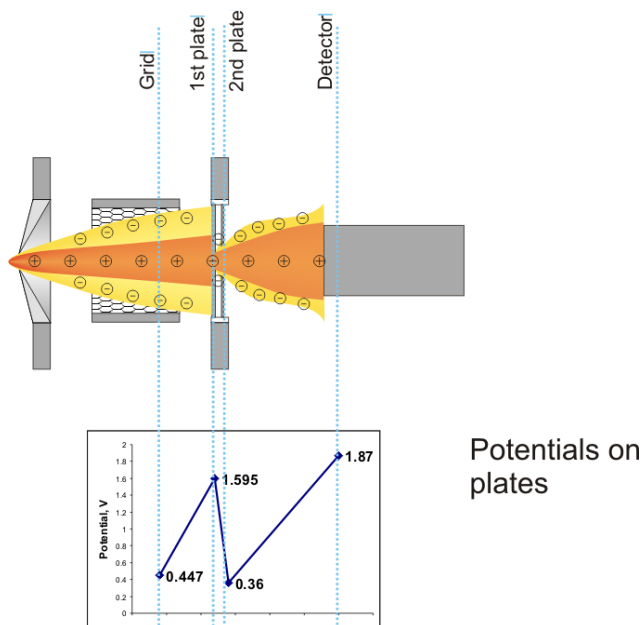


Figure 4.14. The sketch of the electrodes where the induced potentials from the plasma were measured. The potential was measured on one electrode, while the other electrodes were floating.

This must be considered a result of the high electron mobility, allowing them to move further from the axis than the ionic species and thereby reduce the potential in the outer part of the expanding jet. Thus the center of the expansion becomes relatively enriched in positively charged ions leading to a higher potential here. The rapid drop in the potential from 1.6 V to 0.36 over 0.3 mm between the 1<sup>st</sup> and 2<sup>nd</sup> extraction electrode would indicate that the difference in electron and ion mobility in this region is already sufficient to achieve a remarkable charge separation at this stage in the plasma expansion.

#### 4.3.3. The Ion Funnel Installed with Extraction Interface

With the ion funnel placed between the extraction interface and detector the current obtained were dramatically smaller in all experiments. When all funnel electrodes were grounded the current dropped to nA instead of  $\mu$ A as observed previously. Additionally, it was not anymore possible to apply voltages more negative than -100 V to the 2<sup>nd</sup> extraction electrode without creating a secondary discharge inside the funnel region (Figure 4.15). Apparently, even with the full pump speed applied (45 m<sup>3</sup>/h), the pressure inside the funnel region is too high to allow operating the extraction interface in a mode that reduces ion dispersion significantly.

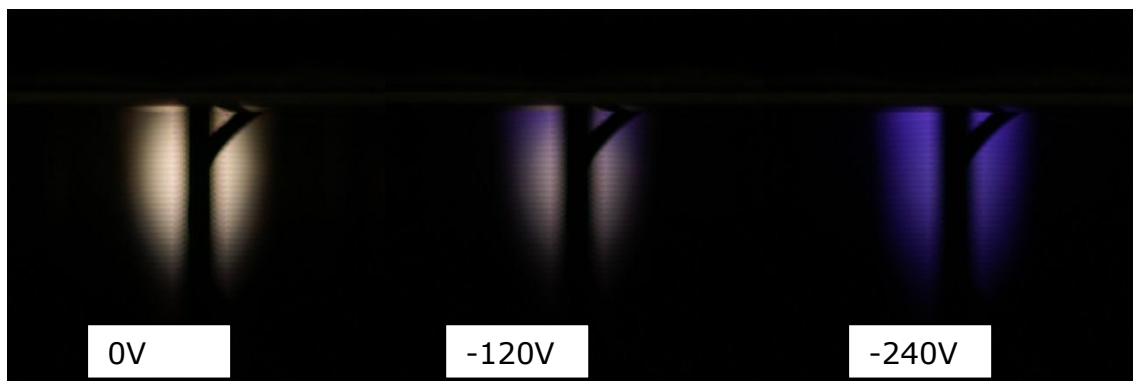


Figure 4.15: Photographs of the ion funnel installed after the extraction interface. The blue shine, appearing at voltages below -100 V applied to the 2<sup>nd</sup> extraction electrode indicates formation of a secondary discharge.

As the previous experiments indicated that higher current through the extraction interface can also be achieved by biasing the 2<sup>nd</sup> extraction interface to positive voltage, this option was explored instead. The initial studies were concerned with the influence of the potentials applied to the three electrodes in the extraction interface. All experiments here were carried out with the turbomolecular pump switched on to increase the transmission from the funnel to the third vacuum stage (Figure 4.4.B). Without this pressure gradient, the currents were lower by at least 2 orders of magnitude. Figure 4.16 show the dependency on the positive offset for the three electrodes with the ion funnel electrodes and detector set to ground potential. In all three cases the highest increase of the current is observed for the applied potential range from 0 V to 5 V. At more positive potential offset the measured current increase



get smoother. It was also notable that due to the electrical conductivity of the expanding plasma the voltage applied to the one electrode was altering the potential of the neighboring electrodes as well. Thus, increasing the voltage at the grid for example led to an increase of the voltage measured at the 1<sup>st</sup> and 2<sup>nd</sup> extraction interface. For the further studies these potentials were thus optimized for highest currents on a daily basis. The optimized potentials varied typically within 1 to 2 V which is largely attributed to minute changes in the plasma potential of the ion source.

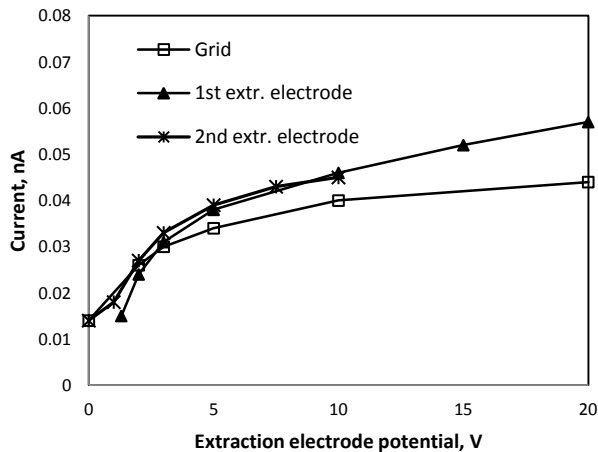


Figure 4.16: Influence of the DC potential applied on the current measured after the ion funnel. All funnel electrodes and detector at 0V potential.

The influence of the potentials along the funnel and the detector was investigated at fixed potential gradient at certain point, which guarantees constant acceleration along the certain electrodes. Two series were measured at constant potential gradient between the plasma and the detector with different forms of the potential field in between and two curves have been measured at constant potential gradient along the funnel, but different acceleration downstream (Figure 4.17).

The 1<sup>st</sup> funnel electrode had a minimal effect on the ion beam since it is located far away from the center of the beam and the initial potential along the ion funnel was mostly determined by the 2<sup>nd</sup> extraction electrode offset. Most crucial for the ion transmission potentials were those at the end of the ion funnel and detector's offset since they determine the slope of the potential field. Therefore the 1<sup>st</sup> funnel electrode for all experiments was set to ground potential.

In figure 4.17 shows the dependence on the last funnel electrode offset at different values of the detector and the 2<sup>nd</sup> last funnel electrode.

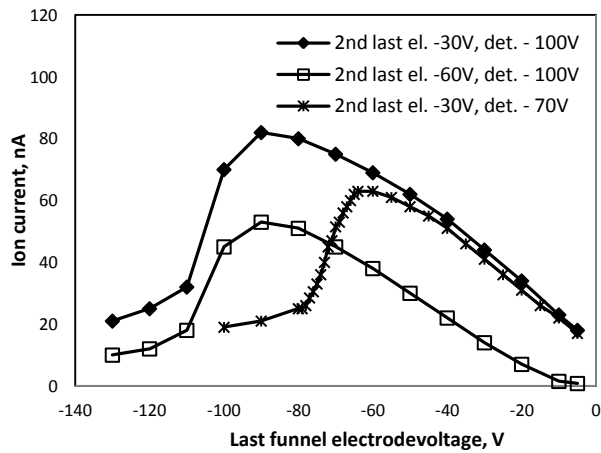


Figure 4.17. Dependence of the measured current on the last funnel electrode potential at fixed 2<sup>nd</sup> last Funnel electrode and detector voltages.

- Turbo pump on.
- Grid +2.7 V,
- 1 extr plate = +3.5 V,
- 2<sup>nd</sup> extr. plate = +4.3 V,
- 1<sup>st</sup> funnel electrode = 0 V,
- 2<sup>nd</sup> last funnel electrode = -30 V or -60 V,
- Detector: -70 V or -100 V.

In all the cases the measured current increases at decreasing last funnel electrode offset until the point, where it is about 10 V more positive than the detector potential. Moving towards negative potentials, there was a steep decrease of the signal until the exit funnel electrode potential was 10 V less than the detector. At this point and farther to more negative voltages, the signal continued to decrease, but much slower. The curves on the plot can be separated into the two groups, firstly when the detector potential was fixed at -100 V and secondly when the 2<sup>nd</sup> last funnel electrode was fixed at -30 V, which creates a constant DC potential along the funnel.

If the detector potential was fixed at -100 V and a comparison of the two curves with the 2<sup>nd</sup> last funnel electrode was set to -30 and -60 V, the main difference was the total ion current, while the shape of the curves were similar. Both curves had the same maximum positions. Hence, the maximum measured current depends on the potential slope between the funnel outlet and the detector. When the potential gradient between the funnel and the detector was less than 10 V, the decrease of the potential field was not enough to attract ions from the funnel and the current dropped dramatically. The overall transmission depends on the potential field at the end of the ion funnel. A 30 V difference between two last funnel electrodes gave ~30 % lower signal than when the difference was 60 V. To pull ions out from the funnel the potential gradient between the last two funnel electrodes should be as high as possible. Otherwise ions will be lost on the funnel walls due to their high concentration at the funnel exit.

When the funnel DC gradient (potential gradient between the 1<sup>st</sup> and the 2<sup>nd</sup> last funnel electrodes) was fixed at 30 V, the maximum ion transmission was determined by the detector voltage. Both curves at the 2<sup>nd</sup> last ion funnel electrode and the detector potentials -70 V and -100 V have similar slopes until a -50 V offset on the last funnel electrode was reached. But the maximum transmission for both cases occurs when the last funnel electrode was set 10 V higher than the detector.

Therefore it is preferable to have a mean DC gradient within the ion funnel, and approximately 30 V difference between the last two ion funnel electrodes, with the detector set to 10 V less than the last funnel electrode.

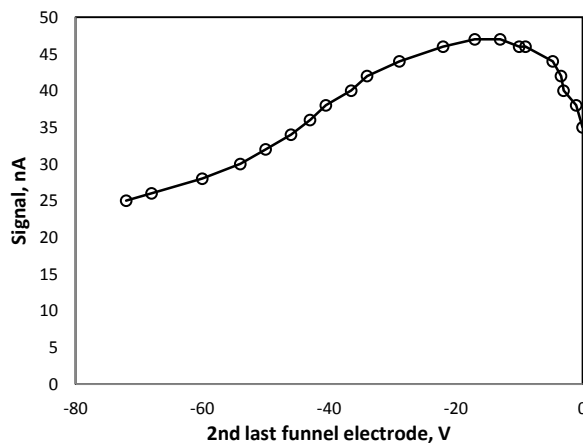


Figure 4.18. Dependence of the measured current on the 2<sup>nd</sup> last funnel electrode potential at fixed other voltages. Last ion funnel electrode: -60 V. detector potential: -70 V.

With a potential of -70 V applied to the detector, the measured current could be increased in dependence on the DC gradient applied along the funnel determined by the 2<sup>nd</sup> last funnel electrode potential (Figure 4.18). Currents of up to 50 nA were obtained.

However addition of the RF field to the ion funnel always led to instantaneous loss of current. Figure 4.19 shows this as an example for 600 kHz frequency and different pressures in the funnel chamber. Frequencies up to 2 MHz were tested but did not show substantial differences in the profiles. A major influence however was obtained when varying the pressure in the funnel chamber, with lower pressure (87 Pa, figure 4.19) leading to higher current than operation at 100 or 200 Pa, where similar currents were obtained. RF-amplitudes higher than 100 V however resulted in almost indistinguishable currents independent on pressure. From these results it appears that the largest fraction of ions is already lost within the ion funnel and this fraction increases with higher pressure due to collisional cooling of ions with the axial motion. Thus a successively smaller fraction of the ions has sufficient kinetic energy to proceed beyond the effective potential at the funnel exit at increasing RF amplitudes.

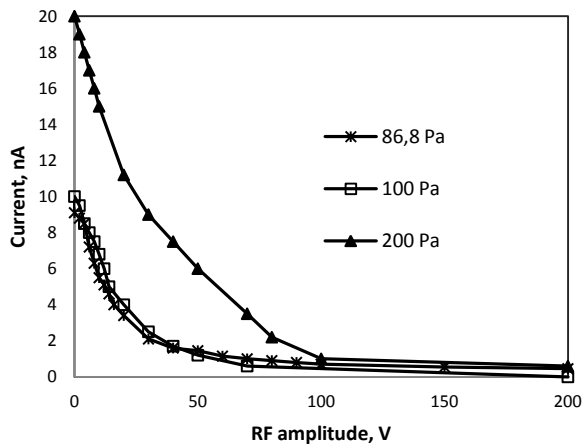


Figure 4.19. Dependence of the measured current on the RF amplitude (RF frequency – 600 kHz) at different pressures in the 2<sup>nd</sup> chamber. Potentials of the electrodes: grid 1.5 V, 1<sup>st</sup> extraction electrode 2V, 2<sup>nd</sup> extraction electrode 2.3 V, 1<sup>st</sup> ion funnel electrode -5V, 2<sup>nd</sup> last ion funnel electrode -30 V, last ion funnel electrode -60 V, detector potential -70 V.

#### 4.4. Angular Resolved Current Measurements

To investigate additionally the angular spread of the ions exiting the ion funnel, the Faraday type detector was exchanged by the detection system rotating relative the exit aperture. The detector surface was biased by -10 V relative to the front screen in order to ensure almost complete collection of the ions while maintaining the angular resolution, while the screen was adjusted relative to the potential applied to the funnel exit aperture. This approach was chosen to test which fraction of ions can be collected at the various angles. Low energy ions leaving the funnel would be also detectable at more negative potential applied to the detector surface even when they are outside the solid angle formed by the funnel exit and the square opening of the detector. The extraction interface electrodes were set to constant values during all these studies: the grid was set to +0.75 V, and both extraction plates were set to +2.5 V. The first studies were carried out without RF field applied when changing the DC gradients along the funnel. Like in the previous experiments, the first funnel electrode was maintained at ground potential and the gradient adjusted by varying only the voltage applied to the funnel exit electrodes. The last two electrodes were set to identical potential. The potential applied to the detector screen (further on termed “Delta Potential”) was applied relative to the funnel exit electrodes, i.e. a delta potential of -60 V with a DC-gradient on 60 V for the ion funnel correspond to an absolute voltage of -120 V at the detector screen and -130 V at the measurement electrode. As expected, ion currents maximize for the axial position of the detector. With increasing detector angle, the signal rapidly decreased until an angle of 7 degrees was reached (Figure 4.20). For wider angles, the signal decrease was usually far less pronounced and depended significantly on the delta potential and DC

gradient applied in the funnel. The widest spread was observed for the fully grounded ion funnel with the highest delta potential applied. With a DC gradient of 60 V on the other hand there was almost no dependence on the delta potential anymore. The maximum measured current at the axial position of the detector was also dependent on the DC gradient: the highest signal was measured with the grounded funnel while at a DC gradient 60 V the maximum measured current was similar to the case when the delta potential was 0 V, independent of the potential field between the funnel and the detector.

#### 4.4.1. DC Influence

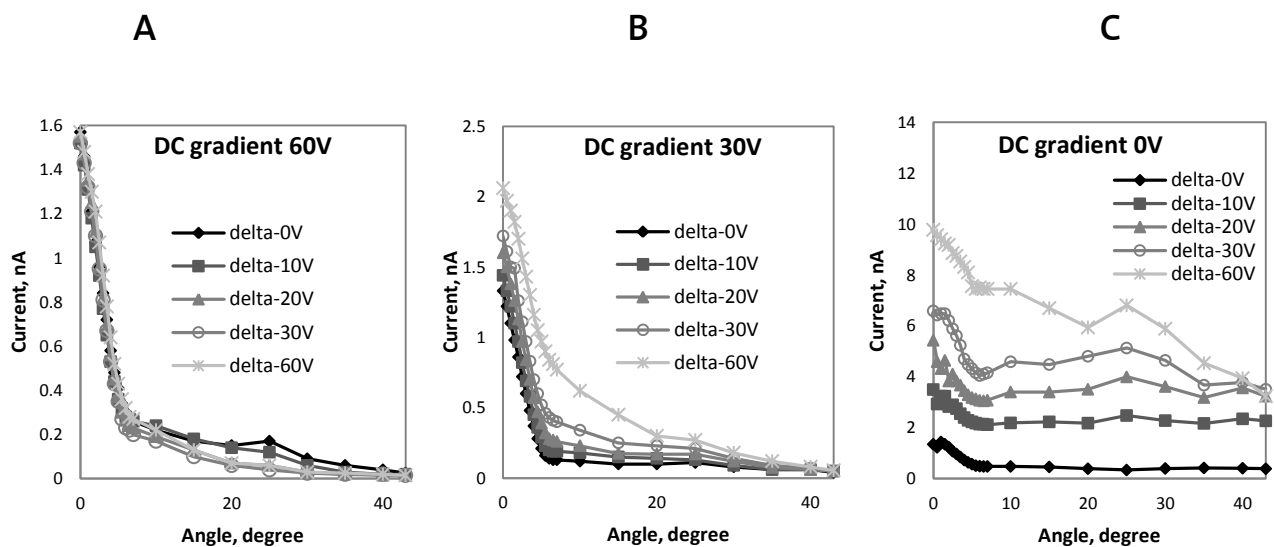


Figure 4.20. Dependence of the measured current on the DC voltage and the Delta potential between the ion funnel and the front foil without RF field. Dry Ar, DC gradient – 0 V (C), -30 V (B) or -60 V (A). 1<sup>st</sup> chamber pressure – 520 Pa, 2<sup>nd</sup> chamber pressure – 50 Pa.

With zero DC gradient, the measured ion current was strongly dependent on the delta potential between the funnel and the detector. Moving the detector screen potential towards negative values increased the ion current not only in the axial direction, but also at off-axis positions. As a result, a broad angular distribution was observed (Figure 4.20.C).

The additional DC field suppressed the maximum ion current at the axial position and especially the “tail” towards 45 degree angle relative to the axial position. At about 7 degrees there was a point of inflection of the signal curve. At higher angles, the ion current maintained very low values although the current could be increased by increasing the potential gap (Delta potential) between the funnel outlet and the detector (Figure 4.20.B). At higher DC fields, ions were less sensitive to the potential gap after the funnel, and the ion current was almost the same for all the delta values (Figure 4.20.C).

The ions insensitiveness to the potential gap after the ion funnel can be a result of their kinetic energies. Without any DC voltage applied, ions leave the funnel with a low axial energy. The negative potential of the detector (or front foil in this case) attracts these slow moving ions. Since the ions do not leave this region quickly enough in an axial direction, the negative potential field of the detector could attract most of the ions even from off-axis position, which resulted in a broad tail in the angular distribution graph.

The higher DC field resulted in an acceleration of the ions axially towards the ion funnel outlet. Since the axial component of the ion velocity was higher, the same negative potential on the detector in off-axis positions produced the same mean radial velocity component with less displacement of ions from their initial trajectory. Therefore a higher DC gradient should result in less tailing, and that was observed in this case (Figure 4.20 C-B-A).

It was observed that the total measured ion current decreased with increasing DC gradient. All the series have the same fast drop of the ion current from 0 to approximately 7 degrees, and then there was a point of inflection, and then there was a tail. The difference between the maximum ion current and the current at the inflection point was almost the same for all series – at about 1.5 nA. So it could be that there are two populations of ions: slow ions that can be attracted by the negative detector offset and fast ions that have almost the same spread and are not sensitive to the detector potential. The DC gradient cuts off part of the slow ions while the fast ions remain, and pass to the detector.

It also could be that the ion funnel does not affect the central ion beam. There should be a higher pressure inside the funnel than outside, so ions may isolate the central part of the beam from the external field. The funnel outlet has a 3 mm diameter that is significantly larger than the Debye length. As a result the ion beam passes through the funnel undisturbed and has a constant contribution to the total ion current measured. Other parts of the beam may pass through or be lost on the funnel walls depending on conditions.

#### **4.4.2. RF Influence**

The applied RF field should create potential barriers at the funnel walls, which theoretically should lead to better ion confinement within the funnel, but based on the results in figures 4.19 instead lead to a reduction in the measured signal. A more detail investigation of the ion expansion downstream of the funnel outlet is presented in figure 4.21.

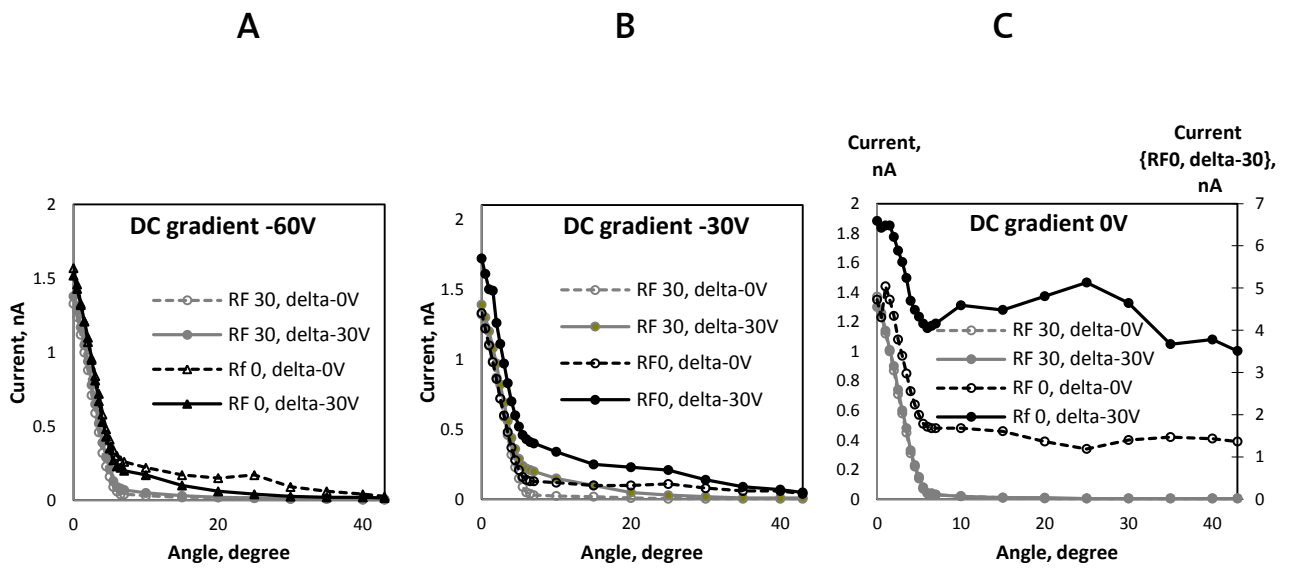


Figure 4.21. Dependence of the measured current on the RF field and Delta potential.

Dry Ar, RF amplitude – 0 or 30 V, DC gradient – 0 V (C), -30 V (B) or -60 V (A).

The angular dependence of the measured current in the presence of a RF field basically has the same shape as it had without the RF field. There was a dramatical decrease of the measured current from the axial position to the  $\sim 7$  degree radial displacement of the detector. When the detector was set outside this angle, then the signal forms a “tail” towards 45 degree with an almost linear decay of the intensity.

The similarity was more pronounced for the data at higher DC fields, since the effects of the DC and RF fields were similar. There measured current with the similar axial intensity of about  $\sim 1.5$  nA decreases dramatically towards the 7 degree displacement of the detector. The points of inflection of both dependencies are the same, though the signal at the greater angular displacement is lower when the RF field is applied than with the DC field. The charts with the RF field applied appear to be similar to the limiting case of the applied DC field. At the greater DC gradients the curves were shifted downward towards the curves with the RF field applied. There was no significant difference between the curves at different DC fields when the RF field was applied. The measured current was also insensitive to any difference in the DC gradient and the extraction voltages on the metal sheet.

There are two possible explanations for the effect of the RF field. One is that a more dense ion flow at the ion funnel exit resulted in a larger space-charge effect and consequently in the ion loss. But this could also result in a broader angular distribution of ions at the funnel exit. On the other hand it is possible that low energy ions were trapped within the potential walls formed between the electrodes and only central part of the beam was transported through the funnel.

The DC voltage of -60 V (Figure 4.20.A) was similar to that of the RF field (both series). This could be due to the limitation that only the central axially directed ion beam can pass the potential barrier at the funnel exit and reach the detector. A very low tail of all curves suggests that expansion after the ion funnel exit was not significant. Otherwise a broad visible tail should be observed as was observed for a DC of 0V and a Delta of -60 V (Figure 4.20.C.).

The same limitation on the total ion current transmitted can also be explained as energy discrimination. Only the ions which have an energy sufficient to break through the potential walls at the ion exit can pass the ion funnel and move towards the detector.

#### 4.4.3. Comparison of Dry Plasma and Wet Plasma

Since the influence of the RF field was very different for the dry argon plasma and wet plasma, it was very important to find an explanation for this. Knowing the angular distribution of ions could help to add clarity to knowing at which point the ions were lost.

For this purpose the data for the dry argon plasma was compared for the same conditions, but when the blank solution has been sampled into the plasma. The result is presented in figure 4.22.

*Dry Ar vs Blank*

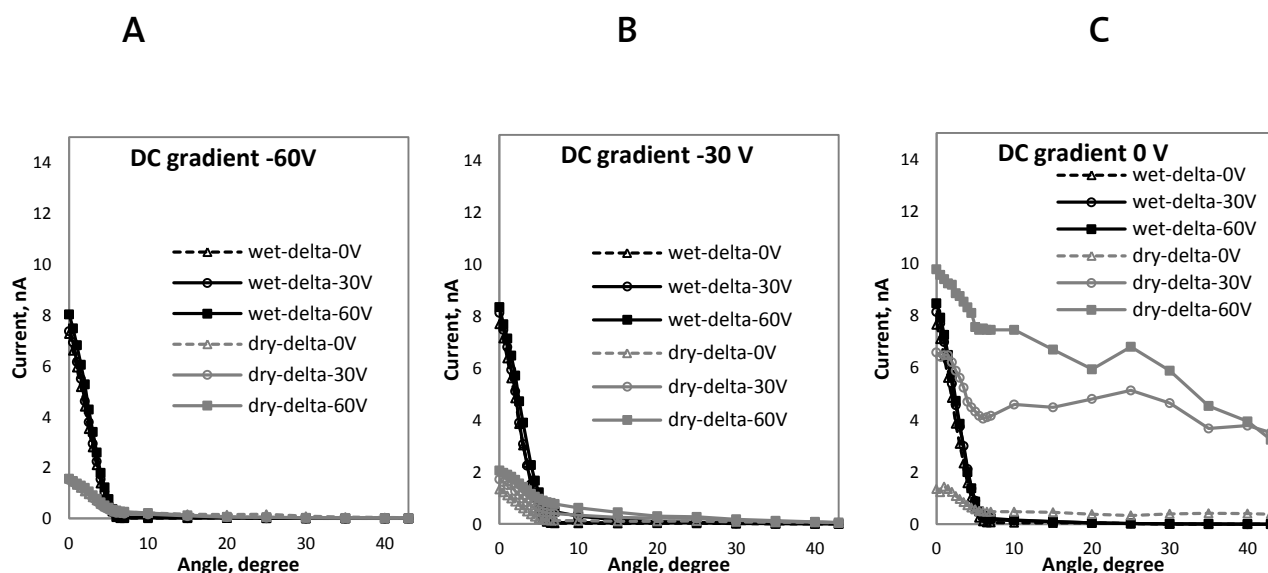


Figure 4.22. Dependence of the measured current on the detector angle at different Delta potentials and plasma humidity with the installed metal sheet in front of the detector.

Dry Ar (dry plasma) or nebulized 1% HNO<sub>3</sub> (wet plasma), RF amplitude 0 V, DC gradient – 0 V (C), -30 V (B) or -60 V (A).



As previously described, the ion distribution of the wet plasma was similar to the distribution in the dry argon plasma. There was a steep decrease of the measured current till  $\sim 7$  degrees. At displacements of the detector farther off axis than this, the signal drastically decreases.

The main difference of wet plasma from the dry argon plasma was the intensity of the measured current on-axis position and the “tail” observed at the angles of more than 7 degrees. The intensity of the measured current of the wet plasma in the center of the expanding beam was  $\sim 5$ -fold higher than the current of the dry plasma at the same condition, observed at the flat potential field between the funnel and the foil. The “tail” was closer to zero, resulting in a lower signal even at small displacements of the detector at angles greater than 7 degrees.

The ion motion is strongly dependent on the plasma composition. That means that the addition of the solvent to the plasma will change temperature, pressure, ion energies, and consequently the ion distribution. Corresponding to the data in [31] the water in the central part is present in form of atomic hydrogen and atomic oxygen. Due to the higher thermal conductivity of hydrogen the thermal conductivity of the mixture is higher in presence of the water. Therefore the temperature of the central channel is expected to be higher for the wet plasma. This fact was also confirmed by the experimental measurements of the pressure, which always slightly decreased when the blank solution was nebulized (531 Pa for dry Ar and 517 Pa for the wet plasma in the 1<sup>st</sup> pressure stage).

The increased plasma temperature in the central channel of the expanding beam leads to higher ion kinetic energy. Therefore higher kinetic energies should be more effective in breaking the potential barrier of the ion funnel if the energy discrimination hypothesis is taken into account. This results in a good agreement with experiment. Under the same conditions (DC gradient, Delta value) the total ion current was approximately 5 times higher in the presence of the blank solution than for the dry Ar only (Figure 4.22.C.).

The low tail and the insensitivity of the signal to the Delta and DC gradient also contributed to the assumption that ions have higher energy in a higher DC gradient.

#### **4.4.4. Influence of the Potential Gap Between the Ion Funnel and the Extraction Plate (Delta)**

The potential gap between the ion funnel exit and the detector (Delta) has a significant value but only for low energy ions (Figure 4.20.C.).

If it was assumed that a broad cloud of slow ions was leaving the ion funnel then a relatively strong negative field on the metal sheet should attract these ions to the detector. Even the ions that had trajectories off the central axis could be driven to the detector if their initial velocity was low.

In the case of accelerated ions (with applied DC gradient – Figures A and B) the ion motion was more directed and the time during which ions were exposed to the field was shorter. As a result these ions could not be trapped at angles larger than the natural beam width at the same values of the Delta

potential. As a result, only minor differences were observed for different Delta potentials at high DC gradients, applied RF fields, or with a wet plasma (Figures 4.22).

#### 4.4.5. Pressure Influence

Pressure changes when the turbomolecular pump was on or off did not have a significant effect on the angular distribution of the ions. However, the total ion current was slightly higher when the pump was off. This might be because of the higher density and therefore reduced expansion of the ion beam after the exit from the funnel. The higher pressure would then result in a secondary discharge between the detector surface and the metal sheet when the sheet was floating and the detector was set to a potential of less than -20 V.

#### 4.5. Conclusions

The addition of the additional pressure stage before the funnel resulted in a decrease in the pressure in the 2<sup>nd</sup> stage by at least one order of magnitude, which makes the pressure in this stage suitable for the use of the ion funnel. The pressure in the 1<sup>st</sup> and 2<sup>nd</sup> stage can be regulated by the pumping efficiency and the orifice diameter of the plate separating 1<sup>st</sup> and 2<sup>nd</sup> pressure stages.

The choice of the aperture was determined by monitoring the pressure and the measured current. Since the plasma beam expanded in the 1<sup>st</sup> pressure stage and had a radially diffuse structure, the dependence of the pressure in the 2<sup>nd</sup> chamber on the pressure in the 1<sup>st</sup> chamber was a linear relation to the orifice diameter instead of being proportional to the area of the aperture. The measured current increased one order of magnitude when using a 1.5 mm orifice compared to using a 1 mm orifice. When changing from the 1.5 mm orifice to the 2 mm orifice the increase was small. Consideration of these two factors and the need for appropriate pressures resulted in the choice of a separator plate with a 1.5 mm orifice diameter.

The extraction interface, which was initially modeled using Simlon, consisted of two extraction plates and an additional circular grid which surrounded the expanding plasma. Although the Simlon model predicted efficient focusing at the 2<sup>nd</sup> extraction plate, no significant improvement was found with negative potentials on the 2<sup>nd</sup> extraction plate. It appears that the plasma density at this stage was too high, so that the plasma created an electrical conductive connection between all the electrodes of the extraction interface. This made it ineffective to apply potentials to the extraction interface, which were significantly different from the potential of the plasma, which was assumed to be approximately +2.5 V for the conditions used. The maximum of the measured current was observed when all of the electrodes of the extraction interface had potentials near to that of the plasma.

The influence of the extraction electrode potentials on the measured current was significant only when no further driving force was applied to the system. Then increases of up to 7 times were obtained

by setting the potentials on the extraction interface to  $\sim +5$  V. The gain of the signal was only a few percent when a potential gradient was applied to the ion funnel.

The most important effect on the measured current was the potential gradient between the 2<sup>nd</sup> and 3<sup>rd</sup> pressure stages. It was found, that the most crucial point in the ion funnel was the exit. There the DC gradient along the funnel can be moderate, but the gradient between the two last funnel electrodes have to be at least 20 V. This negative well at the funnel exit provided an effective force to pull ions from the funnel. The same potential was applied to the region between the ion funnel and the detector. The potential barrier significantly decreased the measured signal and, for the efficient collection of ions after the funnel, the detector needed to be at least 10 V less than that of the last funnel electrode. A greater potential gradient was not necessary since no significant gain of the signal was achieved. Taking into consideration the quadrupole limitation to operate with low energy ions, further acceleration using a negative detector offset was not necessary and was undesirable.

The RF field was not found to have a focusing effect, although no electrical breakdown occurred up to an amplitude of 200 V. This confirmed that the plasma density was reduced so that there was no conductive media within the funnel. The humidity of the plasma was very important for the experiments with the RF field applied. With the dry Ar plasma, the signal drops dramatically with an increase in the RF amplitude while for a wet plasma (with a nebulized blank solution) the signal was insensitive to the RF field. This difference reveals the dependence of the number of ions, which were lost inside the ion funnel, on their kinetic energies. The kinetic energy of the ions determines the ability of ions to penetrate the potential barriers created by the RF field along the funnel walls. In the case, where the ion funnel was limited to the maximum transmission, any additional disturbance such as thermal movements would cause a space-charge effect on the increased width of the potential walls from the increase in the RF amplitude which would cause an additional ion loss.

It is possible that the reason for the failure with the confinement effect using the ion funnel was that the pressure inside the funnel was too high. The measured outside pressure was around 90 Pa, but within the funnel it was expected to be several times higher [70]. Too high of a load to the funnel (1.5 mm orifice between the 1<sup>st</sup> and the 2<sup>nd</sup> chambers instead of 0.8 mm of the skimmer orifice) could result in an overload in the funnel. Sub-optimal geometry in the funnel may be also a reason for the system being far away from the conditions, where the ion funnel can use its benefits as an ion guide. A more detail study of the effect of both DC and RF field is needed to understand how these fields change the ion beam, and to understand the role of the water vapor in the plasma.

Applying a DC gradient along the funnel or the RF-field to the electrodes significantly suppressed the ion current and the ion spread after the funnel exit. The axial ion current had the same limit of approximately 1.45  $\mu$ A for the highest RF and DC voltages. This can be explained by the energy or the direction of motion discrimination. Low energy ions that do not move axially are lost by collision with the ion funnel walls due to DC potential acceleration or by trapping within potential walls formed between electrodes.

A focusing effect of the RF-amplitude was not apparent in either wet or dry plasma conditions, indicating that the ion current at the funnel exit aperture was limited by space charge effects.

The kinetic energy distribution was related to plasma conditions. Increasing humidity of the plasma lowers the temperature and enhanced the abundance of ions with higher kinetic energy. As a result a larger number of ions had an energy high enough to pass through the potential barriers and be detected and were less deflected by the space-charge effect inside the funnel. This energy distribution for the wet plasma was less sensitive to the operating conditions of the ion funnel.

Since all the applied fields resulted in a reduction in the measured current, the ion funnel was most likely already limited to the highest ion transmission. Most of the ions, which have an axial direction of the movement inside the funnel will pass through the funnel orifice and be detected. Therefore, an increase of the initial kinetic energy by the water vapor in the plasma results in the higher signal. When the initial kinetic energy was small (ions were thermalized within the funnel), an additional field lead to ion losses. When it was the DC field, the ions were accelerated towards the funnel electrodes and were lost by collision with the funnel walls. When the RF field was applied, a large fraction of ions were lost by being trapped in the potential wells. As a result, in both cases only those ions, which have an initial axial direction and high enough energy, can pass through the funnel. Other were deflected and lost.

Based on these measurements, future studies need to be performed at lower pressures in the 2<sup>nd</sup> chamber. It would also be useful to alter the parameters of the funnel, even though these parameters are restricted by the pressures, which must be maintained in order to be able to use turbomolecular pumps and a quadrupole mass analyzer.

## 5. Plasma Extraction through a Nozzle Interface.

---

### 5.1 Introduction

A divergent nozzle expands from a small diameter aperture to a wider opening in the direction of flow. It provides a transformation of the thermal energy of hot plasma into directed flow due to the pressure difference across the axis of the nozzle [34]. The traditional ICPMS sampler cone can be considered as a special case of a nozzle with large opening angle. The expansion of the plasma downstream of the sampler occurs with an acceleration of the plasma to supersonic velocities accompanied by the formation of a barrel shock structure and a perpendicular Mach disc.

The principle of the supersonic expansion in an ICPMS interface for an ideal gas was described by Douglas and French [34]. The expanding plasma passes into a region of reduced pressure and expands. During this process the kinetic energy of the gas is converted into directed motion causing cooling and acceleration. Since the flow static pressure at the nozzle exit is higher than in the surrounding chamber, the flow expands until it reaches the background pressure forming a barrel shock structure and developing a sheath layer, where the background gas penetrates into the jet core [84]. The barrel shock structure ends up with a Mach disc perpendicular to the jet axis. Subsequent weaker Mach discs can also be formed when the expanding gas is reheated in and sufficiently accelerated to become supersonic again until another structure is formed.

The gas flow parameters are influenced by the pressure and temperature of the plasma and the nozzle geometry. It has been found, that for given operating conditions there is an optimal cross-sectional ratio of a nozzle exit to throat (expansion ratio), which significantly reduces the shockwaves downstream the nozzles. The expansion ratio is typically larger for higher 1<sup>st</sup> stage gas pressure and nozzle divergent length and smaller for higher gas temperatures and nozzle throat diameter [85,86].

In the conventionally employed sampler-skimmer interfaces the skimmer tip is located inside the zone of silence to minimize the influence of the secondary processes occurring within the shock structure. Omitting the skimmer leads to the formation of the Mach disc (chapters 3 – 4) before the ions are introduced into the next vacuum stage. A reduction of the effect of the shock structures in the 1<sup>st</sup> vacuum chamber may be achieved by implementing nozzles, providing a smoother expansion of the plasma jet.

Such an approach has been proposed in [87] already in combination with an ion funnel for cooling and confining a high energy ion beam (Figure 5.1).

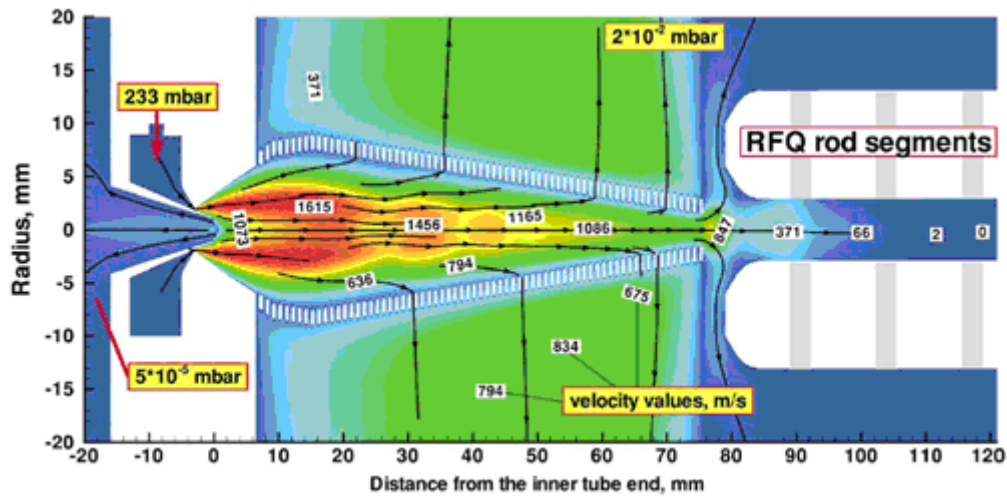


Figure 5.1. The scheme of a nozzle-based extraction interface with ion funnel for high energy ion cooling, including numerical simulation of gas velocities in the expansion [87].

In this configuration ions are carried by the supersonic jet out of the nozzle and enter the RF-only ion funnel. The RF funnel is here used as a filter to remove excess buffer gas, without need for a skimmer cone.

Such a smoother and narrower expansion of the plasma should result in a less pronounced or at least smoother shock structure, which should decrease the interaction of ions with a background gas. A smoother gas expansion should thus prevent ion recombination and the secondary ion formation within the boundaries of the shock structure. The smoothness of the expanding beam is a function of the nozzle geometry and thus a detailed investigation was carried out to determine suitable nozzle geometry and to understand the effect of the nozzle opening angle on the shape and electric characteristics of the expanding plasma. Visual observation of the jet and measurements of the ion current profiles vs. distance was carried out in order to determine the shape and the degree of expansion of the plasma jet. Additionally, ICPMS spectra were acquired with different nozzle geometries to determine changes in the ion composition and kinetic energies for the conventional sampler and nozzle-based vacuum interface.

## 5.2 Experimental

The experiments were carried out on two different instruments. Optical investigation and total current measurement of the plasma were carried out using the experimental setup described in chapter 4. The system was operated without the additional extraction interface and the sampler and nozzles were mounted directly in the water-cooled copper front plate. Electric currents were measured with different configurations, depending on the experiment. For measurements of total transmission through the sampler or nozzles the cylindrical steel rod the same as previously was used. For analysis of

the currents on and through the skimmer a specific holder was made that allowed positioning the skimmer at variable distance relative to the sampler or nozzle orifice. This holder consisted of a threaded tube of 39 mm outer and 35 mm inner diameter, with a thread lead of 1 mm. It was made from anodized aluminum for electrical insulation from the housing. Electric contact to the skimmer allowed an electric potential to be applied and to register the electric currents in dependence on axial position of the skimmer within the plasma expansion. A second detector electrode could be placed inside the cylindrical holder to allow measurement of the current transmitted through the skimmer cone as well. This detector consisted of a stainless steel rod mounted in a wheel-like support fitting exactly inside the skimmer holder. The end facing towards the skimmer aperture was equipped with either a 0.5 mm or 10 mm diameter plate for charge collection. The front of this plate was in all cases positioned at the skimmer base. Currents were measured by an ammeter (414S Picoammeter, Keithley Instruments, Cleveland, USA) connected via feed throughs to the skimmer holder ("outer current") or central electrode ("inner current"). The first chamber vacuum was maintained by the S25B rotary vane pump and the TurboVac 361 turbomolecular pump was connected to evacuate the second chamber when required. Pressure in the first chamber was monitored by the Baratron absolute pressure gauge. ICP operating parameters were identical to those used. Figure 5.1 shows a sketch of the instrumental set up with the inner detector installed.

Measurement of the inner and outer currents was carried out in the following way: first, the nozzle or sampler was installed and the ICP started. Then the ion current was measured with the turbo pump off depending on the detector offset. After 6 minutes warm up the voltage on the inner or outer electrodes was adjusted and the current registered for different potentials. Then the turbo pump was turned on, the system was allowed to stabilize for 10 minutes and the same series of measurements was repeated. After this the plasma was turned off and the nozzle / sampler were changed. Since the skimmer holder was not water cooled, skimmer and holder heated up when in contact with the plasma expansion. Thus, at least 30 min cool down was required before an experiment with another nozzle or different position of the skimmer was started. To avoid a temperature influence on the measured current, all the data were acquired during the same time interval after the plasma had ignited. Typically, 30 s were required to acquire the data unless the current was near zero and correspondingly exhibited a greater noise. The delay, however, was never longer than 1 min. The signal fluctuation was typically in order of 5% and the mean value was recorded.

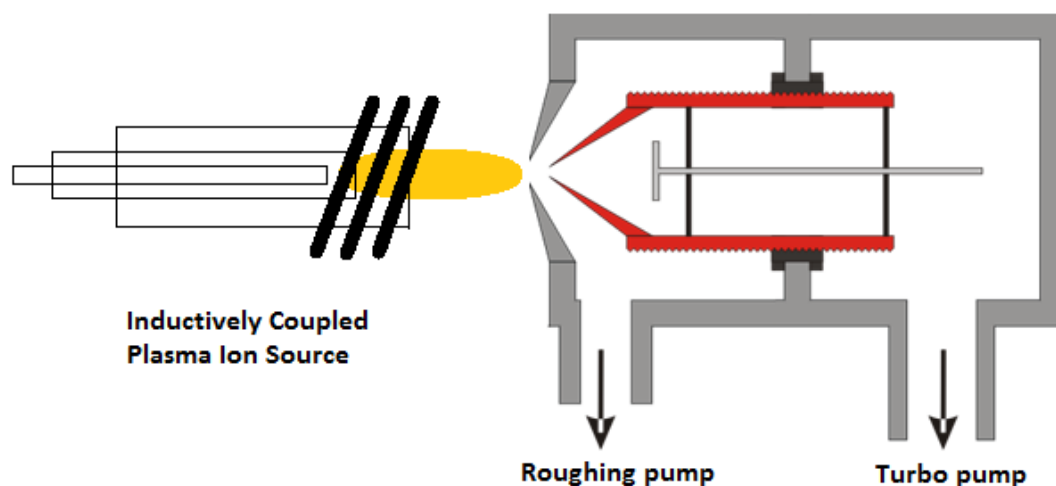


Figure 5.2. Sketch of the instrumental setup with the adjustable skimmer and the inner electrode for current measurements. Red part: Detection zone of the “outer current”. Grey inner electrode for the “inner current”.

Photographs of the expanding plasma were taken with a digital camera (Sony A100) through the glass plate covering the two vacuum chambers. Acquisition parameters and observation distance were kept constant for all photographs (ISO 100, focal length 200 mm, exposure 0.6 s, F Number f/20, manual exposure program, auto white balance)

### 5.2.1. Nozzles

A series of nozzles with different opening angles were constructed in a way that a base holder was made, where interchangeable inserts could be placed inside. The base had the same outer dimensions as the standard sampler and was manufactured from stainless steel (Figure 5.3.). The inserts were inserted into the holder from the top without further sealing. Nozzles with angles of 7, 8, 10, 15, 20, 25 and 30° and the standard sampler with an opening angle of 56° were used in the experiments. All nozzles have an orifice diameter of 1.1 mm, identical to the standard sampler.



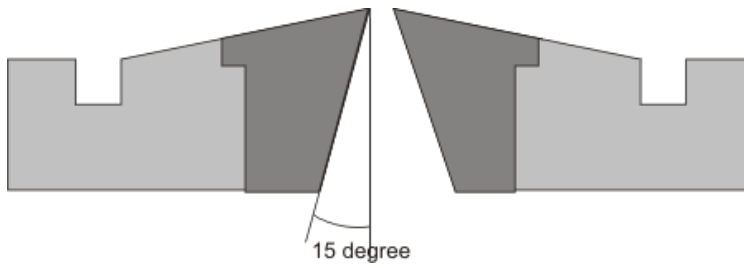


Figure 5.3. The sketch of the 15° nozzle with the exchangeable core (dark grey) mounted into the holder (light grey).

### 5.3 Results and discussion

#### 5.3.1 The plasma expansion as a function of the nozzle opening angle

Images of the plasma expansion into the first vacuum chamber, held at 520 Pa, are shown in figure 5.4 for different nozzles in comparison to the conventional sampler. It can be seen that the opening angle has a clear influence on the structure of the expansion and the intensity of the emission in the Mach disk and barrel shock. The narrower the nozzle exit, the more confined appears the emission structure.

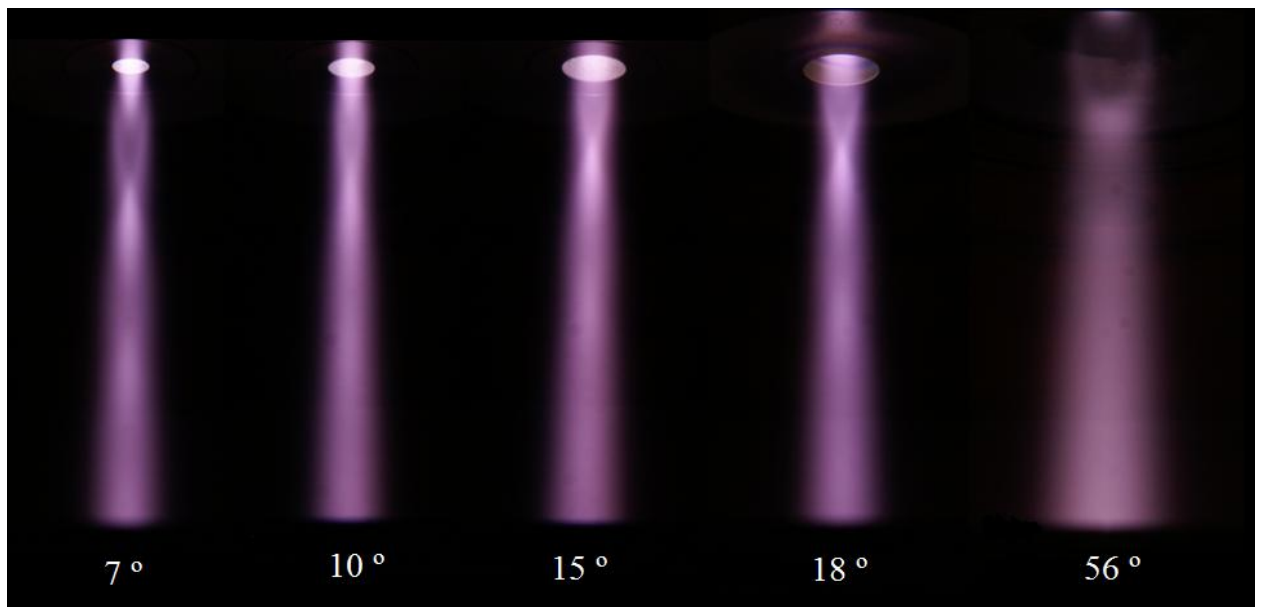
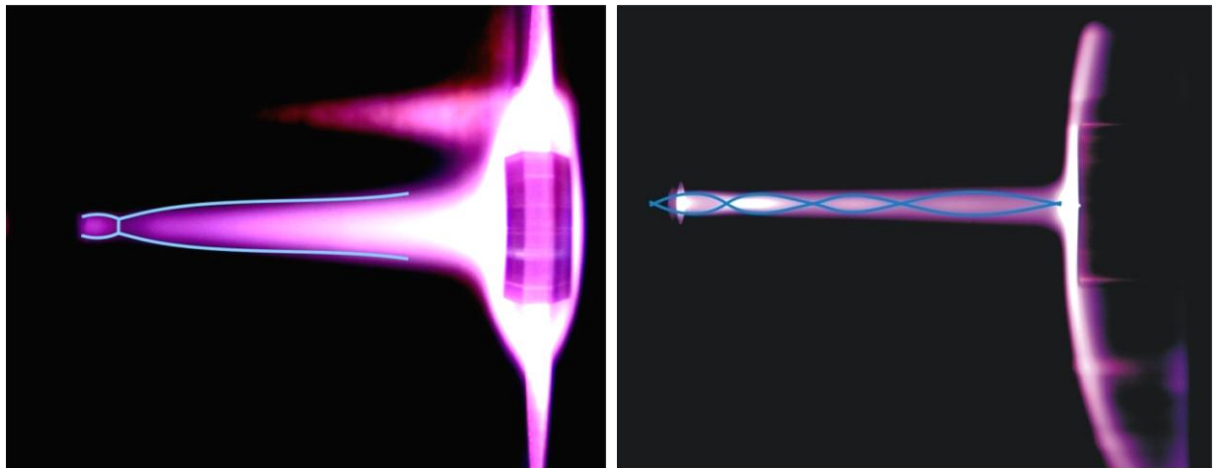


Figure 5.4. The plasma expansion into the first vacuum chamber at different nozzle opening angles. The plasma was extracted into the first vacuum chamber held at a pressure of 520 Pa.

The standard sampler showed the faintest and most diffuse structure but with a clearly visible Mach disk and barrel shock structure. Decreasing the opening angle to  $18^\circ$  shows a much more confined structure with the Mach disc changing to a node with repetitions appearing at regular intervals. Further decreasing the nozzle angle confines the expansion even more and the additional Mach nodes appear more pronounced for example with the  $7^\circ$  nozzle.

The structure of the plasma can be better compared when increasing the contrast in the picture, as shown in figure 5.5. These photographs indicate that no additional Mach disc is formed when the conventional sampler is used, while the  $18^\circ$  nozzle leads to the formation of even 3 nodes.



*Figure 5.5 The plasma expansion at enhanced contrast for the sampler (left) and  $18^\circ$  nozzle (right) The pictures were taken with the rod detector in place, mounted at a distance of 8 cm.*

The distance between the sampler/nozzle orifice and the Mach disc (or nodes for the nozzles) depends on the pressure but also on the nozzle's opening angle as listed in table 5.1. The distance increases for smaller angles and with decreasing pressure. The distances were estimated from the photographs based on the distance between the detector rod surface and the sampler/nozzle aperture. The position of the narrow and bright points in the jet structure is considered to represent the Mach disc/node. For the nozzles several nodes could usually be identified but estimating the position of the last knot was less precise because of the smoother flow. Of the different nozzles, the one with an opening angle of  $10^\circ$  provided the smoothest flow and only 2 clearly visible nodes.

Table 5.1. Mach discs/node position for different nozzles and the conventional sampler (distance to the orifice).

Nozzle, degree	Pressure, Pa	1 <sup>st</sup> node, mm	2 <sup>nd</sup> node, mm	3 <sup>rd</sup> node, mm
7	381	26	49	
	519	21	36	
	692	19	30	42
	865	18	27	40
8	387	23	39	
	519	21	34	49
	692	19	29	43
	865	18	27	40
10	375	23	37	
	519	21	33	
	692	18	28	
	865	17		
15	363	20	33	
	519	17	28	44
	692	16	27	36
	865	14	26	35
18	398	20	34	
	519	17	30	43
	692	16	26	39
	865	15	24	36
sampler	381	22		
	519	17		
	692	16		
	865	15		

### 5.3.2. Electric properties of the plasma expansion

The electric current downstream the conventional sampler and the different nozzles was initially determined using the cylindrical rod detector. The dependence on detector potential is shown in figure 5.6.

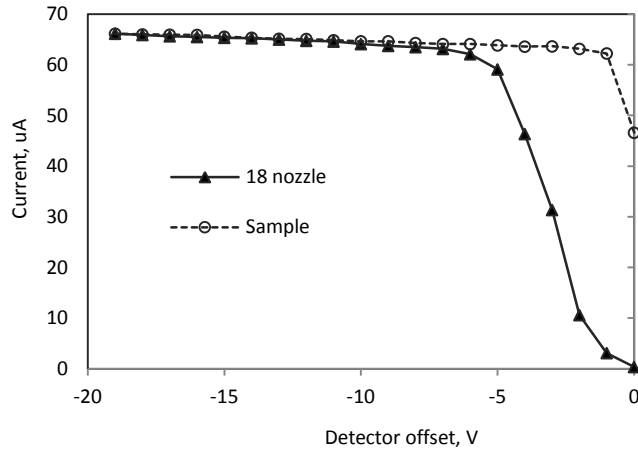


Figure 5.6. Dependence of the current measured via the cylindrical rod detector on potential offset with the sampler (dotted line) and 18 ° nozzle (solid line). The distance between the detector and the sampler or nozzle orifice is 1.3 mm.

An increase of the current in dependence of the detector offset is different for the sampler and the 18° nozzle. For the sampler the steepest increase in current is observed between 0 and -1V, where the grounded detector leads to a fairly unstable signal, while the current remains practically stable at more negative potentials. With the 18° nozzle on the other hand practically no current is observed at 0 V and more negative potentials lead to successively higher currents until -7 V, where the current shows the same trend as the sampler.

Since the major difference of the plasma jets formed by nozzle or sampler is the density and the width of the jet, the difference dependencies on detector offset can be considered a result of the change in Debye length and the radial charge separation. As the plasma expands as quasi-neutral, the net current of the expanding plasma jet is low [23]. The wider dissipation of the plasma jet downstream the sampler leads to a larger Debye length in comparison with the nozzle. Thus even a relatively small potential of -1V applied to the detector is sufficient to achieve repulsion of the electrons and a positive current is measured for the detector potential slightly lower than that of the ICP. Based on the previous results, the plasma potential can be assumed to be at about +2.5 V and thus the potential difference to the grounded detector is sufficient to detect the positive ion current. In case of the nozzle the plasma density remains high over a wider distance and the shorter Debye length requires a greater negative offset to achieve electron repulsion. This causes the shift of the curve in figure 5.6 for the nozzle towards more negative potentials applied to the detector.

The dependence of the current measured on the distance between sampler or nozzle and the detector surface is shown in figure 5.1 for different potentials applied to the detector. The net current generally decreases with distance for both the sampler and the 18° nozzle in a similar way when the potential is sufficiently negative. When the potential applied to the detector is within the range of the steep increase shown in figure 5.6 however, the dependency is more complex and shows greater variability. It appears that the actual current registered is far more affected by subtle changes in the experimental set up where small variations in potential can lead to significant changes in the current response. For a potential bias corresponding to the plateau region shown in figure 5.6. on the other hand, the registered current decreases almost linearly with distance and shows no significant difference between using the sampler or the nozzle.

Changing the distance of the detector was accompanied by a visible change in the structure of the plasma “wings” (Appendix, figure 8.1). For wide distances the “wings” were bent downstream in direction of the plasma jet, while close to the orifice, they bended upstream. The inversion occurs at a distance of about 3 cm. This indicates that there is a substantial change in the gas dynamics, which might affect the measured current by an additional interaction with the grounded chamber walls.

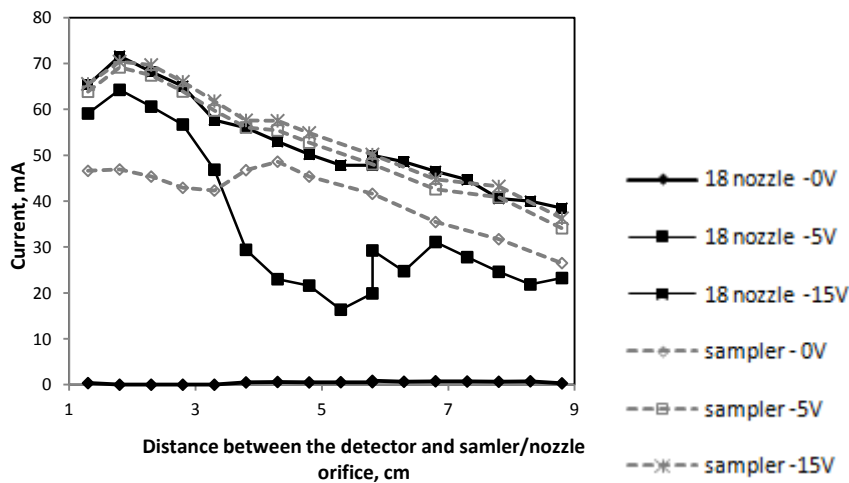


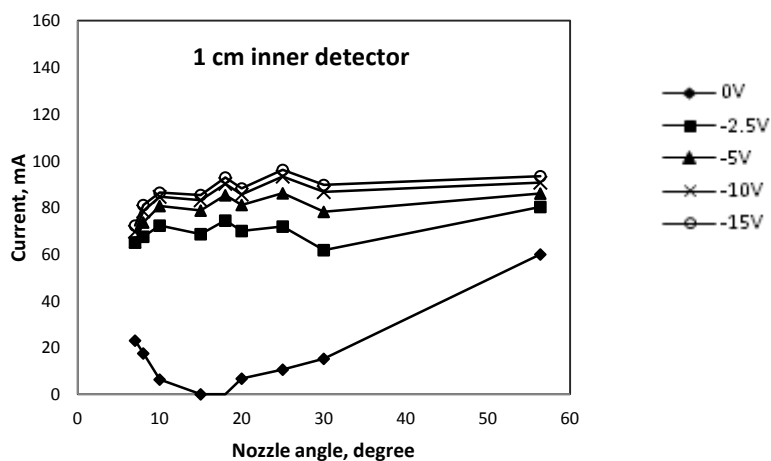
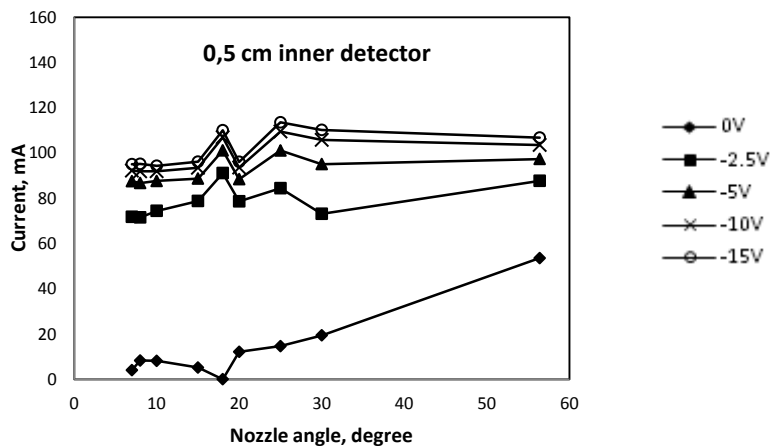
Figure 5.7. Dependence of the measured current on the distance and the detector offset for the sampler (s) and 18° nozzle (n) with different potential applied to the cylindrical rod detector.

The similar absolute currents and their dependence on distance with the detector biased by -15 V for the sampler and the 18° nozzle indicates that this potential is sufficient for electron repulsion near the detector surface provided that the separation is sufficiently large. For the nearest position of the detector however the current decreased, indicating that the plasma density is still sufficiently high to shield the electric field from the core. It would also mean that the large detector surface used in these

experiments collect a similar number of charges from the expanding plasma (for a negative potential applied) and that the dissipation of the expansion plays a minor role. The decay of the current measured is thus probably caused by ion-electron recombination during the expansion rather than the radial spread of the expanding plasma.

### 5.3.3. The ion current in the 1<sup>st</sup> and 2<sup>nd</sup> pressure stages

To estimate the degree of dissipation of the ions during the expansion, the skimmer-type and the two inner detectors were used. The outer current measured by via the skimmer and its holder resembles the fraction of ions moving off-axis during the expansion while the inner current downstream the skimmer corresponds to the portion of the jet transmitted to the 2<sup>nd</sup> pressure stage. The different sizes of the inner detector electrode may further shed a light on the dispersion of the ions downstream the skimmer orifice.



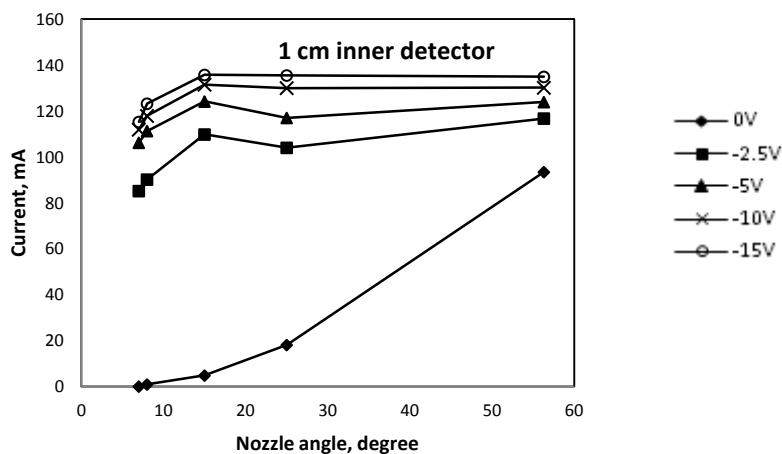


Figure 5.8. The current measured on the skimmer and its holder surfaces (outer current) for the different opening nozzle angles with grounded inner detector of 0.5 cm (top) and 1 cm (middle and bottom) diameter while varying the potential bias applied to the skimmer. The skimmer tip is located at the nozzle/sampler base, 8 mm downstream the orifice. The turbomolecular pump in the 2<sup>nd</sup> chamber was switched on.

The dependence of the current measured on the skimmer orifice (“outer current”) is shown in figure 5.8. Like with the rod detector, the measured current increased for more negative detector potentials. The spread between the current measured at the grounded and negatively biased detectors is in this case also greater for the smaller nozzles. The variability of the data is most likely a result of slight variation in the experimental conditions due to the plasma shutdown necessary to exchange the nozzles but the trend was reproducible (middle and bottom plots in figure 5.8).

With -15 V potential at the detector the, difference in ion currents for the nozzles and the sampler is within 20-30 %, with slight decrease for nozzles with an opening angle less than 18°. But the dependence on the nozzle angle increased significantly when the skimmer was grounded. The decrease of the outer current at the smaller nozzles results from the less pronounced dissipation of the plasma jet (Figure 5.4): the smaller jet diameter leads to a greater fraction of ions to pass through the skimmer orifice. Additionally, the confinement of the jet leads to greater flux of electrons to the skimmer surface, thus reducing the net current measured. Inside the skimmer holder the ions still can be detected by the inner walls, provided that the potential difference is sufficient. With the skimmer grounded, ion trajectories are dominated by the drag force of the gas. Since most of the jet, which passes through the skimmer aperture, does not reach the skimmer holder, the signal decreases with decreasing opening angles as shown in figures 5.9. Interestingly, the additional pump in the 2<sup>nd</sup> stage (downstream the skimmer) had no significant effect on the measured current, indicating that the gas dynamics within the skimmer throat are barely affected by the pressure in the second vacuum chamber.

The total current, measured by the inner detector, exhibits a completely different dependence on the nozzle angle than the outer current measured on the skimmer surface and its holder (Figure 5.9).

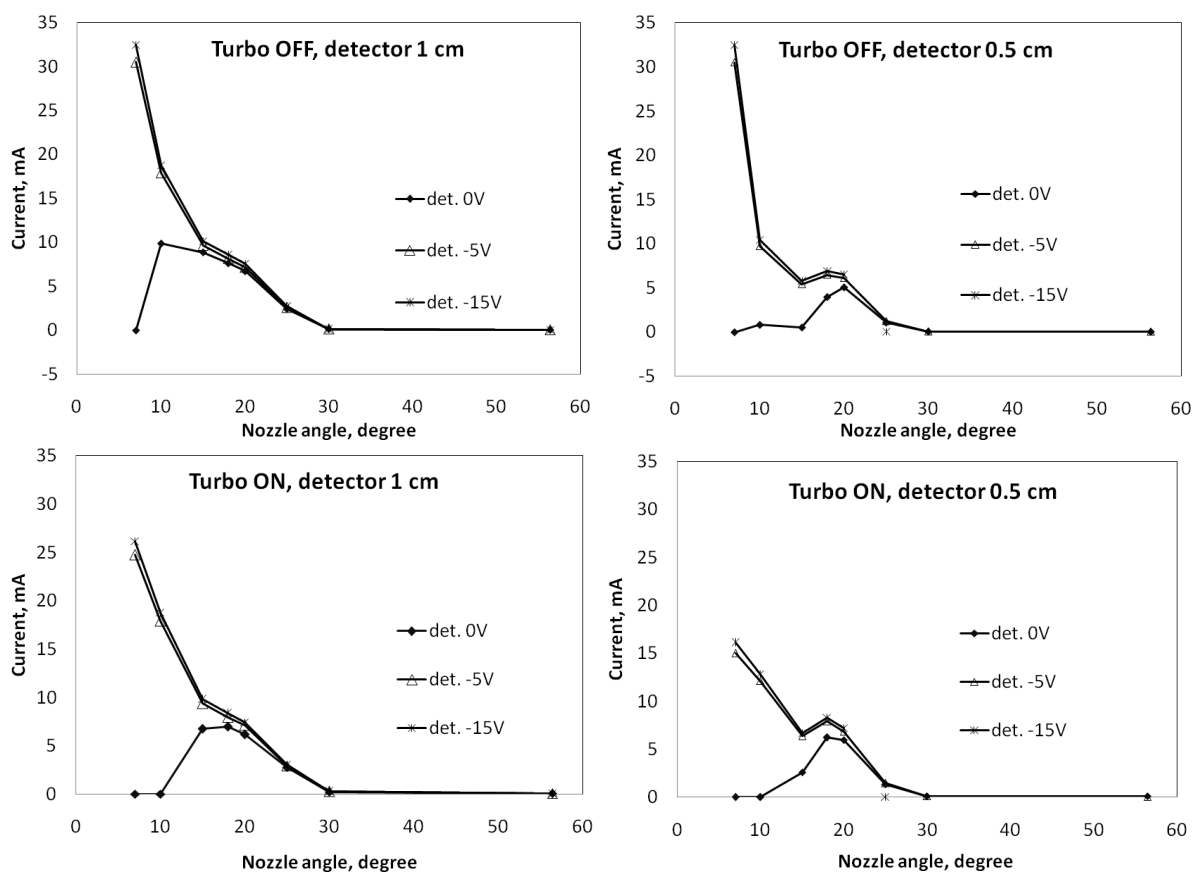


Figure 5.9. Dependence of the inner current measured downstream the skimmer on the nozzle angle and the detector bias. Detector disc diameter is 1 cm (left) or 0.5 cm (right). The turbomolecular pump at the second vacuum chamber was switched off (top) or on (bottom). The skimmer tip is at the nozzle/sampler base and grounded.

In figure 5.9 the dependencies of the measured current on the nozzle opening angle are presented: for the turbo pump switched off and on and for the inner detector diameter of 0.5 cm and 1.0 cm. The trends are similar irrespective of an additional pressure gradient between the 1<sup>st</sup> and 2<sup>nd</sup> chamber (i.e. turbomolecular pump switched off or on): the current increased with narrower opening angles from the sampler towards the 18 - 20 ° nozzles. At narrower nozzles however the signal was strongly dependent on the detector potential applied. With the detector grounded, it decreased to almost zero again for the nozzles with 7° - 8° opening angle, while the increase continued when negative bias was applied to the detector. However, the variability of the current observed is broader for the narrower nozzles when the turbomolecular pump was off, i.e. equal pressure in before and behind the skimmer. The major differences found for the two inner detectors are the intensity of the current and the width of the intermediate peak observed at the 18 - 20 ° nozzles. The current registered is however not proportional to the detector surface, indicating that the radial ion distribution in the expansion is also not homogeneous. For the inner detector diameter of 0.5 cm the signals showed a more pronounced maximum at the nozzle opening angles around 20°, while for the 1 cm inner detector diameter the peak appears to be broadened.



The low current measured with the broader nozzles or with the sampler is an indication for a highly dissipated plasma expansion and only a minor part of ions can penetrate through the skimmer orifice. The inner current with the sampler cone was only 0.06% of that measured on the skimmer surface, which is more than 2 orders of magnitude smaller, than is predicted by Douglas and French [34] or Macedone and Farnsworth [35]. Most ions are still moving to the skimmer surface and holder. When the nozzle gets narrower a greater fraction of the beam penetrates through the skimmer and can reach the inner detector, which leads to the signal increase up to 18 - 20 ° nozzles.

Further decrease of the nozzle angle causes different response in dependence on the detector potential. When the detector is grounded, a clear maximum is observed and the current decreases again with narrower nozzles, while a negative bias leads to practically continuous increase of the current. Coinciding with the maximum position for the grounded detector, an intermediate maximum appears also when the negative potential was applied. It is more pronounced for the 0.5 cm detector and appears generally broader with the 1 cm detector. This would indicate that the large nozzle opening angles lead to a highly dissipated beam after the sampler cone and only a small fraction of the ions actually passes the skimmer orifice. For the narrowest nozzles on the other hand a significant fraction of the plasma is transferred through the skimmer and the low current for the grounded detector resembles a balance of ion and electron currents. For the intermediate angles where the local maximum in current is observed, the charge separation occurring during the expansion becomes important. The outer part of the expansion is collected at the skimmer surface. As it carries a slight enrichment of electrons over ions the inner part remains relatively enriched in ions and a net positive current is registered also for the grounded detector.

The current measured when the 2<sup>nd</sup> stage pressure was equal to the 1<sup>st</sup> stage (turbomolecular pump is switched off) was typically higher than with the turbomolecular pump on. This appears to be a consequence of the lower dissipation of the ion beam in the 2<sup>nd</sup> chamber with higher pressure. The ions remain more confined to the expansion axis and a comparable fraction is detected with both detector sizes. It seems that this effect plays the more important role at the narrower nozzles where the ion density at the entrance to the 2<sup>nd</sup> stage is higher. In this case the decrease of the downstream pressure causes greater ion dissipation and reduces the current reaching the detector. Since the measured signal is resulting from integrating the entire detector surface, the influence of the surrounding pressure should be more pronounced for the smaller inner detector, than for the larger one. This is in good agreement with the experimental data: about 100% raise is observed for the 0.5 cm inner detector diameter from the “turbo on” to the “turbo off” cases, while only ~ 25% signal increase has been observed for the 1.0 cm inner detector diameter in the similar case. Another reason can be a different zone of the skimming relative to the Mach disc position, which should affect the ion velocities and the recombination or the secondary ionization degree.

Narrow nozzles form a narrower plasma jet, which leads to higher transmission through the skimmer. But from the other side, the narrower and denser expanding beam has high electron number densities over a longer distance, which means that ion focusing by an external electric field remains difficult. This conductivity can be estimated by the influence of the potential of the skimmer and its holder on the inner detector and vice versa.

It has been observed that potential applied to the skimmer also leads to the potential of the inner detector being shifted towards the values of the skimmer offset, but only when nozzles are used. For the sampler this effect was not observed. This indicates that narrower nozzles lead to electric conductivity between the skimmer and detector, which is also apparent in the dependency of the measured current on the inner detector potential (Figure 5.10). With the skimmer grounded there is an instantaneous increase in the registered net current as soon as the detector is negatively biased. When a potential of -5 V is applied to the skimmer the detector needs to be biased by more than -5 V before the current reached the same value as with the grounded skimmer. Wider nozzles or the sampler do not show this pronounced dependency as a result of the wider dissipation of the expanding plasma. This observation again indicates that the expanding plasma is transferred in its quasi-neutral state into the second vacuum chamber when narrow nozzles are employed and that the only a sufficiently high potential difference between the skimmer and the inner detector leads to charge separation and a detectable net current.

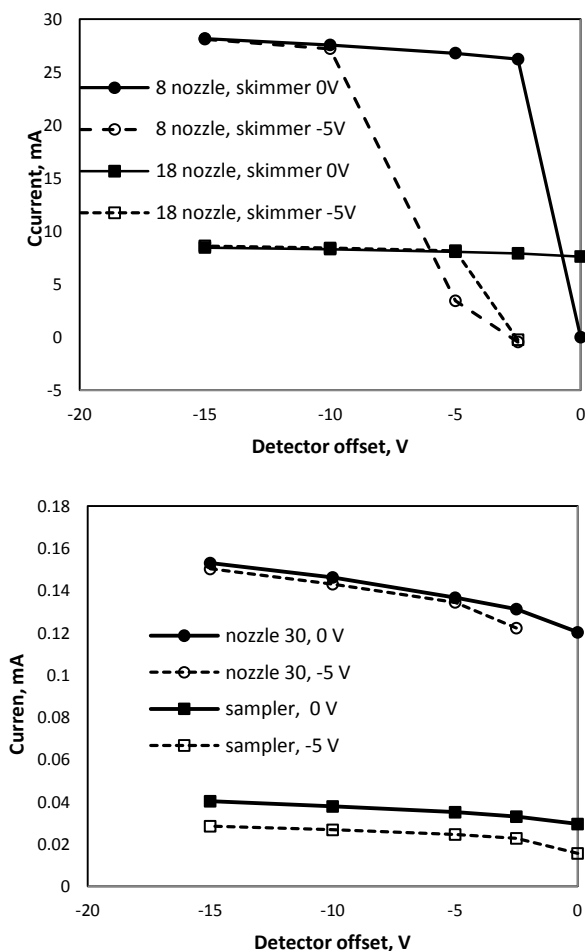


Figure 5.10. Dependence of the measured inner current for the 1 cm detector on the detector offset with the skimmer grounded (solid line) or biased by -5 V (dotted line) for the 8° nozzle (left), the 30° nozzle or the sampler (both right). The skimmer tip is at the nozzle/sampler base.

Some difficulty in comparing the situation with the different nozzle opening angles and the resulting currents are due to the fact that skimming occurs from different regions in the zone of silence, because the respective Mach disc positions change (Table 5.1). Penetration of the background gas, reheating and numerous collisions between ions and gas may thus significantly change the ion concentration during the expansion. Thus the ion currents were measured in dependence on the axial position of the skimmer tip were compared for the conventional sampler and the 18° nozzle while varying pressure in the 1<sup>st</sup> vacuum chamber for the grounded skimmer (Figure 5.11).

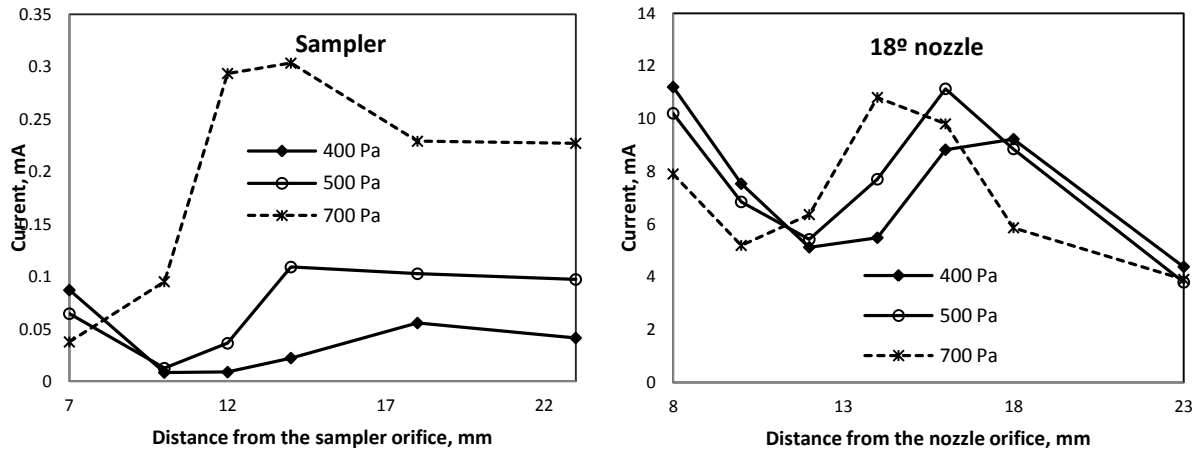


Figure 5.11. Dependence of the measured inner current on the distance between the skimmer tip and the sampler / nozzle orifice for varying pressures in the 1<sup>st</sup> vacuum chamber. Detector offset: -15V. The diameter of the inner detector – 0.5 cm. The turbomolecular pump was switched on and the skimmer grounded.

With the skimmer moving downstream the measured currents shows an initial decrease and a local minimum followed by an increase towards a maximum. The axial position of maximum or minimum depends on the nozzle angle and the pressure in the 1<sup>st</sup> vacuum stage. Both move towards the shorter distances when the 1<sup>st</sup> stage pressure increases and the change of the distance is more pronounced with the conventional sampler. Most notably however is that, while the conventional sampler shows a distinct dependence of the maximum current on pressure, the nozzle does not. The relative differences in current between maximum and minimum however are greater for the nozzle.

The positions where of the currents maximize can be compared with the Mach disc position, determined visually (Table 5.1). For the sampler at 400 Pa the measured maximum is located at about 18 mm downstream the sampler orifice, which would be 4 mm upstream from the Mach disc position. At 500 Pa the peak position is less clear but was estimated at about 15 mm distance, which is ~ 2 mm upstream, while at 700 Pa the maximum current is found at 13 mm distance, which is 3 mm upstream. For the nozzle the maxima are also found at positions slightly upstream the Mach node but the distance appears slightly shorter with 1 – 2 mm.

The local minima for the measured current occur at a position corresponding to approximately half the distance of the Mach Disk for the sampler or 60 – 70 % for the 18° nozzle. The optimum skimming position has been estimated to be at 2/3 of the distance to the Mach disc for the common ELAN sampler [34]. This would correspond to a position near the local minimum in the measured currents in figure 5.11. It is thus very likely that the presence of the skimmer disturbs the expansion to a greater extent than expected and a shock structure is formed inside the skimmer throat. Otherwise one should expect a smoother continuous decrease in current without intermediate minimum until the Mach disk is reached. Moving the skimmer downstream though leads to an increased thermal load to the skimmer tip as it approaches the Mach disk. This can cause the skimmer to glow in this experimental setup and lead to thermionic emission. The currents detected here however are much higher than could be expected at the temperature of glowing Nickel.

Very similar profiles were furthermore observed also when the skimmer was biased by -5V and varying the potential applied to the inner detector. The only notable difference was observed when the inner detector was at ground potential and the registered current dropped to near zero or became even negative. The latter indicates that electrons were emitted from the skimmer reaching the, in this case more positive, inner electrode. This current may have a thermionic component but it is most likely due to the presence of the plasma as a conductive medium penetrating into the second vacuum chamber and enabling the electrons to move towards the inner detector electrode.

#### **5.3.4. ICPMS performance with nozzle interface**

The characteristics and performance of the commercial ELAN 6000 ICPMS with the different nozzles replacing the conventional sampler cone was carried out with modified skimmer cones. This modification was necessary because aperture size of the ELAN 6000 standard skimmer was too large to allow stable operation of the mass spectrometer for nozzle opening angles smaller than 30°. Narrower nozzles caused the pressure in the second vacuum stage of the instrument to exceed the level of  $5 \cdot 10^{-3}$  Pa where all instrument's high voltage supplies are automatically shut off. Thus, two additional skimmers were manufactured from aluminum with orifice diameters of 0.2 mm and 0.4 mm but of identical height.

Using the standard skimmer with a 0.9 mm diameter orifice, measurements could be performed only with the standard sampler of 56° opening angle and the 30° nozzle. The skimmer with 0.4 mm diameter orifice could be used with nozzle angles down to 10° could be used, while the skimmer with 0.2 mm orifice could be used for all nozzles. To lower the pressure in the interface and mass spectrometer an additional rotary vane pump was added to the interface region. The additional pump could also be isolated by means of a shut-off valve. The interface pressure was registered by the Baratron absolute pressure gauge mounted near the intake port of the first rotary vane pump. Ion signal intensities were acquired in the same way as described in Chapter 2 by scanning selected mass ranges and processing the spectral peaks. A solution of the elements studied with a concentration of 10 µg/L in 1 % HNO<sub>3</sub> was aspirated and introduced via the pneumatic nebulizer and cyclonic spray chamber. Additionally, data

from the so called “Autolens Calibration” of the instrument were extracted from the software to estimate changes in the ion kinetic energies. The “Autolens Calibration” evaluates ion signal intensities for selected isotopes across the mass range (from  ${}^7\text{Li}^+$  to  ${}^{238}\text{U}^+$ ) while scanning the voltage applied to the cylindrical lens mounted downstream the skimmer in the second vacuum stage. The voltage leading to the highest signal intensity registered for each isotope is usually increasing with  $m/Q$ . Typical operating voltage ranges are between 4 V for  ${}^7\text{Li}^+$  and 15 V for  ${}^{238}\text{U}^+$  respectively. The linear regression of the optimum voltage vs.  $m/Q$  can give an estimate the ion’s initial kinetic energy or plasma temperature from the slope and the potential of the ion source from the intercept [88]. This relationship is valid when assuming that the ions are accelerated to the velocity of the bulk gas during the expansion into the vacuum stage leading to kinetic energies consisting of a component proportional to  $m/Q$  superimposed to the potential of the ion source. Isotope sensitivities were always acquired under optimized conditions i.e. with the lens voltage set the corresponding optimum in the “Autolens Calibration” by the instrument software.

### 5.3.5. Results

The pressure at the first vacuum stage was not significantly affected by the type of nozzle used but was sensitive to the pump speed applied (Figure 5.12.). It could be reduced from 520 Pa with the single pump to 180 Pa with two pumps in parallel. It was also practically independent on the size of the skimmer orifice diameter. The pressure in the mass spectrometer region on the other hand increased systematically when nozzles with smaller opening angles were installed. It started to increase notably when nozzle’s the opening angle decreased below  $30^\circ$  and the magnitude of the increase depended on the orifice diameter of the skimmer used. The pressure limit of the mass spectrometer was reached exceeded with nozzle angles below  $30^\circ$  when using the 0.9 mm standard skimmer or  $10^\circ$  for the 0.4 mm skimmer. With the 0.2 mm skimmer aperture, all nozzles could be used.

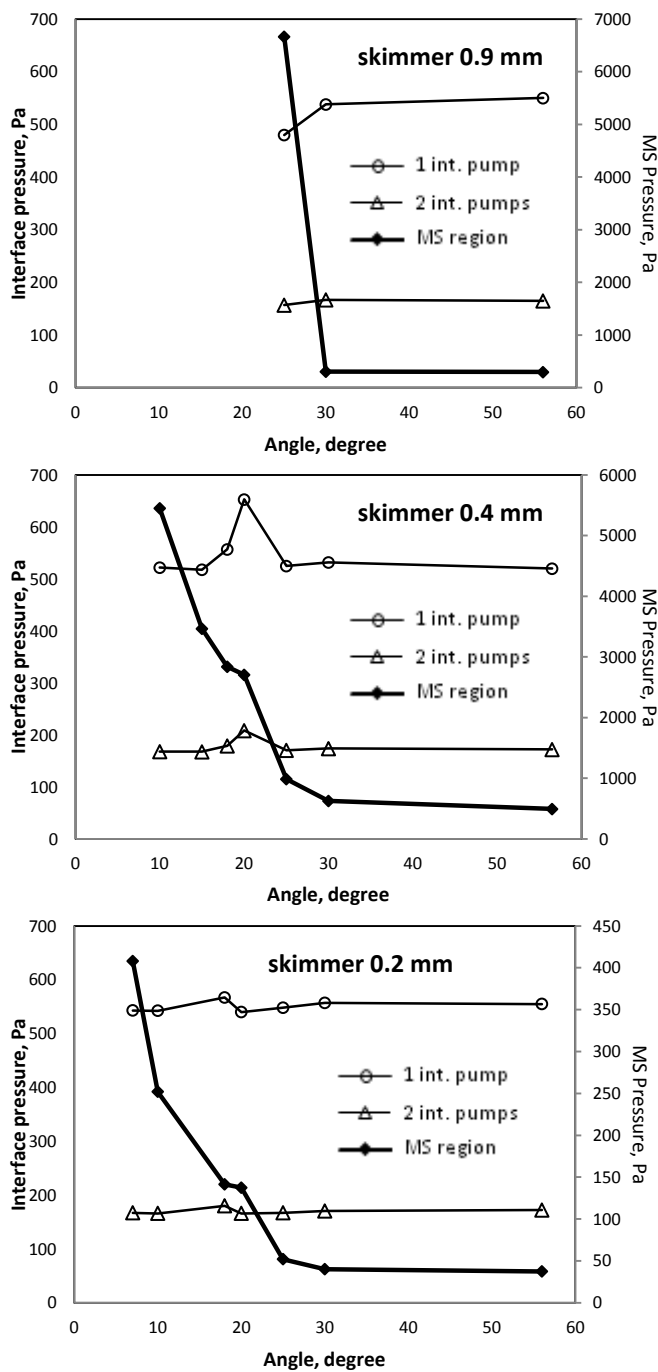


Figure 5.12. Dependence vacuum conditions inside the first stage (1 and 2 interface pumps applied) and mass spectrometer region for the different nozzles and skimmer types used. Interface pressures are shown for the additional pump switched off and on.

The signal intensities for the 10 µg/L multi-element solution, obtained with the different nozzle opening angles and different skimmer orifice diameters, are presented in figure 5.13. The highest sensitivities were still observed with the 0.9 mm skimmer and only a slight difference is observed for the standard sampler compared to the 30° nozzle. Operation with single or dual interface pumps did also not result in a remarkable change of the signal intensities in general. Ce<sup>+</sup> showed a slight increase when

the additional pump was added but the remaining isotopes showed similar sensitivity. A slightly higher sensitivity is observed for ions at low  $m/Q$  with the  $30^\circ$  nozzle. With the 0.4 mm skimmer on the other hand, the sensitivities were comparably low and the effect of the additional pump more pronounced. The different nozzles showed a pronounced trend with a sensitivity maximum for most isotopes at nozzle angles between  $25^\circ$  and  $30^\circ$ . With the 0.2 mm skimmer the signal intensities were the lowest and the influence of the additional pump was not as pronounced anymore. The effect of the nozzle angle however was highly special in this case. Again a sensitivity maximum was found around  $30^\circ$  opening angle but smaller opening angles led to lower sensitivity and a minimum was observed around  $10^\circ - 18^\circ$  where the additional pump resulted slightly higher sensitivities. Further reduced nozzle angles lead then to an increase in sensitivity again but only little effect with the additional pump.

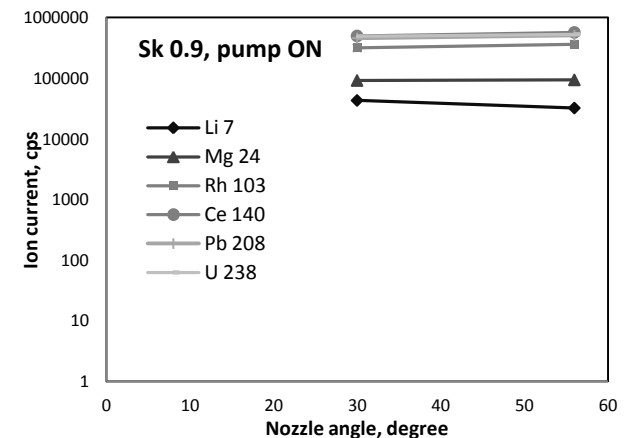
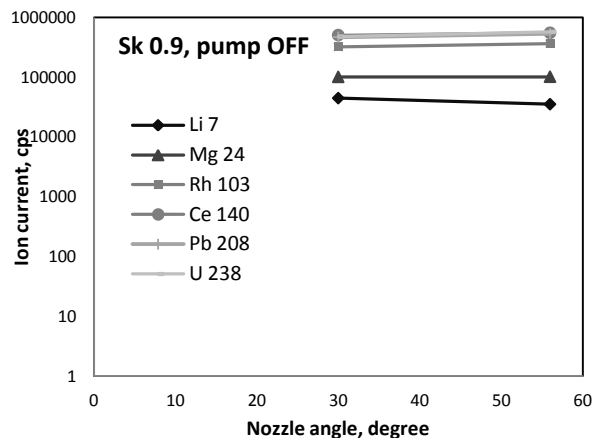
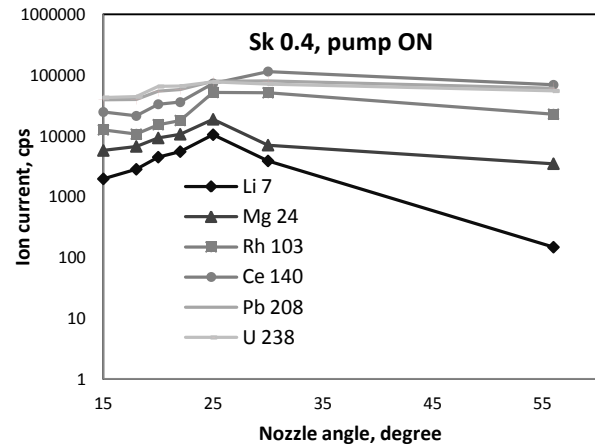
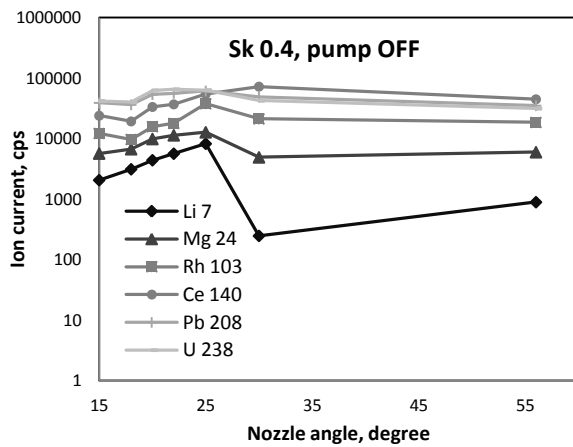
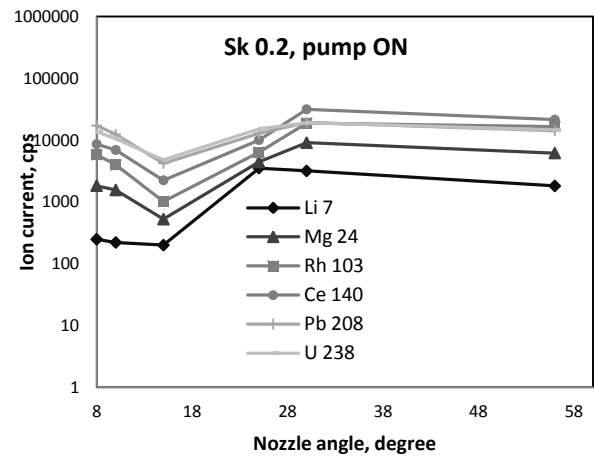
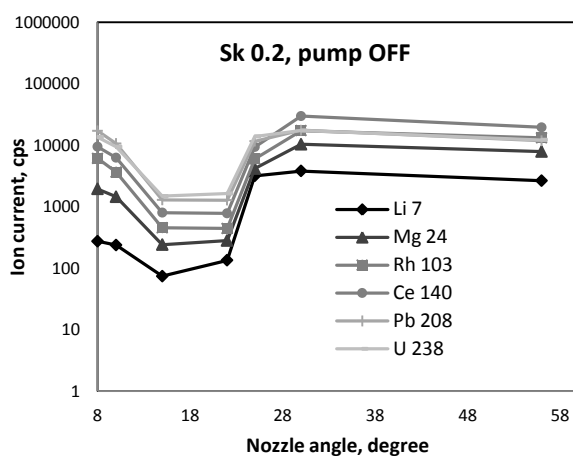


Figure 5.13. Dependence of the ion signal intensities on nozzle opening angles for different elements studied. Skimmer diameters were 0.9 mm (top), 0.4 mm (middle) and 0.2 mm (bottom) and the additional interface pump is switched off (left) or on (right). All Intensities were corrected for isotopic abundance.

Together with the ion signal intensities, the change in oxide ion formation was monitored via  $\text{CeO}^+/\text{Ce}^+$  in all experiments as displayed in figure 5.14. In all cases there was no significant influence of the additional pump but the oxide ion formation rather followed very closely the same pattern as the pressure in the mass spectrometer region (Figure 5.11.). With the 0.9 mm skimmer the  $\text{CeO}^+/\text{Ce}^+$  ratio was always in a about 2.5 % which is typical for the instrument under optimized plasma operating conditions. A similar level was also found when the skimmers with smaller apertures were used together with the standard sampler cone and the 30 ° nozzle. Smaller nozzle angles however always led to increased oxide formation rates reaching up to 25% for the 7° nozzle.

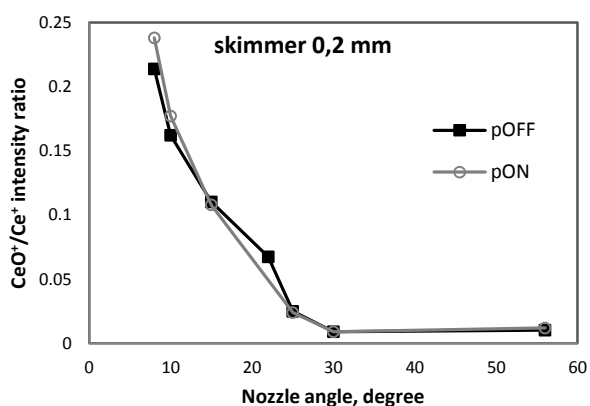


Figure 5.14. Dependence of the  $\text{CeO}^+/\text{Ce}^+$  intensity ratio on the skimmer diameter, nozzle angle and the additional interface pump (switched off or on).

The non-spectral background as monitored via  $m/Q$  220 was showing a very similar trend and increased in line with the pressure in the mass spectrometer region, while their values decreased when using smaller skimmer orifices with the same sampler or nozzle (Figure 5.15.).



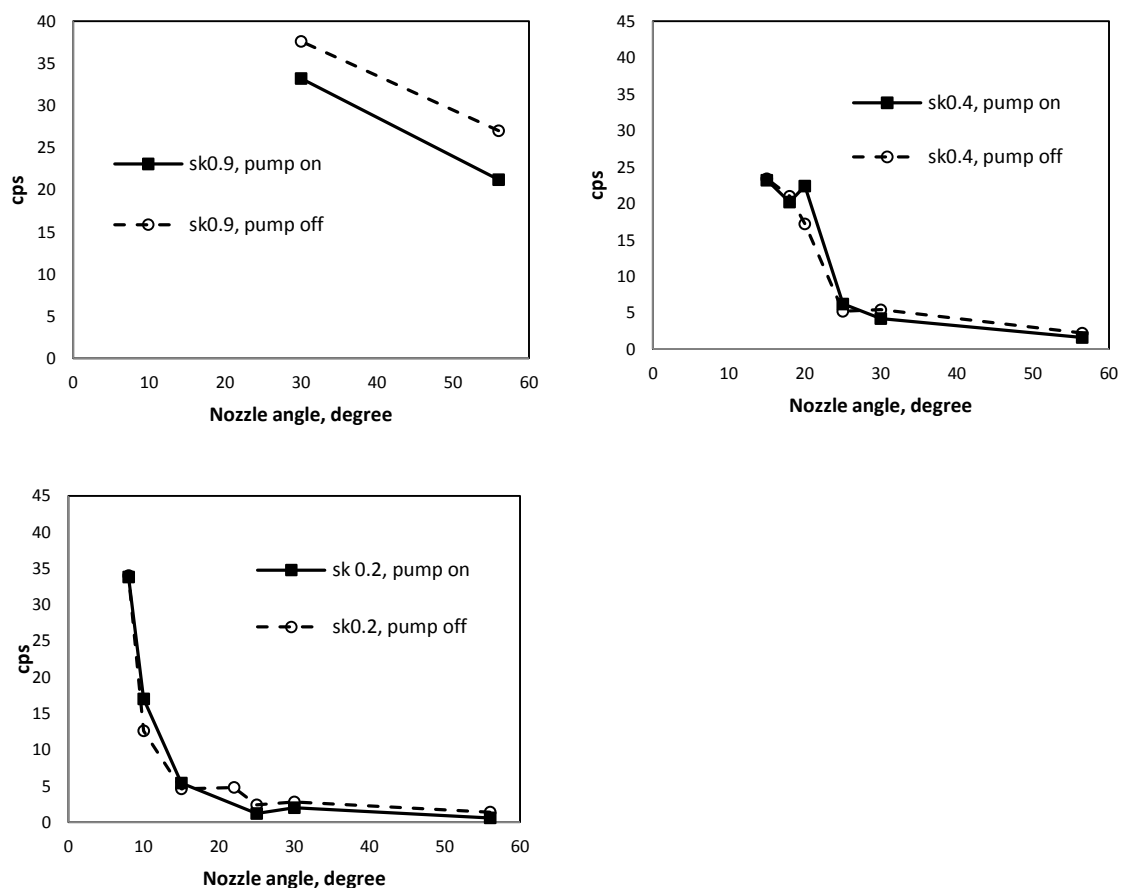


Figure 5.15. Dependence of the background ( $m/Q$ : 220) on the nozzle angles for different skimmer diameters and the additional interface pump switched off and on.

Evaluation of the “Autolens Calibration” data was made based on the optimum voltages determined for  $^{24}\text{Mg}^+$ ,  $^{103}\text{Rh}^+$  and  $^{140}\text{Ce}^+$ . The results, shown in figure 5.16, reveal an obvious transition of the ions kinetic energies. The slope of the calibration, which corresponds to the increase of kinetic energy with  $m/Q$ , shows only small variability for the standard sampler and the  $30^\circ$  nozzle but continuously decreases with further smaller nozzle opening angles. Beyond an angle of  $20^\circ$  the slope was found to be almost 2 orders of magnitude less than with the standard sampler, regardless of the skimmer orifice diameter used. The intercept of the calibration on the other hand appears not to be influenced by the nozzles opening angles to a large degree. The intercept is always within a range of 3 – 5 Volts and exhibited no systematic variation.

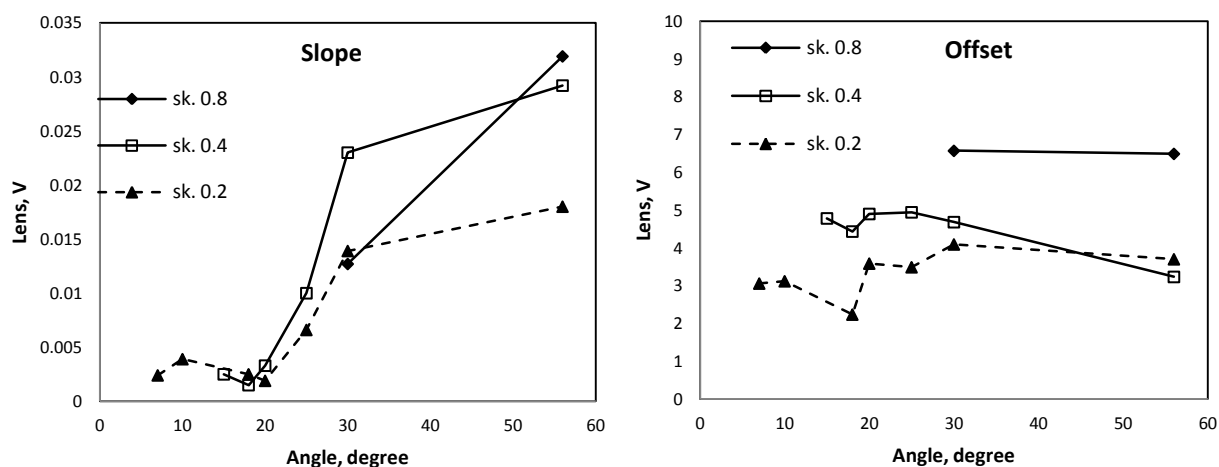


Figure 5.16. Dependence of the instrument's "Autolens Calibration" slope and intercept on the nozzle angle and the skimmer orifice diameter. Additional interface pump is switched off.

These observations indicate that the only mass dependent component of the ion acceleration is substantially affected by the change of the supersonic expansion within the vacuum interface. The skimmer orifice diameter affects the mass dependent component in a similar way with smaller orifice apertures yielding smaller slopes. These observations can be explained when assuming a continuous restriction of the free expansion of the plasma jet next to and within the skimmer orifice. The more confined expansion leads to an increase in gas density within the skimmer throat and thus a higher collision frequency. This leads to more efficient thermalization of the ions and the free supersonic expansion is successively stopped as the nozzle opening angle or the skimmer orifice diameter decreases. The ion kinetic energies are then increasingly determined by the plasma potential within the skimmer rather than by the gas dynamics of the supersonic expansion. This leads to a reduction of kinetic the energies and also can explain the lower sensitivities observed as the nozzle angle is decreasing because the fraction of ions that has sufficient kinetic energy to travel further downstream through the entrance aperture of the mass spectrometer decreases. The lower slopes however should also lead to less mass discrimination due to space charge effects, which was not observed in these experiments. It must be thus assumed that the mass discrimination is dominated by the radial distribution of the different isotopes, with lower  $m/Q$  remaining relatively depleted in the central part of the expansion. The increase of the  $CeO^+/Ce^+$  ratio and non-spectral background intensity can just as well be explained by increasing collision frequencies inside the skimmer throat when the expansion becomes more confined. What remains unclear at the moment is the increase in sensitivity observed for the 0.2 mm skimmer orifice and the smallest nozzle angles. Compared to the 0.4 mm skimmer orifice, it appears that the sensitivities are lower for nozzles with opening angles between  $10^\circ$  and  $25^\circ$  are used. It may be a result of a change of the shock structure which for these nozzle angles leads to such a dramatic perturbation of the expansion that the ions are effectively removed from the beam. The smaller opening angles might then lead to a relaxation of this perturbation and a slightly higher ion transmission. Pressure alone appears not to be a viable explanation because the continuous increase in oxide formation and non-spectral background intensities are suggesting that collision frequencies

follow a regular trend with nozzle opening angle. Eventually, however, the expansion from the 20° and 18° nozzles are more significantly disturbed by the skimmer and further reflections inside the skimmer walls lead to a greater disturbance of the ion extraction and this effect is less pronounced for the supersonic expansion from the smaller nozzles. One further aspect that would have to be considered but could not be assessed within these experiments is the change in the temperature at the skimmer tip. The more confined expansion would shift the thermal load at the skimmer closer to its tip and the surface temperature may additionally affect the characteristics of the gas dynamics during the transfer to the second vacuum stage.

## 5.4 Summary

The plasma jet extracted via nozzles exhibits a denser and more confined structure than the one formed by the conventional sampler cone. The supersonic expansion, characterized by the barrel shock structure with the perpendicular Mach disc occurring with the sampler, changes into more spindle-like structures where the terminal shock structure forms nodes instead of the flat Mach disc. Depending on the nozzle opening angle, these nodes were observed to occur at wider distances from the nozzle aperture as its opening angle decreased. Usually a series of transitions between supersonic and subsonic expansion is observed as indicated by a series of “Mach nodes” along the axis of the expansion. The total current registered within the first vacuum stage, however, remained practically unaffected whether the conventional sampler or a narrower nozzle were used. Similarly, the ion signal intensities measured for the conventional sampler and the 30° nozzle were very similar, indicating that the nozzle inner surface has only little effect on the ion number density of the extracted plasma. There was also no significant difference of the net current measured via the skimmer at different downstream positions, provided that the detector areas was larger than the plasma expansion and biased by more than -10 V. But when the detector was grounded or only slightly biased, the difference between the nozzle and the sampler was more pronounced. The current profile was shifted towards by about 5V towards more negative potentials for the nozzle compared with the sampler. The low and unstable currents observed with grounded or moderately biased detector and the nozzle indicates that electron repulsion requires much higher potential gradients for the nozzles than with the sampler. Despite the fact that the expanding plasma was not found to have a uniform charge distribution, even over a distance of only 0.3 mm (Chapter 4.4), the large collection area of the cylindrical rod detector or the skimmer would integrate over the entire plasma region. Thus, especially for the nozzles, the cross section of the expansion does not exceed that of the cylindrical detector, while the sampler creates a wider expansion of the jet and the charge separation is more pronounced.

The radial spread of ions and ion transmission to the 2<sup>nd</sup> stage has been estimated via the currents measured on the skimmer surface and the inner detector, located downstream the skimmer. Based on these data, the transmission increases from the 0.06% for the sampler to ~ 10% for the 18° nozzle and ~ 42% for the 7° nozzle. Thus the transmission efficiency for the sampler is significantly lower than the percentage ranges estimated by Douglas and French [34], while the total current registered downstream the skimmer was similar. It should be noted however that the skimmer orifice was

enlarged from 0.9 to 3 mm during these experiments due to erosion from the sharp tip. Accordingly, using the standard skimmer should result in even smaller transmission efficiency. The outer current increased for nozzles with larger opening angle in accordance with the wider expansion of the plasma jet. For smaller nozzle opening angles a greater fraction of the expanding jet is transmitted through the skimmer aperture to the next stage and the inhomogeneous charge distribution additionally reduces the contribution of ions relative to the electrons reaching the skimmer surface. Both effects reduce the net positive current detectable at the skimmer. There was no effect of the pressure in the 2<sup>nd</sup> vacuum chamber on the outer current indicating the flow dynamics downstream the skimmer orifice are not affecting the conditions of the plasma expansion in the 1<sup>st</sup> vacuum stage significantly. The potential applied to the inner detector however had a direct influence on the current measured via the skimmer unless the sampler was used. This would indicate that the density of the plasma expanding from the nozzles into the skimmer throat can still form an electrically conductive medium between the skimmer and the inner detector.

The inner current showed more complex dependencies. It was found to be highly sensitive to the skimmer potential, with negative skimmer potentials leading to higher measured current as soon as the detector bias was sufficiently negative. With the grounded or only moderately biased inner detector the potential difference was not sufficient to achieve charge separation and close to zero or even negative currents were obtained.

The inner current was significantly affected by the nozzle angle and an up to 1000-fold increase has been observed from using the sampler to the 7° nozzle. With the 18° – 20° nozzles a local maximum of the inner current has been observed when the detector was grounded. For the negatively biased detector, farther decreasing nozzle opening angles led to a steep increase of the measured current. Considering the skimmer aperture diameter and the radius of the plasma jet formed, the nozzles with opening angles below 18° led to almost complete transmission into the 2<sup>nd</sup> pressure stage. The increased density and the narrower spread of the plasma jet thus responsible the increase of the inner current, while at the same time the increase in electron transmission leads to almost zero net current the detector grounded.

The dissipation of the ions downstream the skimmer can be estimated by the comparison of the inner current measured with the inner detectors of 0.5 cm and 1 cm diameter. Despite 4 times smaller area of the 0.5 cm detector however, the intensity dropped to only 70% – 80%, which indicates that the majority of the ions is moving within a region smaller than 1 cm at the skimmer base, where the detector was located.

The transmission into the 2<sup>nd</sup> vacuum stage also depended on the skimming position. When the skimmer tip was positioned inside the zone of silence, the current initially decreased with increasing distance to the sampler or nozzle in line with the decrease of the plasma density along the expansion axis.

As the Mach disk or node is approached, the measured inner current increased and a maximum was observed about 3 mm upstream the Mach disc position for the sampler and around 1.5 mm

upstream for the 18° nozzle. The background pressure had only minor influence on the position of the local maximum and minimum but changed mainly the width of the current peak. The occurrence of his maximum may either be due to the higher confined plasma within the barrel shock structure, which causes greater fraction of the plasma to be transmitted to the next stage or secondary ion formation due to the high collision rate inside the Mach disc.

Further downstream from the position of maximum current, the skimmer should be located in close proximity of the Mach disc. Despite the further confinement of the expanding plasma however, the current decreases continuously. The most likely explanation for this deviation is an interaction of the skimmer tip with the plasma expansion. The colder surface of the skimmer may lead to the formation of a boundary layer and additional shock formation inside the skimmer throat. The corresponding disturbance of the free expansion would thus randomize the directed motion of the expansion and reduce the transmission through the skimmer orifice.

Attempts to use the nozzles in the Elan 6000 ICPMS were complicated by the high gas load into the 2<sup>nd</sup> and 3<sup>rd</sup> vacuum stages when using the nozzles. The pressure in the mass spectrometer in this case increased significantly and eventually caused the high voltages of the quadrupole MS ad detector to be shut down automatically. With the common skimmer (0.9 mm diameter) only nozzles with opening angles up to 30° could be used. The specifically made skimmers with orifice apertures of 0.2 and 0.4 mm diameter made it possible to make a series of measurements with the different nozzles. The 0.4 mm skimmer could be used for the nozzle with opening angles down to 10°, while the vacuum could be sustained with all nozzles and the 0.2 mm skimmer. The pressure in the high vacuum region began to increase most significantly for nozzles with opening angles below the 25°, while the pressure in the interface region remained practically unaffected by the nozzle used.

Unfortunately there was no benefit from using especially the narrowest nozzles since the non-spectral background and the oxide formation increased dramatically together with the pressure in the MS chamber. The measured ion signals also showed a complex dependence on the nozzle angle. Changing from the conventional sampler to an opening angle of 30° only led to minute changes in sensitivity for all skimmers used. Further decreasing opening angles caused the sensitivity to drop dramatically with the 0.2 mm skimmer, with a minimum for nozzles with opening angles between 15° and 22°. Even narrower nozzles then caused the intensity to increase again. For the 0.4 mm skimmer the sensitivity changes showed a pronounced dependence on the isotopes with lower  $m/Q$  showing highest sensitivities for the 25° nozzle, while high  $m/Q$  were continuously suppressed with decreasing nozzle opening angle. Together with the trends observed in the “Autolens Calibration” one must conclude that the expansion characteristics for nozzles narrower than 25° have a dramatic effect on the transmission of the plasma through the skimmer orifice. Under these conditions, the energy distribution of the different  $m/Q$  narrows substantially, which must be a result of a high collision frequency effectively cooling the expanding plasma.

One needs to state at this point that these first attempts to using nozzles in an ICPMS vacuum interface did not yield highly promising results. At least with the instrument used in this study, the dramatic effect on the high vacuum precluded the use of conventional skimmer sizes and thus the

instrument sensitivity could not be improved. Nonetheless, these experiments have shown that a generally higher transmission can be achieved through a nozzle to extract the atmospheric plasma. In order to investigate whether this can be translated in to true ion signals for ICPMS measurements the vacuum system would have to be modified significantly. Especially the situation inside the skimmer throat appears to be limiting the attainable performance with the instrument used here. An improvement may be achievable when much greater pump speeds are applied in the 2<sup>nd</sup> vacuum stage or another means that might accelerate the expansion of the gas and reduce the collision frequency, without at the same time losing the ions together with the gas.

## 6. Conclusion and Outlook

---

Adaption of an ion funnel as ion guide for ions extracted from an atmospheric inductively coupled plasma ion source has been studied in this work. Initial tests had shown for the first time that an ion funnel of specific geometry can be utilized to transfer also elemental ions through the 2<sup>nd</sup> vacuum stage of a modified commercial ICPMS instrument. Ion transmission of the configuration developed here was however generally lower than in the original ICPMS configuration with the single cylindrical lens instead. At optimized conditions, ion transmission was lower in average by one order of magnitude compared with the conventional setup. The ion transmission was nevertheless sensitive to the RD and DC fields applied, indicating that the funnel can be used as transfer element instead of the classical ion optics. Transmission was maximized when applying an RF field with amplitudes in the range of 25V to 50V at 600 MHz frequency and a DC gradient of 20V to 40V along the funnel axis. Parameters for optimum ion transmission were found to depend on  $m/Q$ . Lower  $m/Q$  optimized at higher RF-frequencies, which is agreement to the theoretical transmission properties of a stacked ring electrode guide. Higher values of DC gradient and Rf amplitude however, usually, deteriorated the mass resolution of the quadrupole MS, most likely due to fringe fields or a too high ion energy spread at the funnel exit.

Partly enclosing the ion funnel enabled its operation as a gas collision cell for the use of reactive or non-reactive gases. An effective reduction  $Ar^+$  and Ar-containing molecular ions was observed with  $N_2$  and  $H_2$ . The latter is rather favorable in this context as it does not affect the transmission of low  $m/Q$  analyte ions to a great extent.

The coupling of the ion funnel directly downstream the sampler cone in an ICPMS vacuum interface however was not possible because the high electron number density within the plasma expansion just after the sampler orifice led to electric shorting between the funnel electrodes and a breakdown of the RF-field inside the funnel. An additional pumping stage before the ion funnel was again necessary to reduce the plasma load. This ensured stable operation of the RF field and allowed operation of the funnel in a wider pressure range. The additional extraction interface tested in this configuration however did not yield better ion transmission through the funnel. The extraction electrodes, being in contact with the dense conductive plasma, could not be operated at sufficiently high potential because of the formation of a secondary discharge. Nonetheless initial tests could be carried using lower extraction voltages and the funnel operating in a pressure regime of up to the mbar range, which would improve collisional damping inside the funnel and enhance its ion confinement capabilities. It could be shown that the DC gradient along the funnel increased the current measured downstream the exit aperture. These studies also showed that the potential applied to the funnel outlet is most critical in this regard. The highest transmission was observed when at least 30 V difference were applied to the two last ion funnel electrodes. The potential difference to the detector for total current measurements should also be greater than 10 V in order to ensure charge separation within the expansion and efficient collection of ions exiting the funnel. The RF field however did not have any

positive effect on the ion transmission in this set up. This is most likely due to space charge effects, limiting the total current through the smallest apertures at the funnel exit to several nA. Due to the high number density of  $\text{Ar}^+$  ions in the plasma expansion however, the fraction of analyte ions will remain marginal and an effective improvement in ICPMS performance is not to be expected under these conditions.

The angular resolved measurements however revealed an interesting behavior of the ions exiting the ion funnel. Their radial spread after ion funnel exit aperture was largest when no field was applied to the ion funnel. Application of DC or RF fields caused the angular spread to become narrower without significantly affecting the current measured at the axis. The DC and RF fields thus cut away the fraction of ions from the entire beam that has too low kinetic energies to overcome the effective potential at the exit of the ion funnel. This characteristic makes the ion therefore comparable to an electrically controllable aperture, which might have applications in ion beam steering and control in other mass spectrometry applications.

It is nonetheless apparent that the present configuration of an ion funnel is far from optimum as ion transfer device in an ICPMS instrument. Since there is no observed improvement in ion transmission by applying the RF field, the ion current within the funnel is still limited by space-charge effects. The RF amplitude results in a higher effective potential and deeper trapping potential wells, causing an additional loss of ions. Thus, further studies have to be carried out to modify the interface and allow transformation of the plasma beam into an ion beam of appropriate energy distribution and composition, which can be efficiently transmitted by the ion funnel.

An attempt to increase ion transmission through the first vacuum stage was made by investigating the effect of nozzles instead of the conventional sampler. These studies indicated that the expansion can be significantly affected by the geometry of the nozzle. Decreasing the opening angle led to narrowing of the jet and reveals a significant change in the shock structure by forming multiple nodes instead of the Mach disk observed with the standard sampler.

Due to the higher plasma density in the expansion, the ion current transmitted through the skimmer orifice can be substantially increased. With this increase in plasma density an electrically conductive medium can be present within the skimmer throat, which affects the potentials and current measurements of downstream electrode and detector. Thus, smaller the nozzle opening angles lead to a situation similar to installing the ion funnel directly downstream of the sampler, where the high density of the charged particles led to the electrical shorting.

The degree of dissipation in the 1<sup>st</sup> vacuum stage is remarkably different for the sampler and 18° nozzle but the measured total ion current appears to be similar provided that the detector surface is large enough to cover the majority of the plasma expansion. In this case the current measured for the 18° nozzle and sampler was highly similar, when the detector bias was below -7 V in order to achieve repulsion of the electrons and collection of ions. When positioned near the nozzle exit however, the density of the plasma may be still high and a charge separation requires significantly higher fields due to the shorter Debye length.



Due to the higher density of the plasma jet formed by the nozzle, the Debye length is shorter and a greater bias is required in this case. The close agreement of the measured current in dependence on distance between orifice and the detector is most likely due to ion- electron recombination.

The transmission to the 2<sup>nd</sup> chamber through the skimmer orifice is determined by the nozzle angle, which is responsible for the width of the jet as a whole and the Mach disc position for a given background pressure. The dependence on pressure is according to conventional theory of a supersonic expansion even though the position of the Mach disk according to observation was slightly further downstream than assumed by Douglas and French [34]. A similar deviation is apparent from the dependence of the ion currents measured for increasing separation between skimmer and nozzle or sampler. It was further confirmed by numerical simulations of the fluid dynamics.

It was however interesting to note that the currents measured downstream the skimmer showed a minimum when the skimmer aperture was placed at about half the distance upstream from the Mach disc for the sampler and at 60 – 70 % of the distance for the 18° nozzle. An intermediate maximum was observed at about 3 mm upstream from the Mach disc for the sampler and only 1 mm for the nozzle. This local minimum may be caused by the shock structure in the skimmer throat, which disturbing the free expansion of the plasma jet significantly. It appears though that current measurements carried out under these conditions are not a clear representation of the ion transmission as registered with a conventional ICPMS instrument.

The conventional ELAN 6000 instrument operated with the sampler exchanged to the nozzles revealed a significant influence of the nozzle opening angle on the instrumental operating conditions. Most notably was the increase in background pressure in the high vacuum region caused by the nozzles. Despite doubling the pump speed at the first vacuum stage, the pressure limit of the instrument was exceeded already for the 25° nozzle when operating the standard 0.9 mm orifice skimmer. Only by reduction of the orifice to 0.2 mm all nozzles could be used.

The analyte sensitivity however dropped together with the skimmer diameter, which indicates that despite the higher fraction of the plasma transferred to the 2<sup>nd</sup> vacuum stage (as indicated by the pressure increase) a relatively smaller fraction of ions reaches the mass spectrometer. The highest sensitivity was also still attainable with the conventional sampler, while decreasing the nozzle opening angle usually led to progressively lower ion signal intensities. An exception was present for the 0.2 mm skimmer orifice where nozzles with opening angles smaller than 20° lead to an increase again, without however reaching the sensitivity for the sampler or the 30° nozzle. Another peculiarity was the trend towards smaller mass discrimination for smaller nozzle opening angles between 20° and 30°, especially with the 0.4 mm skimmer orifice. In any case however, the high density of the plasma expansion when using nozzles was causing a significant increase in the formation of molecular oxide ions and an increase in the non-spectral background. Both parameters were very closely correlating with the background pressure measured in the high vacuum region and result from the increase in collision frequency in the expansion near the skimmer orifice. This is also resulting in a narrower energy distribution of the ions transported into the 2<sup>nd</sup> vacuum stage, causing the mass-dependence of the optimum ion lens setting to become comparable for all  $m/Q$ .

Although the operation of the ICPMS with the nozzles did not yield improvements in instrument performance, the results of these studies may allow drawing some conclusions that can help to understand the general processes occurring within the vacuum interface and even open up new directions to improve the performance. Most interesting is the decrease in ion energy spread. This characteristic may allow designing ion optics configurations with better transmission across the range of  $m/Q$  required in elemental mass spectrometry and reduce the instrumental mass bias in isotope ratio determinations. Even though concomitant increase in oxide ions observed will be a severe limitation with solution based sample introduction methods, it may be a viable approach for applications where a “dry” plasma is sampled like with laser ablation. It will require to further study the effect of skimming position and pressure inside the 2<sup>nd</sup> vacuum stage, which could not be investigated in depth in this study but might be the key factor in order to retain or improve analyte sensitivity.

Using the ion funnel with an ICP ion source will in general require to overcome the space charge limit at the funnel exit aperture. Especially due to the thermalization of the ions inside the funnel at elevated pressure, the maximum current that may be transferred through the ion funnel is low. This problem may be attenuated by several ways. One approach could be reducing the ion current of  $\text{Ar}^+$  specifically by charge exchange with hydrogen. Even though this would not yield a net reduction of the total current present in the funnel, the resulting ions would be of much lower  $m/Q$ , which could be removed by selecting operating for the ion funnel that causes rejection of  $\text{H}_3^+$  via the low  $m/Q$  cut-off of the RF-field. All isotopes typically determined by ICPMS have higher  $m/Q$  and should thus be less affected. Another approach or an addition to the previous strategy could be to modify the ion funnel geometry in order to accommodate a higher total current also at the funnel exit.

The observation that the ion funnel used in these studies showed some characteristics of a size adjustable aperture would also be of advantage for example with sector field mass spectrometers as it might be useful as a contact-free entrance slit for adjusting the mass resolving power of the instrument.

The use of the ion funnel may further be advantageous to elemental mass spectrometry applications when using different ion sources that produce lower initial currents such as laser ablation mass spectrometry (LAMMS), which also suffers from a wide ion kinetic energy spread of the ions, making an efficient ion collection by electrostatic ion optics arrangements difficult. Since the ion beam is not dominated by a high current of background ions like in an ICP the demands for selectivity are moderate and the lower energy spread and high ion confinement may allow reducing the crater sizes compared with currently used approaches without sacrificing analyte sensitivity. Another technique where the ion funnel may be of interest is a combination with a miniaturized glow discharge (GD) source at intermediate pressure. The GD operates in a comparable pressure regime as an ion funnel [89] and current sources also exhibit an appreciable energy spread. It might thus be interesting to install an ion funnel in close proximity to the glow and thereby achieve high collection efficiency and high transfer efficiency through the ion optics into the MS.

## 7. Reference List

---

- [1] C.A. Heinrich, T. Pettke, W.E. Halter, M. Aigner-Torres, A. Audétat, D. Günther, et al., Quantitative multi-element analysis of minerals, fluid and melt inclusions by laser-ablation inductively-coupled-plasma mass-spectrometry, *Geochim. Cosmochim. Acta.* 67 (2003) 3473–3497.
- [2] B.S. Kamber, Geochemical fingerprinting: 40 years of analytical development and real world applications, *Appl. Geochemistry.* 24 (2009) 1074–1086.
- [3] S. Gschwind, L. Flamigni, J. Koch, O. Borovinskaya, S. Groh, K. Niemax, et al., Capabilities of inductively coupled plasma mass spectrometry for the detection of nanoparticles carried by monodisperse microdroplets, *J. Anal. At. Spectrom.* 26 (2011) 1166.
- [4] A.A. Ammann, Inductively coupled plasma mass spectrometry ( ICP MS ): a versatile tool, *J. Mass Spectrom.* 42 (2007) 419–427.
- [5] T.U. Schlegel, M. Wälle, M. Steele-MacInnis, C.A. Heinrich, Accurate and precise quantification of major and trace element compositions of calcic–sodic fluid inclusions by combined microthermometry and LA-ICPMS analysis, *Chem. Geol.* 334 (2012) 144–153.
- [6] J.R. Darling, C.D. Storey, M. Engi, Allanite U–Th–Pb geochronology by laser ablation ICPMS, *Chem. Geol.* 292–293 (2012) 103–115.
- [7] G. Raber, N. Stock, P. Hanel, M. Murko, J. Navratilova, K. a. Francesconi, An improved HPLC–ICPMS method for determining inorganic arsenic in food: Application to rice, wheat and tuna fish, *Food Chem.* 134 (2012) 524–532.
- [8] S. Gong, N. Chen, Q. Wang, T.M. Kusky, L. Wang, L. Zhang, et al., Early Paleoproterozoic magmatism in the Quanji Massif, northeastern margin of the Qinghai–Tibet Plateau and its tectonic significance: LA-ICPMS U–Pb zircon geochronology and geochemistry, *Gondwana Res.* 21 (2012) 152–166.
- [9] A. Marsala, T. Wagner, M. Wälle, Late-metamorphic veins record deep ingression of meteoric water: A LA-ICPMS fluid inclusion study from the fold-and-thrust belt of the Rhenish Massif, Germany, *Chem. Geol.* 351 (2013) 134–153.
- [10] M.A. Fehr, M. Rehkämper, A.N. Halliday, Application of MC-ICPMS to the precise determination of tellurium isotope compositions in chondrites, iron meteorites and sulfides, *Int. J. Mass Spectrom.* 232 (2004) 83–94.
- [11] S.G. Nielsen, M. Rehkämper, J. Baker, A.N. Halliday, The precise and accurate determination of thallium isotope compositions and concentrations for water samples by MC-ICPMS, *Chem. Geol.* 204 (2004) 109–124.
- [12] J. Kosler, U – Pb dating of detrital zircons for sediment provenance studies — a comparison of laser ablation ICPMS and SIMS techniques, *Chem. Geol.* 182 (2002) 605–618.
- [13] A.N. Halliday, D.-C. Lee, J.N. Christensen, M. Rehkämper, W. Yi, X. Luo, et al., Applications of multiple collector-ICPMS to cosmochemistry , geochemistry , and paleoceanography, *Geochim. Cosmochim. Acta.* 62 (1998) 919–940.
- [14] M.E. Ketterer, S.C. Szechenyi, Determination of plutonium and other transuranic elements by inductively coupled plasma mass spectrometry: A historical perspective and new frontiers in the environmental sciences, *Spectrochim. Acta Part B At. Spectrosc.* 63 (2008) 719–737.
- [15] D.J. Lowe, Tephrochronology and its application: A review, *Quat. Geochronol.* 6 (2011) 107–153.

- [16] A.L. de Souza, M.E.B. Cotrim, M.A.F. Pires, An overview of spectrometric techniques and sample preparation for the determination of impurities in uranium nuclear fuel grade, *Microchem. J.* 106 (2013) 194–201.
- [17] J.S. Becker, Applications of inductively coupled plasma mass spectrometry and laser ablation inductively coupled plasma mass spectrometry in materials science, *Spectrochim. Acta Part B At. Spectrosc.* 57 (2002) 1805–1820.
- [18] K.-C. Hsu, C.-C. Sun, Y.-L. Huang, Arsenic speciation in biomedical sciences: recent advances and applications., *Kaohsiung J. Med. Sci.* 27 (2011) 382–9.
- [19] R. Yin, X. Feng, W. Shi, Application of the stable-isotope system to the study of sources and fate of Hg in the environment: A review, *Appl. Geochemistry.* 25 (2010) 1467–1477.
- [20] P. Rodríguez-González, J.M. Marchante-Gayón, J.I. García Alonso, A. Sanz-Medel, Isotope dilution analysis for elemental speciation: a tutorial review, *Spectrochim. Acta Part B At. Spectrosc.* 60 (2005) 151–207.
- [21] R.S. Houk, V.A. Fassel, G.D. Flesch, H.J. Svec, A.L. Gray, C.E. Taylor, Inductively coupled argon plasma as an ion source for mass spectrometric determination of trace elements, *Anal. Chem.* 52 (1980) 2283–2289.
- [22] D.J. Douglas, J.B. French, Elemental Analysis with a microwave induced plasma quadrupole mass spectrometry, *Anal. Chem.* 53 (1981) 37–41.
- [23] H. Niu, R.S. Houk, Fundamental aspects of ion extraction in inductively coupled plasma mass spectrometry, *Spectrochim. Acta Part B At. Spectrosc.* 51 (1996) 779–815.
- [24] D. Günther, H.P. Longerich, S.E. Ackson, A new enhanced sensitivity quadrupole inductively coupled plasma-mass spectrometer, *Can. J. App. Spec.* 40 (1995) 111–116.
- [25] B.S. Green, B.D. Mapstone, G. Carlos, G.A. Begg, *Tropical Fish Otoliths: Information for Assessment, Management and Ecology*, Springer Dordrecht Heidelberg London New York, Dordrecht, 2009.
- [26] R. Thomas, *Practical Guide to ICP-MS*, Marcel Dekker, Inc, 2008.
- [27] P. Gaines, Sample Introduction for ICP-MS and ICP-OES, *Spectroscopy.* 20 (2005) 20 – 23.
- [28] D. Günther, B. Hattendorf, Solid sample analysis using laser ablation inductively coupled plasma mass spectrometry, *Trends Anal. Chem.* 24 (2005) 255–265.
- [29] J. Košler, Laser ablation ICP—MS — a new dating tool in Earth science, *Proc. Geol. Assoc.* 118 (2007) 19–24.
- [30] R.H. Wendt, V.A. Fassel, Emission spectrometric methods of analysis. Emission spectrometric determination of sodium and lithium in tungsten bronzes, *Spectrochim. Acta Part B At. Spectrosc.* 21 (1965) 1691–1695.
- [31] Y.Q. Tang, C. Trassy, Inductively coupled plasma: the role of water in axial excitation temperatures, *Spectrochim. Acta Part B At. Spectrosc.* 41 (1986) 143 – 150.
- [32] J.A. Olivares, R.S. Houk, Ion Sampling for Inductively Coupled Plasma Mass Spectrometry, *Anal. Chem.* 57 (1985) 2674–2679.
- [33] R. Campargue, Progress in Overexpanded Supersonic Jets and Skimmered Molecular Beams in Free Jet Zones of Silence, *J. Phys. Chem.* 88 (1984) 4466 – 4474.

- [34] D.J. Douglas, J.B. French, Gas Dynamics of the Inductively Coupled Plasma Mass Spectrometry Interface, *J. Anal. At. Spectrom.* 3 (1988) 743 – 747.
- [35] J.H. MacEdone, A.A. Mills, P.B. Farnsworth, Optical measurements of ion trajectories through the vacuum interface of an inductively coupled plasma mass spectrometer., *Appl. Spectrosc.* 58 (2004) 463–7.
- [36] H.B. Lim, R.S. Houk, J.S. Crain, Langmuir probe measurements of potential inside a supersonic jet extracted from an inductively coupled plasma, *Spectrochim. Acta Part B At. Spectrosc.* 44 (1989) 989–998.
- [37] D.M. Chambers, B.S. Ross, G.M. Hieftje, Fundamental studies of the sampling process in an inductively coupled plasma mass spectrometer-III . Monitoring the ion beam, *Spectrochim. Acta Part B At. Spectrosc.* 46 (1991) 785 – 804.
- [38] X. Chen, R.S. Houk, Spatially resolved measurements of ion density behind the skimmer of an inductively coupled plasma mass spectrometer, *Spectrochim. Acta Part B At. Spectrosc.* 51 (1996) 41–54.
- [39] R.S.U. Houk, Y. Zhai, Comparison of mass spectrometric and optical measurements of temperature and electron density in the inductively coupled plasma during mass spectrometric sampling, *Spectrochim. Acta Part B At. Spectrosc.* 56 (2001) 1055 – 1067.
- [40] R.L. Spencer, J. Krogel, J. Palmer, A. Payne, A. Sampson, W. Somers, et al., Modeling the gas flow upstream and in the sampling nozzle of the inductively coupled plasma mass spectrometer via the Direct Simulation Monte Carlo algorithm, *Spectrochim. Acta Part B At. Spectrosc.* 64 (2009) 215–221.
- [41] W.N. Radicic, J.B. Olsen, R. V. Nielson, J.H. Macedone, P.B. Farnsworth, Characterization of the supersonic expansion in the vacuum interface of an inductively coupled plasma mass spectrometer by high-resolution diode laser spectroscopy, *Spectrochim. Acta Part B At. Spectrosc.* 61 (2006) 686–695.
- [42] P.B. Farnsworth, R.L. Spencer, W.N. Radicic, N. Taylor, J. Macedone, H. Ma, A comparison of ion and atom behavior in the first stage of an inductively coupled plasma mass spectrometer vacuum interface: Evidence of the effect of an ambipolar electric field, *Spectrochim. Acta Part B At. Spectrosc.* 64 (2009) 905–910.
- [43] N. Taylor, P.B. Farnsworth, Experimental characterization of the effect of skimmer cone design on shock formation and ion transmission efficiency in the vacuum interface of an inductively coupled plasma mass spectrometer, *Spectrochim. Acta Part B At. Spectrosc.* 69 (2012) 2–8.
- [44] H. Niu, R.S. Houk, Langmuir probe measurements of the ion extraction process in inductively coupled plasma mass spectrometry-I . Spatially resolved determination of electron density and electron temperature, *Spectrochim. Acta Part B At. Spectrosc.* 49B (1994) 1283–1303.
- [45] S.D. Tanner, Space charge in ICP-MS: calculation and implications \*, *Spectrochim. Acta Part B At. Spectrosc.* 47 (1992) 809–823.
- [46] J.W. Olesik, M.P. Dziewatkoski, Time-resolved measurements of individual ion cloud signals to investigate space-charge effects in Plasma Mass Spectrometry, *J. Am. Soc. Mass Spectrom.* 7 (1995) 362–367.
- [47] D. Beauchemin, J.W. McLaren, S.S. Berman, Study of the effects of concomitant elements in inductively coupled plasma mass spectrometry, *Spectrochim. Acta Part B At. Spectrosc.* 42 (1987) 467 – 490.
- [48] M.M. Fraser, D. Beauchemin, Effect of concomitant elements on the distribution of ions in inductively coupled plasma-mass spectroscopy. Part 1. Elemental ions, *Spectrochim. Acta Part B At. Spectrosc.* 55 (2000) 1705–1731.

- [49] E.H. Larsen, S. Stürup, Carbon-enhanced inductively coupled plasma mass spectrometric detection of arsenic and selenium and its application to arsenic speciation, *J. Anal. At. Spectrom.* 9 (1994) 1099 – 1105.
- [50] J. Koch, L. Flamigni, S. Gschwind, S. Allner, H. Longerich, D. Günther, Accelerated evaporation of microdroplets at ambient conditions for the on-line analysis of nanoparticles by inductively-coupled plasma mass spectrometry, *J. Anal. At. Spectrom.* 28 (2013) 1707 – 1717.
- [51] C. Agatemor, D. Beauchemin, Matrix effects in inductively coupled plasma mass spectrometry: a review., *Anal. Chim. Acta.* 706 (2011) 66–83.
- [52] G.R. Gillson, D.J. Douglas, J.E. Fulford, K.W. Halligan, S.D. Tanner, Nonspectroscopic interelement interferences in inductively coupled plasma mass spectrometry, *Anal. Chem.* 60 (1988) 1472–1474.
- [53] B.S. Ross, G.M. Hiefje, Alteration of the ion-optic lens configuration to eliminate mass- dependent matrix-interference effects in inductively coupled plasma-mass spectrometry, *Spectrochim. Acta Part B At. Spectrosc.* 46 (1991) 1263 – 1273.
- [54] S.D. Tanner, D.J. Douglas, J.B. French, Gas and Ion Dynamics of a Three-Aperture Vacuum Interface for Inductively Coupled Plasma-Mass Spectrometry, *Appl. Spectrosc.* 48 (1994) 1373–1378.
- [55] S.D. Tanner, L.M. Cousins, D.J. Douglas, Reduction of Space Charge Effects Using a Three-Aperture Gas Dynamic Vacuum Interface for Inductively Coupled Plasma-Mass Spectrometry, *Appl. Spectrosc.* 48 (1994) 1367–1372.
- [56] N. Praphairaksit, R.S. Houk, Reduction of Space Charge Effects in Inductively Coupled Plasma Mass Spectrometry Using a Supplemental Electron Source inside the Skimmer: Ion Transmission and Mass Spectral Characteristics, *Anal. Chem.* 72 (2000) 2356–2361.
- [57] N. Praphairaksit, R.S. Houk, Reduction of Mass Bias and Matrix Effects in Inductively Coupled Plasma Mass Spectrometry with a Supplemental Electron Source in a Negative Extraction Lens, *Anal. Chem.* 72 (2000) 4435–4440.
- [58] N. Praphairaksit, R.S. Houk, Attenuation of matrix effects in inductively coupled plasma mass spectrometry with a supplemental electron source inside the skimmer, *Anal. Chem.* 72 (2000) 2351–2355.
- [59] S. Moussalami, W. Chen, B. a. Collings, D.J. Douglas, High intensity ion beams from an atmospheric pressure inductively coupled plasma, *Rev. Sci. Instrum.* 73 (2002) 884.
- [60] K. Hu, R.S. Houk, Inductively coupled plasma mass spectrometry with an electrically floating sampling interface., *J. Am. Soc. Mass Spectrom.* 4 (1993) 733–41.
- [61] K. Hu, P.S. Clemons, R.S. Houk, Inductively coupled plasma mass spectrometry with an enlarged sampling orifice and offset Ion Lens. I. Ion trajectories and detector performance., *J. Am. Soc. Mass Spectrom.* 4 (1993) 16–27.
- [62] I. Kalinitchenko, X.D. Wang, B. Sturman, Simple and Effective Control of Spectral Overlap Interferences in ICP-MS, *Spectroscopy.* (2008) 38 – 46.
- [63] D.J. Douglas, Applications of collision dynamics in quadrupole mass spectrometry, *J. Am. Soc. Mass Spectrom.* 9 (1998) 101–113.
- [64] J.P. Turner, D.J. Mills, E. Schroder, G. Lapitajs, G. Jung, L.A. Iacone, et al., Instrumentation for low- and high-resolution ICPMS, in: *Inductively Coupled Plasma Mass Spectrom.*, 1998: pp. 421–501.

- [65] I. Feldmann, N. Jakubowski, D. Stuewer, Application of a hexapole collision and reaction cell in ICP-MS Part I: Instrumental aspects and operational optimization, *J. Anal. Chem.* 365 (1999) 415–421.
- [66] S.D. Tanner, V.I. Baranov, D.R. Bandura, Reaction cells and collision cells for ICP-MS: a tutorial review, *Spectrochim. Acta Part B At. Spectrosc.* 57 (2002) 1361–1452.
- [67] G.C. Eiden, C.J. Barinaga, D.W. Koppenaal, Selective Removal of Plasma Matrix Ions in Plasma Source Mass Spectrometry, *J. Anal. At. Spectrom.* 11 (1996) 317 – 322.
- [68] S.A. Shaffer, K. Tang, G.A. Anderson, D.C. Prior, H.R. Udseth, R.D. Smith, A Novel Ion Funnel for Focusing Ions at Elevated Pressure Using Electrospray Ionization Mass Spectrometry, 11 (1997) 1813–1817.
- [69] S.A. Shaffer, D.C. Prior, G.A. Anderson, H.R. Udseth, R.D. Smith, An ion funnel interface for improved ion focusing and sensitivity using electrospray ionization mass spectrometry., *Anal. Chem.* 70 (1998) 4111–9.
- [70] S.A. Shaffer, A. Tolmachev, D.C. Prior, G.A. Anderson, H.R. Udseth, R.D. Smith, Characterization of an improved electrodynamic ion funnel interface for electrospray ionization mass spectrometry., *Anal. Chem.* 71 (1999) 2957–64.
- [71] D. Gerlich, Inhomogeneous rf fields : a versatile tool for the study of processes with slow ions, *Adv. Chem. Phys.* 82 (1992) 1 – 176.
- [72] A. V. Tolmachev, T. Kim, H.R. Udseth, R.D. Smith, T.H. Bailey, J.H. Futrell, Simulation-based optimization of the electrodynamic ion funnel for high sensitivity electrospray ionization mass spectrometry, *Int. J. Mass Spectrom.* 203 (2000) 31–47.
- [73] J.S. Page, A. V Tolmachev, K. Tang, R.D. Smith, Theoretical and experimental evaluation of the low m/z transmission of an electrodynamic ion funnel., *J. Am. Soc. Mass Spectrom.* 17 (2006) 586–92.
- [74] R.T. Kelly, A. V Tolmachev, J.S. Page, K. Tang, R.D. Smith, P.O. Box, The ion funnel: theory, implementations, and applications, *Mass Spectrom. Rev.* 29 (2010) 294–312.
- [75] S. Heinz, J. Äystö, D. Habs, S. Hegewisch, J. Huikari, a. Nieminen, et al., A radio frequency ring electrode cooler for low-energy ion beams, *Nucl. Instruments Methods Phys. Res. Sect. A Accel. Spectrometers, Detect. Assoc. Equip.* 533 (2004) 239–247.
- [76] T. Kim, H.R. Udseth, R.D. Smith, Improved Ion Transmission from Atmospheric Pressure to High Vacuum Using a Multicapillary Inlet and Electrodynamic Ion Funnel Interface, *Anal. Chem.* 72 (2000) 5014–5019.
- [77] T. Kim, A. V. Tolmachev, R. Harkewicz, D.C. Prior, G. Anderson, H.R. Udseth, et al., Design and Implementation of a New Electrodynamic Ion Funnel, *Anal. Chem.* 72 (2000) 2247–2255.
- [78] T. Wyttenbach, P.R. Kemper, M.T. Bowers, Design of a new electrospray ion mobility mass spectrometer, *Int. J. Mass Spectrom.* 212 (2001) 13–23.
- [79] B.H. Clowers, Y.M. Ibrahim, D.C. Prior, W.F. Danielson, M.E. Belov, R.D. Smith, Enhanced ion utilization efficiency using an electrodynamic ion funnel trap as an injection mechanism for ion mobility spectrometry., *Anal. Chem.* 80 (2008) 612–23.
- [80] L. Meier, C. Berchtold, S. Schmid, R. Zenobi, Sensitive detection of drug vapors using an ion funnel interface for secondary electrospray ionization mass spectrometry., *J. Mass Spectrom.* 47 (2012) 555–9.
- [81] L. Meier, C. Berchtold, S. Schmid, R. Zenobi, Extractive electrospray ionization mass spectrometry-enhanced sensitivity using an ion funnel, *Anal. Chem.* 84 (2012) 2076–80.

- [82] D. Beauchemin, Current status of ICP-MS, *Compr. Anal. Chem.* 34 (2000) 1 – 212.
- [83] D.J. Douglas, J.B. French, An improved interface for inductively coupled plasma-mass, *Spectrochim. Acta Part B At. Spectrosc.* 41 (1986) 197–204.
- [84] S. Yin, M. Zhang, Z. Guo, H. Liao, X. Wang, Numerical investigations on the effect of total pressure and nozzle divergent length on the flow character and particle impact velocity in cold spraying, *Surf. Coatings Technol.* 232 (2013) 290–297.
- [85] T.-C. Jen, L. Li, W. Cui, Q. Chen, X. Zhang, Numerical investigations on cold gas dynamic spray process with nano- and microsize particles, *Int. J. Heat Mass Transf.* 48 (2005) 4384–4396.
- [86] W.-Y. Li, H. Liao, G. Douchy, C. Coddet, Optimal design of a cold spray nozzle by numerical analysis of particle velocity and experimental validation with 316L stainless steel powder, *Mater. Des.* 28 (2007) 2129–2137.
- [87] V.L. Varentsov, D. Habs, A cooler for intense low-energy ion beams, *Nucl. Instruments Methods Phys. Res. Sect. A Accel. Spectrometers, Detect. Assoc. Equip.* 490 (2002) 16–29.
- [88] S.D. Tanner, Plasma temperature from ion kinetic energies and implications for the source of diatomic oxide ions in inductively coupled plasma mass spectrometry, *J. Anal. At. Spectrom.* 8 (1993) 891–897.
- [89] M. Tarik, G. Lotito, J. a. Whitby, J. Koch, K. Fuhrer, M. Gonin, et al., Development and fundamental investigation of Laser Ablation Glow Discharge Time-Of-Flight Mass Spectrometry (LA-GD-TOFMS), *Spectrochim. Acta Part B At. Spectrosc.* 64 (2009) 262–270.



## 8. Appendix

---

### 8.1. Simlon simulations parameters:

Hardware:

- Aperture diameter – 1-2.5 mm
- Number of plates – 2, 3
- Angle of plates border in the aperture -  $90^\circ$ ,  $45^\circ$ ,  $30^\circ$
- Thickness of plates – 0.3, 0.5 mm
- Thickness of isolator – 0.3, 0.5 mm

Ions:

- Total ions number – 101
- Ion Mass – 40 amu
- Initial ion's kinetic energy – 3eV

Simulation parameters:

- Coulomb repulsion as  $1 \cdot 10^{-10}$  C- $1 \cdot 10^{-14}$  C
- Potential of plasma - +3V

Models:

- Only Coulomb repulsion
- Damping factor (DF) = 0.5 (every iteration:  $A_1 = A_0 - V \cdot DF$  for every x, y, and z). DF=const.
- DFFconst.  $DF_0 = 0.5$  and lineary decreased to 0 at the last X coordinate.
- $A_{1x} = A_{0x} - V_x \cdot DF$
- DFFconst.  $DF_0 = 0.5$  and lineary decreased to 0 at the last X coordinate.
- $V(\text{average}) = 0.5 \text{ mm} / \mu\text{s}$  (result of a simulation by CFX).
- $A_{ix} = A_{0x} - (V_x - V_x(\text{average})) \cdot DF$
- Collision Model:
  - Probability of collision = 2/3 per point Random changes of the ion speed:  $V = V_0 \cdot (1 + \text{rnd})$ , where  $\text{rnd} = -1..1$
  - Three velocity components change.

A series of simulations with Simlon software gave the optimum parameters at around +5 V for the front plate and -100 V for the second plate, where both plates had a thickness of 0.3 mm and the distance between them was 0.3 mm. The 1<sup>st</sup> plate diameter was set to 1.5 mm. Both plates have an edge cut at  $45^\circ$ , which gave a diameter of the second plate of 2.7 mm.

The effect of focusing potentials based on simulations is presented in figure 3.4. The collisional mode was an additional script, which added a random change to the velocity components with a probability of  $2/3$  (calculated probability of collision per step for the given pressure regime). The free path of Ar ions at a 100 Pa pressure was calculated to be 0.15 mm. Based on this value and the geometrical parameters of the system the value of  $2/3$  was selected.

## 8.2. Reflections of the plasma from the cylindrical detector

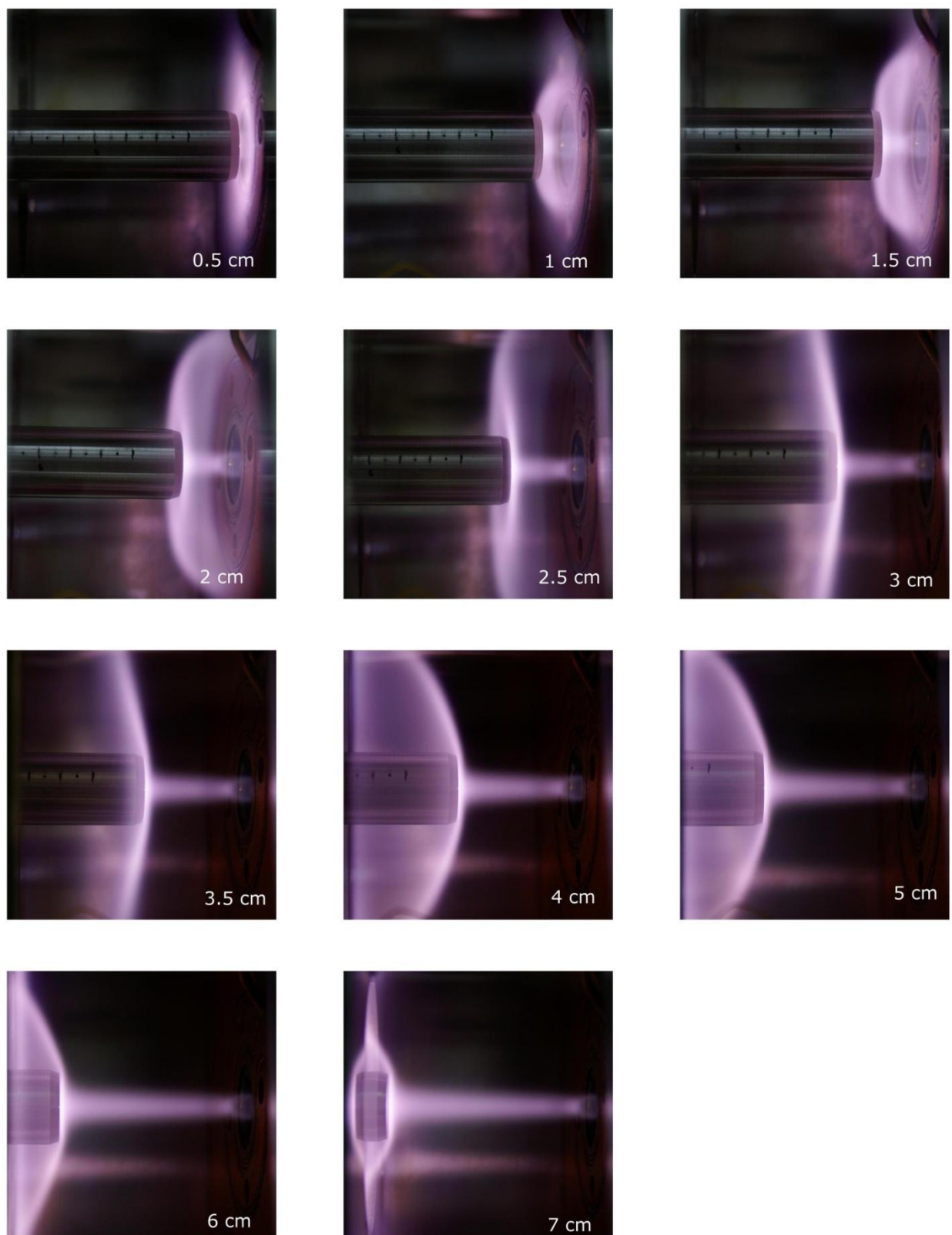


*Figure 8.1. Plasma reflections from the surface of the cylindrical detector at different distances between the detector and the front plate.*



## 9. Acronyms and Abbreviations

---

amu	Atomic Mass Unit
C	Coulomb
cm	Centimeter
cps	Counts per Second
D	Debye
D <sub>o</sub>	Sampler aperture diameter
DC	Direct Current
E	Energy
e	Electron Charge
EESI	Extractive Electro Spray Ionization
ESI	Electro Spray Ionization
eV	Electron Volt
ETH	Eidgenössische Technische Hochschule
fA	Femtoampere
g	Gram
GD	Glow Discharge
I	Electric Current
ICP	Inductively Coupled Plasma
ICPMS	Inductively Coupled Plasma Mass Spectrometer
ICPOES	Inductively Coupled Plasma Optical Emission Spectrometry
IF	Ion Funnel
IRZ	Initial Radiation Zone
K	Kelvin
kHz	Kilohertz
L	Liter
LA	Laser Ablation
LA-ICPMS	Laser Ablation Inductively Coupled Plasma Mass Spectrometry
LAMS	Laser Ablation Mass Spectrometry
M	Mole
m	Mass
m <sub>e</sub>	Mass of the Electron
m <sub>ion</sub>	Mass of an Ion
m/Q	Mass to Charge Ratio
mg	Milligram
min	Minute
mL	Milliliter
MΩ	Megaohm
MS	Mass Spectrometer
ms	Millisecond

$\mu\text{A}$	Microampere
$\mu\text{F}$	Microfarad
$\mu\text{g}$	Microgram
MHz	Megahertz
$\mu\text{L}$	Microliter
$\mu\text{m}$	Micrometer
nA	Nanoampere
NAZ	Normal Analytical Zone
ng	Nanogram
nm	Nanometer
P	Perveance
$P_{\text{max}}$	Maximum Perveance
Pa	Pascal
r	Radius
RF	Radio Frequency
SESI	Secondary Electro Spray Ionization
T	Absolute Temperature
$T_0$	Temperature of Plasma Source
TOFMS	Time of Flight Mass Spectrometer
V	Volts
$V_{\text{pp}}$	Voltage peak to peak
W	Watts

## 10. Curriculum Vitae

---

Name Tatiana Egorova  
Born 13.02.1983, Petrozavodsk, Russia

### Education:

---

1989 - 1994 Elementary School Kremjonky, Russia  
1994 - 1995 Secondary school Kremjonky, Russia  
1995 - 1996 Gimnasium Kremjonky, Russia  
1996 - 2000 Physico-mathematical Lycée Protvino, Russia

### Academical Education:

---

2000 - 2005 Student in Lomonosov Moscow State University  
14.06.2005 Diploma with Honor in Analytical Chemistry  
2007 - 2013 PhD in Chemistry, group of Prof. Detlef Günther at the Laboratory of Inorganic Chemistry at ETH-Zürich, Zürich, Switzerland

### Employment:

---

2004 - 2006 Tester, "Advanced Chemical Development Inc.", Canada  
2006 – 2007 Leader Manager, "Spectroscopy Systems" Moscow, Russia  
2009 – 2012 Teaching assistant for the practical course of Analytical chemistry (AAS and IC techniques) for students at ETH Zurich (Zurich CH)